EXAMINING THE EFFECTS OF EPIGENETIC MODULATION ON IDH MUTANT GBM CELLS

by

Alişan KAYABÖLEN

A Dissertation Submitted to the

Graduate School of Health Sciences in Partial Fulfillment of the Requirements for the Degree of

Doctor of Philosophy

in

Cellular and Molecular Medicine

KOÇ ÜNİVERSİTESİ

Dec 24, 2019

Examining the Effects of Epigenetic Modulation on IDH Mutant GBM Cell

Koç University

Graduate School of Health Sciences

This is to certify that I have examined this copy of a doctoral dissertation by

Alişan KAYABÖLEN

and have found that it is complete and satisfactory in all respects,

and that any and all revisions required by the final

examining committee have been made

Committee Members:

_____

Assoc. Prof. Tuğba Bağcı-Önder (Advisor)

_____

Assoc. Prof. Tamer Önder

_____

Assoc. Prof. Ceyda Açılan Ayhan

_____

Prof. Batu Erman

_____

Assoc. Prof. Tolga Emre

Date _____

To my beloved family including the future one…

ABSTRACT

Examining the Effects of Epigenetic Modulation on IDH Mutant GBM Cells

Alişan KAYABÖLEN

Doctor of Philosophy in Cellular and Molecular Medicine

December 24, 2019

Mutations in *IDH1* and *IDH2* genes are common in low grade gliomas and secondary GBM and are known to cause a distinct epigenetic landscape in these tumors. To interrogate the epigenetic vulnerabilities of IDH-mutant gliomas, we performed a chemical screen with inhibitors of chromatin modifiers and identified 5-azacytidine, Chaetocin, GSK-J4 and Belinostat as potent agents against primary IDH1-mutant cell lines. Testing the combinatorial efficacy of these agents, we demonstrated GSK-J4 and Belinostat combination as a very effective treatment for the IDH1-mutant glioma cells. Engineering established cell lines to ectopically express $IDH1^{R132H}$, we showed that IDH1-mutant cells adopted a different transcriptome with changes in stress-related pathways that were reversible with the mutant IDH1 inhibitor, GSK864. The combination of GSK-J4 and Belinostat was highly effective on $IDH1^{R132H}$ cells, but not on wt glioma cells or non-malignant fibroblasts and astrocytes. The cell death induced by GSK-J4 and Belinostat combination involved the induction of cell cycle arrest and apoptosis. RNA sequencing analyses revealed activation of inflammatory and unfolded protein response pathways in IDH1-mutant cells upon treatment with GSK-J4 and Belinostat conferring increased stress to glioma cells. Specifically, GSK-J4 induced ATF4-mediated integrated stress response (ISR) and Belinostat induced cell cycle arrest in primary IDH1-mutant glioma cells, which were accompanied by *DDIT3*/CHOP-dependent upregulation of apoptosis. Moreover, to dissect out the responsible target histone demethylase, we undertook genetic approach and demonstrated that CRISPR/Cas9 mediated ablation of both KDM6A and KDM6B phenocopied the effects of GSK-J4 in IDH1-mutant cells. Finally, GSK-J4 and Belinostat combination significantly decreased tumor growth and increased survival in an orthotopic model in mice. Together, these results suggest a potential combination epigenetic therapy against IDH1-mutant gliomas.

ÖZETÇE

IDH Mutant GBM Hücrelerinde Epigenetik Düzenlemelerin Etkilerinin İncelenmesi

Alişan KAYABÖLEN

Hücresel ve Moleküler Tıp, Doktora

24 Aralık 2019

IDH1 ve IDH2 genlerindeki mutasyonlar düşük dereceli gliomlar ve ikincil GBM tümörlerinde görülmekte olup, belirleyici epigenetik farklılıklara sebep olduğu bilinmektedir. Epigenetik hassasiyetlerini sorgulamak amacıyla, IDH mutant gliom hücrelerinde kromatin düzenleyici inhibitörlerinin bulunduğu kütüphane ile gerçekleştirdiğimiz kimyasal tarama sonucunda bu hücreleri yüksek oranda etkileyen 5-azacytidine, Chaetocin, GSK-J4 ve Belionstat kimyasalları tanımlanmıştır. Belirlenen ajanların kombinasyon durumunda verimleri test edildiğinde, GSK-J4 ve Belinostat kombinasyonunun IDH mutant gliomlarda hücre canlılığını önemli ölçüde etkilediği görülmüştür. $IDH1^{R132H}$ mutasyonu hücrelerde ektopik olarak ifade edildiğinde IDH mutant hücrelerinin transkriptomunun ve hücresel stres kaynaklı yolakların değiştiğini, ve bu değişimlerin IDH mutant inhibitörü GSK864 ile geriye döndürülebileceğini gösterdik. GSK-J4 ve Belinostat kombinasyonunun $IDH1^{R132}$ hücrelerinde etkisinin yüksek olduğunu, ancak yabanıl tip gliom hücrelerinde ve malignant olmayan fibroblast ve astrosit hücrelerini etkilemediği görülmüştür. GSK-J4 ve Belinostat kombinasyonu hücre ölümü ve apoptozun indüklenmesini içerir. RNA sekanslama analizleri glioma hücrelerinde artan stresi gösterir biçimde, GSK-J4 ve Belinostat verilen IDH-1 mutant hücrelerinde, inflamatuar ve katlanmamış protein cevabı yolaklarının aktive olduğunu göstermiştir. Özellikle, GSK-J4 indüklenen ATF4 aracılı entegre stres cevabı (ISR) ve Belinostat kaynaklı primer IDH1-mutant glioma hücrelerinde hücre döngüsünün durmasına neden olmuş, bunlara DDIT3/CHOP bağımlı apoptoz eşlik etmiştir. Buna ek olarak, sorumlu hedef histon demetilazını yok etmek için CRISPR/Cas9 aracılı genetik bir yaklaşım ile ve hem KDM6A hem de KDM6B'nin ablasyonunun, IDH1 mutant hücrelerinde GSK-J4'ün etkilerini fenokopi ettiğini gösterdik. Son olarak, GSK-J4 ve Belinostat kombinasyonu, farelerde ortotopik bir modelde tümör büyümesini ve sağkalımı artırmıştır. Bu sonuçlar IDH1-mutant gliomalara karşı potansiyel bir kombinasyon epigenetik tedavi önermektedir.

ACKNOWLEDGEMENTS

Foremost, I would like to express my sincere gratitude to my advisor Dr. Tuğba Bağcı Önder. I am grateful to her for her continuous support, motivation and immense patience. She always believed in me even I had unexpected experimental results and encouraged me to try novel things which satisfied my scientific curiosity. Her continuous guidance has a huge role in my research, experiments and writing of this thesis.

I am also very grateful to Dr. Tamer Önder and Dr. Batu Erman due to their great contributions to my study during thesis progresses, and in my thesis committee. I would also like to thank to other committee members, Dr. Ceyda Açılan Ayhan and Dr. Tolga Emre for their interests in my study and participation and valuable comments in my thesis jury.

I also feel lucky to have the chance to collaborate with Dr. Udo Oppermann, Dr. Adam Cribbs, and Dr. Hiroaki Wakimoto during our project. Their contributions were critical for this study.

I would also like to thank Scientific and Technological Research Council of Turkey (TÜBİTAK) for its PhD thesis grant under BİDEB 2211 program, and Koç University Research Center for Translational Medicine (KUTTAM) for providing financial support to this project.

I am also thankful to all my lab mates who were like my family during the PhD. Especially, Fidan Şeker was with me during all my PhD life and shared whatever she knows together with her close friendship. All the other TBO lab members; Nareg Pınarbaşı, Göktuğ Karabıyık, Filiz Şenbabaoğlu, Ahmet Cingöz, Özlem Yedier Bayram, İlknur Sur, Ali Cenk Aksu, Ezgi Yağmur Kala, Ezgi Özyerli and Birsu Kölemen have huge contributions to me and this study with their great friendships and helpful attitudes which deserve special thanks.

Productive discussions are one of the most important things feeding scientists in every step of their studies. Doing such discussions with close friends are even better, and I am very lucky to do that with Doğancan Özturan, Uğur Akcan and Kenan Sevinç. Even though we are in different labs and working on different topics, it was always exciting to talk about potential projects, novel studies, or sometimes very old but extremely important studies.

During my PhD, I worked with several undergrad students who were ambitious and eager to learn. I thank to Bekir, Simge, Sezan, Kardelen, Cemre, and Mami for their helps in this project.

I would also like to thank all members of METU Orienteering and Navigation Team to keep me a part of the team even if I am far from them. I tasted teamwork, success, enthusiasm, fun, beauty of nature, and many special things with them while subjecting to stressful realities of life and PhD.

There are also some real friends who deserve special thanks. Bilal Kabaklı is my twin brother even if we are not in the same age and do not have blood relation. I feel lucky to be able to share any dreams with him which make both of us stronger and motivated for life. Kübra Narcı is my sister who is always reliable, loyal and cheerful. As she travels to fantastic places, I feel like travelling with her and reading a book she had already read and gave me. Koray İroç and Mustafa Onur Koç are my little brothers. They are one of the main reasons for me to feel young. I am very happy to feel their energy, and loyalty for years. Elif Yurdanur Taşel, Erdinç Taşel and Mehmet Ali Erol are my elder sister and brothers. They have contributed many valuable experiences to my life which are always guided me in many different cases.

For sure, this study and any other accomplishments in my life would not be possible without supports of my family. Therefore, one of the biggest thanks is to my family, to my father Naci Kayabölen, my mother Semra Kayabölen, and my brother Özgür Kayabölen who always trust, believe in and encourage me whatever I did throughout my life.

Finally, there is one person who entered my life with the beginning of my PhD and changed it in the most beautiful way. Whenever I need, whatever I did, she was always with me. Being both a scientific partner and life partner, Gizem Nur Şahin has the most influential role in this study and in my life.

TABLE OF CONTENTS

LIST OF TABLES

LIST OF FIGURES

ABBREVIATIONS

α-KG	α-Ketoglutarate
2-OG	2-Oxoglutarate
2-HG	2-Hydroxyglutarate
aDMA	Asymmetric Dimethyl Arginine
AML	Acute Myeloid Leukemia
ATF	Activating Transcription Factor
BBB	Blood-Brain-Barrier
BET	Bromodomain And Extra-Terminal Motif
BiP	Binding immunoglobulin protein
CNS	Central Nervous System
CRISPR	Clustered Regularly Interspaced Short Palindromic Repeats
CTCL	Cutaneous T-Cell Lymphoma
DNMT	DNA methyltransferase
DSB	Double Strand Break
ECM	Extracellular Matrix
EGF	Epidermal Growth Factor
eIF2	Eukaryotic Initiation Factor 2
EMT	Epithelial to Mesenchymal Transition
ERAD	Endoplasmic Reticulum-Associated Degradation
FDA	Food and Drug Administration
FGF	Fibroblast Growth Factor
GBM	Glioblastoma Multiforme

GCN2	General Control Non-Derepressible 2
GSC	Glioma Stem Cell
G-CIMP	Glioma CpG Island Methylator Phenotype
HAT	Histone Acetyltransferases
HDAC	Histone Deacetylase Inhibitor
HDR	Homology Directed Repair
HIF	Hypoxia Inducable Factor
HMT	Histone Methyltransferase
HRI	Heme-Regulated Inhibitor
HSP	Heat Shock Protein
IDH	Isocitrate Dehydrogenase
IRE1	Inositol-Requiring Enzyme 1
ISR	Integrated Stress Response
JHDM	Jumonji C domain containing Histone Demethylase
KDM	Lysine Demethylase
KMT	Lysine Methyltransferases
LncRNA	Long non-coding RNA
LSD1	Lysine Specific Demethylase 1
MBD	Methyl-CpG Binding Domains
MGMT	Methyl Guanine Methyltransferase
MM	Multiple Myeloma
MMA	Monomethyl Arginine
NHEJ	Non-Homologous End Joining
PAD	Peptidyl-Arginine Deiminase

PDGFR	Platelet Derived Growth Factor Receptor
PERK	PKR-like ER kinase
PKR	Protein Kinase R
PRMT	Protein Arginine Methyltransferase
PTCL	Peripheral T-Cell Lymphoma
PTM	Post-Translational Modifications
RDM	Arginine Demethylases
ROS	Reactive Oxygen Species
SAM	S-Adenosyl-Methionine
SCLC	Small Cell Lung Cancer
sDMA	Symmetric Dimethyl Arginine
SUMO	Small Ubiquitin-Like Modifier
TCGA	The Cancer Genome Atlas
TERT	Telomerase Reverse Transcriptase
TET	Ten-Eleven Translocation
TMZ	Temozolomide
TSG	Tumor Suppressor Gene
uORF	Upstream Open Reading Frame
UPR	Unfolded Protein Response
UTR	Untranslated Region
WHO	World Health Organization

1 INTRODUCTION

1.1 Glioma

Central nervous system (CNS) tumors derived from glial cells are called glioma. Glial cells surround nerve cells in the brain or spinal cord and protect them; and they also support their functions. Glial cells are the most common cell types in the brain, making up ~80% of the brain volume. Gliomas cover almost 30% of all brain tumors and 80% of malignant brain tumors [1]. There are 3 main types of gliomas according to cell origin of the tumor, namely: Astrocytoma, Oligodendroglioma, and Ependymoma.

Ependymoma is a rare type of CNS tumor, which occurs in all age groups but is observed more commonly in children. Oligodendroglioma, observed mostly in adults, is more frequent than ependymoma, but it is still considered a rare CNS tumor type. Astrocytomas are the most common type of gliomas in both children and adults. They are originated from astrocytes or glial precursor cells and can be classified in 4 grades [2]. Grade I astrocytomas are mostly benign and confined. They have almost normal morphology and they divide slowly. Grade II astrocytomas are known as diffuse astrocytoma because of their infiltrative abilities and uncertain boundaries between normal tissue and tumor. However, tumor cells still grow slowly, and they do not have a very abnormal appearance. In grade III astrocytomas, which is called anaplastic astrocytoma, cells are actively dividing, and they have an abnormal appearance. Grade IV astrocytomas are known as glioblastoma multiforme (GBM) and they are the most aggressive type of the gliomas. In GBM, tumor cells have bizarre morphologies and they divide rapidly. As a hallmark of GBM, tumors have necrotic regions in their centers. Low grade astrocytomas or oligodendrogliomas can transform into higher grade gliomas by time and gain aggressive behaviors.

1.1.1 Treatment options in glioma

Glioma is one of the most aggressive tumor types. Highest grade of glioma which is known as GBM is among the deadliest cancers with an average survival of 14-16 months even for patients receiving surgery and chemoradiation [3,4]. Survival rate is higher in low-grade glioma (LGG), however most of the LGGs eventually progress to high-grade glioma, known as secondary GBM [5]. Treatment options mostly lead to slowing down of tumor progression, but unfortunately total cure is not possible. Tumor

heterogeneity, invasive nature of the tumors, and protection by blood-brain barrier (BBB) limiting the tumor delivery of many conventional cancer therapeutics are the main difficulties for a successful treatment in GBM [6].

The first option for a newly diagnosed GBM is the removal of tumor by surgical resection. The main goal in the surgery is complete removal of the tumor. However, since GBM cells invade into the healthy brain tissue, most of the time residual tumor cells remain after the surgery. Therefore, adjuvant therapies should be applied. In some cases, surgery may not be safe because of the specific location of the tumor or the overall health status and the inappropriate clinical parameters of the patient. In such cases, radiation therapy and chemotherapy are the only standard treatment options. In radiation therapy, beams with intense energy, mostly X-rays, are used to eradicate tumor cells via directing beams to the exact coordinates of the tumor in the brain [7]. In chemotherapy, drugs that have the ability to kill the tumor cells are used. Temozolomide (TMZ) is the first FDA-approved drug to be used in GBM [8]. It is a DNA alkylating agent that causes methylation of O^6 and N^7 positions of guanine, leading to DNA damage-induced apoptosis [9]. However, many tumor cells might gain resistance against TMZ by activating DNA repair mechanisms. One of the best-known mechanisms is demethylation of the promoter region of *MGMT* gene [10]. In 2005, Stupp and his colleagues from EORTC and NCIC clinical trials groups suggested an aggressive treatment regimen, which included maximal surgical resection, followed with combination of radiation and TMZ therapy [3]. This protocol, which is known as "Stupp protocol" is now accepted as the standard of care for GBM treatment. However, even with this protocol, average survival was only increased from 12.1 months to 14.6 months. Recently, a monoclonal antibody-based drug, Bevacizumab, targeting the vascular endothelial growth factor (VEGF), is fully approved by FDA for the treatment of recurrent GBM based on a phase III clinical trial [11]. The main purpose of it, by inhibiting VEGF, is to inhibit new blood vessel formation inside and around the tumor and prevent tumor growth and invasion [12]. There are also several other drugs such as lomustine, gliadel, or cisplatin which are used for recurrent GBM [11,13,14]. However, all of these drugs, even with maximal surgery and concomitant radiation therapy, increase the average survival for only few months at most, and are not sufficient to cure GBM.

1.1.2 IDH mutation in glioma

In 2008, an integrated genomic analysis showed that there is a small subset of glioblastoma samples that have a point mutation in *IDH1* gene [15]. Further analyses revealed that *IDH1* mutation is very common in low grade gliomas and secondary GBM (**Figure 1.1**) [16]. Mutations were always found at position 132 in *IDH1* and position 140 or 172 in *IDH2* genes, which changes Arginine amino acid found in active site of both enzymes mostly into Histidine or sometimes into Cysteine, Serine, Glycine, Lysine, Methionine [16]. Mostly, G base is converted to A base at position 395 (G395A) by a point mutation, so wild type Arginine is replaced with Histidine (R132H) in IDH1 enzyme. This happens at the site where Arginine normally forms hydrogen bonds with its substrate, isocitrate [17]. However, due to this mutation, IDH1/2 enzymes gain a new function as described below.

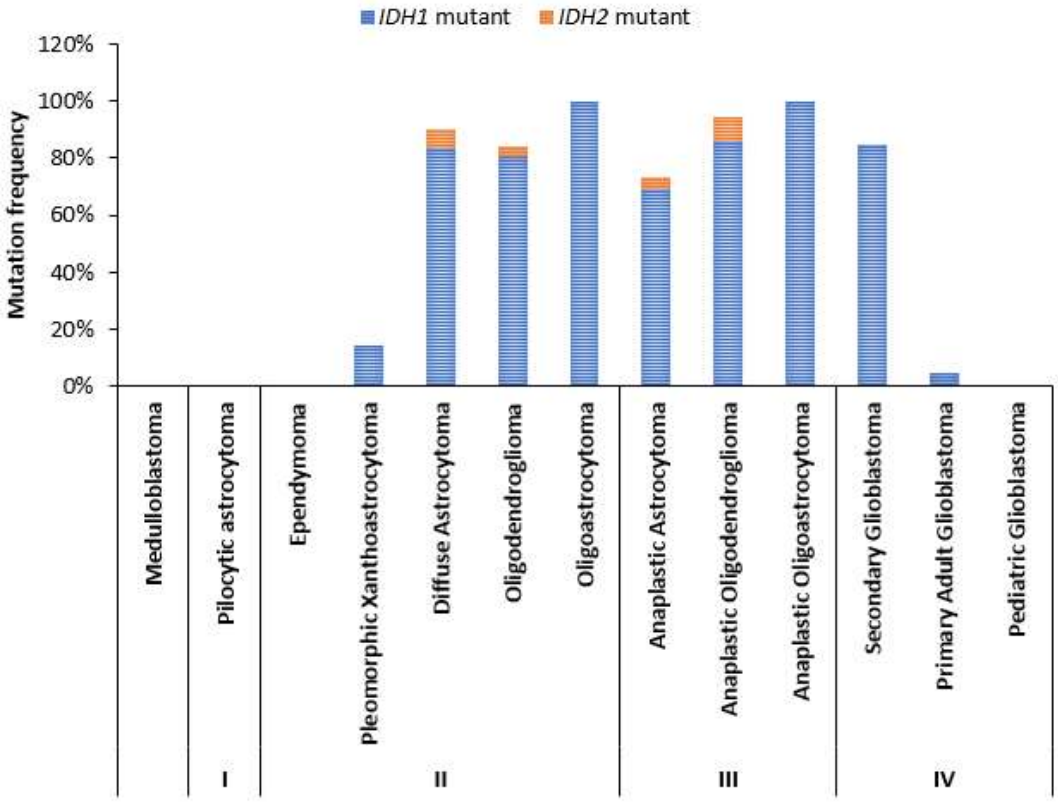

Figure 1.1 Frequency of *IDH1* and *IDH2* mutations in CNS tumors. Figure adapted from [16].

With the identification of these prevalent IDH mutations, World Health Organization (WHO) now includes IDH in its classification scheme. In 2016, WHO

classified glioma according to the *IDH* mutation status [18]. Astrocytoma either diffuse (grade II), anaplastic (grade III) or glioblastoma (grade IV) were classified as IDH-wild type, IDH-mutant or "not other specified" (NOS), which has low evidence for any of the two types or observation of markers for both. *IDH1* mutant tumors mostly have also mutations in *TP53* and *ATRX* genes, which are accepted as markers for astrocytic identity. On the other hand, oligodendroglioma either diffuse (grade II) or anaplastic (grade III) were classified as "IDH-mutant and 1p/19q-codeleted" or NOS. There is no IDH-wild type for oligodendroglioma. Most of the oligodendroglioma have also co-mutations with *IDH1* in *TERT*, *CIC* and *FUBP* genes [19]. In WHO 2016 reports, oligoastrocytoma term is mostly replaced with NOS, but in rare cases, where both molecular markers are found together, it is designated as well. Mostly, IDH-mutant glioma subtypes are associated with longer overall survival. However, there is still no approved treatment specific to IDH-mutant subtypes, which have known potentials to progress towards more aggressive higher-grade types, such as GBM. Therefore, understanding the vulnerabilities of IDH-mutant tumors and identifying novel therapeutics for these tumors are of utmost priority.

1.1.3 Functions of IDH1 enzyme and effect of mutation

Isocitrate dehydrogenase (IDH) is an enzyme produced by *IDH1, IDH2* and *IDH3* genes, and it converts isocitrate to alpha-ketoglutarate (2-oxoglutarate) (**Figure 1.2**). IDH1 is cytosolic isoform of IDH and it is NADP+ dependent. It produces cytosolic NADPH, which is important for lipid synthesis and protection against oxidative stress. It is also required for the activity of 2-OG dependent dioxygenases, such as histone lysine demethylases (KDMs) or DNA demethylases (TET enzymes) [20]. IDH2 and IDH3 are mitochondrial isoforms located in mitochondrial matrix. IDH3 is responsible for catalyzing isocitrate to 2-OG reaction, which is one of the rate-limiting steps in the Tricarboxylic Acid (TCA) cycle. It is NAD+ dependent and produces NADH, which is used to produce ATP in the electron transport chain. IDH2 has a role in energy metabolism by catalyzing reverse reaction, from 2-OG to isocitrate, when needed. Isocitrate can flow through TCA cycle to produce more NADH and energy especially in hypoxic conditions [20].

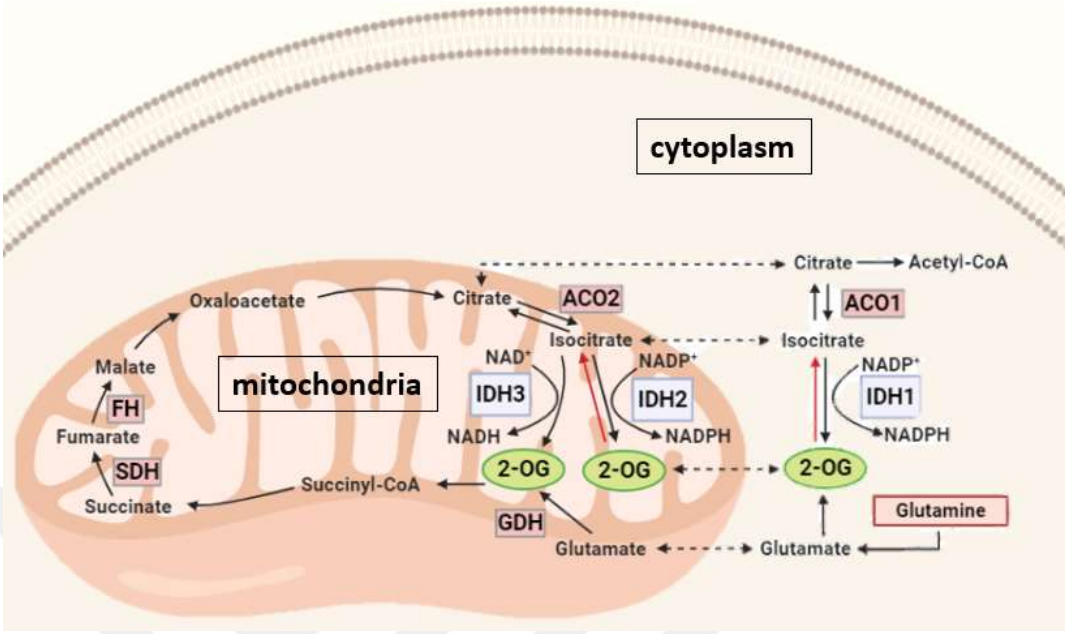

Figure 1.2 The mitochondrial and cytoplasmic roles of IDH family of enzymes. Figure adapted from [20].

Point mutation in *IDH1* or *IDH2* genes leads to a gain-of-function of enzyme. Mutant IDH converts 2-OG produced by wild type IDH enzyme, into 2-hydroxyglutarate (2-HG), which is thought as an oncometabolite [21]. 2-HG acts as an antagonist of 2-OG and inhibits the activities of many 2-OG dependent enzymes, such as TET enzymes or KDMs, which are DNA and histone demethylases, respectively (**Figure 1.3**). Therefore, IDH mutation generates a hypermethylation both in DNA and histones [22,23]. There are also some studies showing that 2-HG inhibits Prolyl Hydroxylase Domain (PHD) enzymes, which are also 2-OG dependent [24,25]. PHD enzymes hydroxylate and lead to degradation of HIF-1α, which is the major transcription factor responsible for cellular survival and proliferation under hypoxic conditions. On the other hand, other groups showed that 2-HG induces PHD activity more than 2-OG itself [26,27]. Therefore, whether 2-HG leads to degradation or stability of HIF-1α, and therefore its role in cellular transformation, is controversial.

Based on clonal evolution analyses in tumor samples, many studies suggested that IDH mutation is the earliest event in tumorigenesis, so it is accepted as a driver mutation in low grade glioma [27–29]. Therefore, inhibition of mutant IDH enzyme with specific inhibitors is considered as a promising strategy to induce differentiation and delay the tumor growth by preventing tumorigenic effects of mutant IDH [30–32]. On the

other hand, it is known that IDH mutant cells grow slower than wild type counterparts. Altered metabolic profile, because of the impaired TCA cycle metabolism [33], inhibition of mTOR and ATP synthase [34], downregulation of LDHA enzyme [35], were thought as the potential reasons for the slow growth observed in IDH mutant glioma. Considering these metabolic deficiencies, exploiting the vulnerabilities of IDH mutant cells by inhibiting crucial pathways for these cells is also offered as an intriguing strategy [36–39].

Similarly, based on uniformity and tumor cell specificity of the *IDH1* mutation, it was shown to be a potential target for immunotherapeutic approach [40]. It was indicated that mutant IDH1-R132H sequence is presented on MHC class II and promotes immunological response in patients with mutant IDH. Considering that it is a suitable epitope for specific targeting, vaccines targeting this epitope were developed and shown to be effective in an intracranial murine glioma model [41]. Moreover, another study demonstrated the immune evasion mechanism in *IDH* mutant glioma by suppression of immune system-recruiting genes and showed that combination of vaccination therapy with specific mutant IDH inhibitors is highly effective in *IDH* mutant glioma models in mice [42].

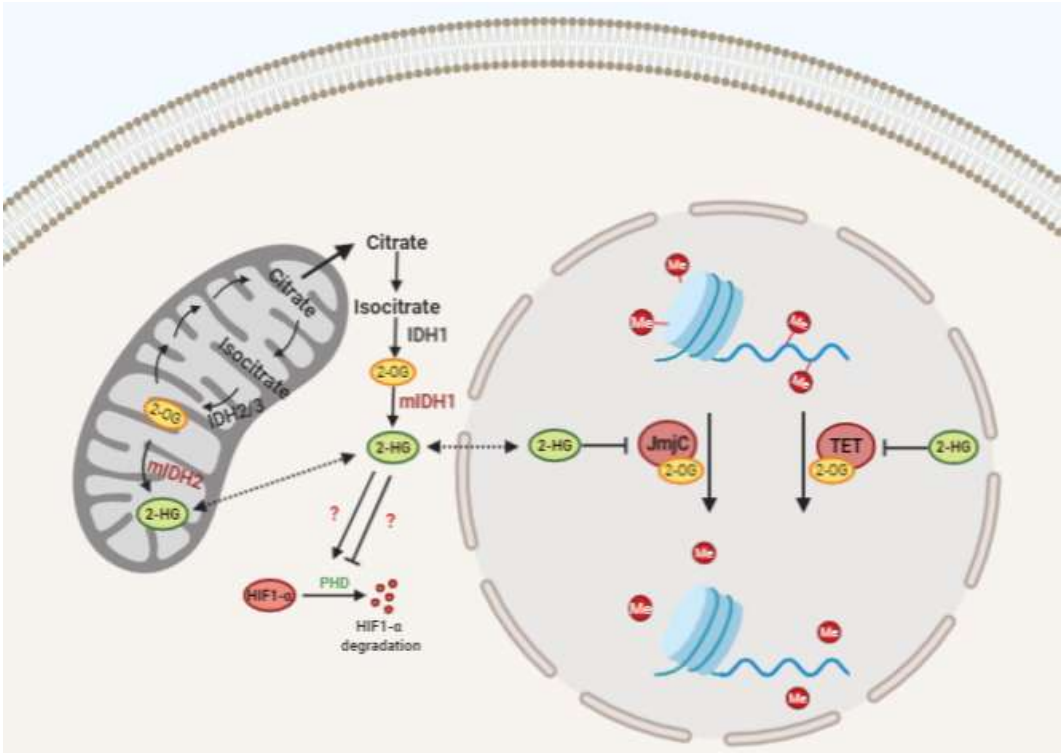

Figure 1.3 Suggested roles of wild type and mutant IDH enzymes in tumorigenesis. Figure adapted from [21].

1.2 Epigenetics

Epigenetics is the field that studies modifications in the chromatin structure without involving changes in DNA sequence. These modifications affect gene expression profiles, may be heritable or may change dynamically. To understand the importance of epigenetics, one may think that all cells in our body have the same genetic code as DNA sequence, however there are many different types of cells and tissues with specialized functions or structures. The main reason of this variety is distinct transcription profile of cells arising from differences in their epigenetic profiles. Epigenetic regulations mainly include DNA methylation, histone modification, chromatin remodeling, and non-coding RNA-associated regulations. Dysregulations in epigenetic modifications may result in abnormal activation or inactivation of genes, which leads to genetic disorders such as cancers, degenerative or metabolic disorders.

1.2.1 DNA methylation

In eukaryotic DNAs, methylation occurs on the 5th carbon of cytosine (5-methylcytosine, or 5-mC) nucleotide followed by a guanine nucleotide, also known as CpG site, where p denotes the phosphate group between bases. Throughout genome, CpG dinucleotides are mainly clustered in the promoter regions of genes and they are known as CpG islands. More than 60% of genes in the human genome include CpG islands in their promoter regions. Methylation of these CpG islands is mostly associated with close chromatin state and gene silencing [43]. On the other hand, CpG regions found throughout the gene body are usually methylated to prevent internal transcription initiation, especially from alternative promoter sites. DNA methylation is also critical for regulation of DNA imprinting, stabilization of repeated genomic sequences such as LINEs and SINEs, silencing of retrotransposons, and inactivation of one of the X-chromosomes in females [44].

DNA methyltransferases (DNMTs) are the enzymes that perform methyl group transfer from S-adenosyl-methionine (SAM) onto the cytosine residues of CpG regions in DNA. DNMT1 is responsible for maintaining existing global methylation pattern in newly synthesized strains during DNA replication, while DNMT3A and 3B can catalyze *de novo* methylation events [45]. Until recently, DNA methylations were considered as stable and to be lost only during DNA replication when DNMTs are inhibited. However,

in 2009 and 2010, by two independent studies, it was shown that Ten-eleven translocation (TET) enzymes, are responsible for the hydroxylation of 5-methylcytosine (5-mC) to 5-hydroxymethylcytosine (5-hmC) [46]. Subsequent studies showed that 5-hmC is the precursor for the removal of these methyl groups from DNA, which proved that TET enzymes are responsible for the active DNA demethylation [47]. TET enzymes, PHD containing enzymes and JmjC domain containing histone demethylases (JHDM), belong to dioxygenase superfamily, which work as 2-oxyglutarate (2-OG) and Fe(II)-dependent in the presence of O_2 [48]. Demethylation of CpGs found in promoter regions mostly correlate with transcriptional activation of the related gene. There are also "reader" proteins containing methyl-CpG binding domains (MBD) that can bind methylated CpG on DNA, and function as transcriptional repressors for the related genes [49] (**Figure 1.4**), as described below.

1.2.2 Post-translational modifications (PTMs) of histones

Histones are positively charged proteins responsible for packaging DNA into condensed, three dimensional structures known as nucleosomes, which are the subunits of the chromatin. In each nucleosome, approximately 146 base pairs (bp) of DNA segment turns almost two times around a histone octamer, which consists of two copies of H2A, H2B, H3 and H4, also known as core histones [50]. Histone H1 is accepted as linker histone which is thought to stabilize chromatin structure by binding to nucleosome core and linker DNA [50]. Other than their structural functions, histones were shown to have important regulatory roles in transcription of genetic information which is known as histone code hypothesis [51]. N-terminal tails of these histones protrude from the nucleosome and are exposed to post-translational, covalent modifications such as acetylation, methylation, phosphorylation, ubiquitinylation, or sumoylation [52]. These modifications are added upon histones or DNA by enzymes known as "writers", recognized by "readers", which affect chromatin structure directly or by recruiting other proteins, and removed by "erasers" (**Figure 1.4**) [53].

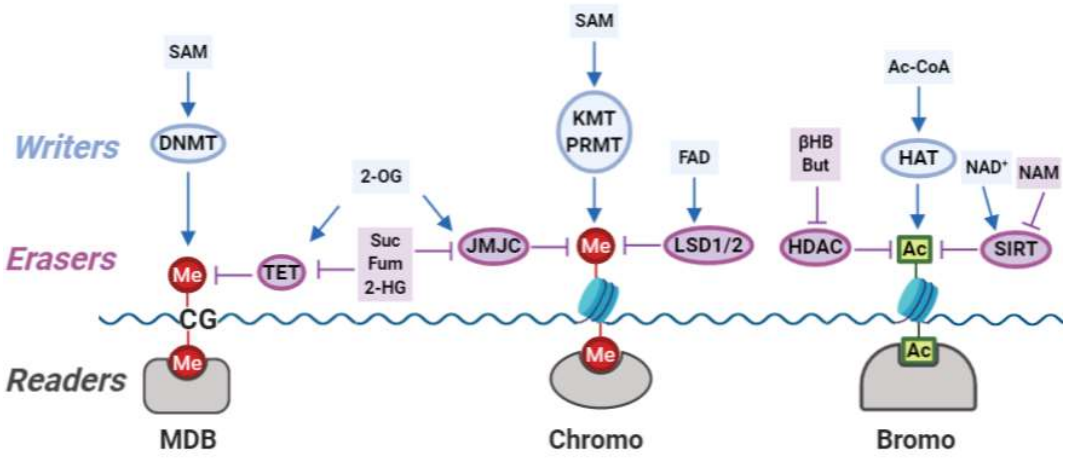

Figure 1.4 Epigenetic modifications on DNA and histone. Figure adapted from [53].

1.2.2.1 Histone acetylation

Acetylation is mostly associated with histone deposition on chromatin and is shown to have important roles in DNA repair. It is mediated by histone acetyltransferases (HATs), which add acetyl groups on the lysine residues of histones and cause loss of positive charges on histones. Neutralized histones bind weaker to the negatively charged DNA leading to open chromatin state and easier binding of transcription factors to DNA. Therefore, histone acetylation is accepted as a gene activation mark. There are different families of HATs based on their sequence similarities, such as GNAT (Gcn5-related N-Acetyltransferases) family, MYST (MOZ, Ybf2/Sas3, Sas2 and Tip60) family and p300/CBP (p300 and the CREB-binding protein) family [54].

Conversely, removal of acetyl groups from lysine residues on histones, which is known as deacetylation and performed by histone deacetylases (HDACs), causes reloading of histones with positive charge. Therefore, histone deacetylation is associated with close chromatin state and accepted as a gene repression mark. HDACs are categorized in 4 classes based on their sequence homologies [55]. HDAC1, HDAC2 and HDAC3, which are found primarily in the nucleus and HDAC8, which is found both in nucleus and cytoplasm, belong to class I. Class II has two subgroups as IIA and IIB. HDAC4, HDAC5, HDAC7 and HDAC9, which are found both in nucleus and cytoplasm belong to Class IIA, while HDAC6 and HDAC10, which are found primarily in cytoplasm, belong to Class IIB. Class III includes sirtuins, which have different structural and mechanistical properties from other HDACs. There are seven known sirtuins in mammals, of which SIRT1 and SIRT2 are found both in nucleus and cytoplasm, SIRT3,

SIRT4 and SIRT5 in mitochondria, and SIRT6 and SIRT7 in nucleus primarily. Class IV have only one member, HDAC 11, which is not homologous to any other HDACs, is found both in nucleus and cytoplasm.

Another protein family is called bromodomain and extra-terminal motif (BET) proteins, which can bind to acetylated lysine residues on histones via their bromodomains (BRD) (**Figure 1.5**) [56]. These proteins can regulate gene expressions by recruiting transcription factors and transcription machinery mostly to distant genomic regions from promoter of related genes.

1.2.2.2 Histone methylation

One of the major modifications on histones is methylation, which is mostly associated with dynamic transcriptional activation and inactivation and is very important during embryonic development. It is mediated by histone methyltransferases (HMTs), which transfer methyl groups from S-adenosyl-methionine (SAM) to the lysine or arginine residues on the histone tails [57]. The enzymes those specifically methylate arginine residues are called protein arginine methyltransferases (PRMTs), while those methylate lysine residues are called lysine methyltransferases (KMTs). Lysine can have mono- (me1), di- (me2), or trimethylation (me3) since it has an NH_3+ group, of which each hydrogen can be replaced by a methyl group. Arginine, on the other hand, has an NH_2+ and a free NH_2 group [58]. If one of the hydrogens in NH_2 group is replaced with methyl group, it is called monomethyl arginine (MMA), while both hydrogens in NH_2 group or one hydrogen from each amino group are replaced with two methyl groups, they are called asymmetric dimethyl arginine (aDMA) or symmetric dimethyl arginine (sDMA), respectively [59]. aDMA is formed by type I PRMTs including PRMT1, PRMT2, PRMT3, PRMT4, PRMT6 and PRMT8, while sDMA is formed by type II PRMTs including PRMT5 and PRMT9. Both type I and type II PRMTs catalyze the formation of MMA as an intermediate for aDMA and sDMA, respectively. On the other hand, PRMT7 which is the only member of type III, is responsible for MMA formation alone.

Unlike acetylation, methylation does not change charges on histones. Therefore, their effects on transcription are determined by effector proteins called ‘readers’ that recognize methylated regions. Specific binding of readers depends on the methylated amino acid, methylation degree (mono-, di-, or tri-) and its position. For instance, arginine methylation of both histones H3 and H4 is mostly accepted as active

transcription mark except for H3R2, and symmetric methylation of H3R8 or H4R3 (**Table 1.1**). On the other hand, di- and trimethylation of H3 at lysine 9 (H3K9) or lysine 27 (H3K27) is associated with close chromatin state and transcriptional silencing, while H3 methylation at lysine 4 (H3K4) is generally associated with transcriptional activation (**Table 1.1**). Mostly, there are many enzymes responsible for the same type of histone methylations. For instance, ASH1L, ASH2L, MLL, SET1A/B and more are able to catalyze H3K4 methylations. Similarly, G9a, GLP, Suv39h1, Suv39h2, and more can catalyze H3K9 methylations. On the other hand, some types of histone methylations are known to be catalyzed by single specific enzymes, such as H3K27 methylations by EZH2, and H3K79 methylations by DOT1L (**Table 1.1**).

Considering the nearly same half-life of histone methylations and histones, it was thought, for a long time, that histone methylations are stable and irreversible [60]. However, following the discovery of LSD1 (KDM1A) as the first histone demethylase (HDM) in 2004 [61], many other HDMs were discovered. As methylation occurs either in arginine or lysine residues of histone tails, there are specific enzymes for the demethylation of each residue. Lysine demethylases (KDMs) are divided into two families; flavin-dependent KDM1s which include KDM1A (LSD1) and KDM1B, and 2-OG and Fe(II)-dependent JmjC domain containing enzymes which include KDM2, KDM3, KDM4, KDM5, KDM6, KDM7 and KDM8 subfamilies [61,62]. Some KDMs such as KDM5 subfamily which demethylates H3K4me2/3, and KDM6 subfamily which demethylates H3K27me2/3, have single specific targets. On the other hand, some of them such as KDM4 subfamily, which demethylates H3K9me2/3 and H3K36me2/3, have more than one target. Similarly, different KDMs may have the same targets. For instance, both KDM3 and KDM7 subfamilies can catalyze H3K9me1/2 demethylations.

Unlike many identified lysine demethylases (KDMs), only few arginine demethylases (RDMs) are known to be responsible for arginine demethylation [63]. PAD2 and PAD4 which are members of peptidyl-arginine deiminase (PAD or PADI) family, are shown to be the first identified arginine demethylases [64,65]. However, both PAD2 and PAD4 remove N^{ω}-methylation on arginine and convert it to citrulline which is neutral in charge and has probably different properties than unmethylated arginine. Therefore, it is claimed that they are not 'true' demethylases [66]. Further studies identified JMJD6, which is a member of JmjC domain containing enzymes family, as an arginine demethylase [67].

A recent study showed that a subset of JmjC containing lysine demethylases can catalyze arginine demethylations as well [66].

There are also reader proteins that recognize and bind methylated histones. Chromodomain (CHD)-containing proteins are the main readers for the methylated lysine residues [68], and Tudor domain-containing proteins are the main readers for the methylated arginine residues on histones [69] (**Figure 1.5**).

Table 1.1 List of known histone methyltransferases and demethylases and their effects on transcription.

Histone	Position	Modification	Responsible enzyme(s)	Known effect on transcription	Reference(s)
H3	R2	Methylation	PRMT5, PRMT6, PRMT7	Repression	70
	K4	Methylation	ASH1L, MLL1-5, SETD1A-B, SETD7, SETMAR	Activation	71
		Demethylation	KDM2B, KDM5A-D, LSD1, LSD2	Repression	61
	R8	Methylation	PRMT5, PRMT2/6	Repression/activation by symmetric/asymmetric methylations	72,73
	K9	Methylation	G9a, GLP, SETDB1-2, SUV39H1-2, PRDM2-3, PRDM16	Repression	74
		Demethylation	JMJD1C, KDM3A-B, KDM4A-E, KDM7A-C, LSD1	Activation	75
	R17	Methylation	CARM1	Activation	75
	R26	Methylation	CARM1	Activation	76
	K27	Methylation	EZH1-2	Repression	77
		Demethylation	KDM6A-C, KDM7A	Activation	78
	K36	Methylation	ASH1L, MMSET, NSD1, SETD2-3, SETMAR, SMYD2, WHSC1L1	Activation	79
		Demethylation	KDM2A-B, KDM4A-C	Repression	80
	K79	Methylation	DOT1L	Activation	81
		Demethylation	KDM2B	Repression	82
H4	R3	Methylation	PRMT1, PRMT3, PRMT5-7	Repression/activation by symmetric/asymmetric methylations	83
	K5	Methylation	SMYD3	Activation	84
	K20	Methylation	SETD8, SUV420H1-2	Repression	85
		Demethylation	KDM7B	Activation	86

1.2.2.3 Histone phosphorylation

Phosphorylation is another type of PTMs of histones, and and it mostly associates with condensation of chromatin during cell division, DNA damage and induction of primary response genes (also known as immediate-early genes) upon a stimulus [87,88]. It takes place on serine, threonine and tyrosine residues of histone tails and is mediated by protein kinases. One of the best-known mechanisms for this modification is phosphorylation of the serine 139 residue on H2AX which is known as γH2AX [89]. H2AX is a variant form of H2A histone; and it is phosphorylated by PI3- family kinases such as ATM, ATR and DNA-PKcs when a double-strand break occurs in DNA. Upon DNA repair, γH2AX is dephosphorylated by phosphatases such as PP2A, PP4, PP6 and Wip1. On the other hand, phosphorylations of the serine 32 on H2B, and serine 10 and serine 28 residues of H3 are thought to be induced by epidermal growth factor (EGF) stimulus and involved in activation of EGF-response genes [90]. Another important mechanism regulated by histone phosphorylation is chromosome compaction during mitosis and meiosis. Phosphorylation of threonine 3, serine 10, threonine 11 and serine 28 residues of histone 3 are shown to be involved in chromatin condensation, and generally used as markers for these events in mitosis and meiosis [91,92].

1.2.2.4 Ubiquitination and SUMOylation

Ubiquitin and SUMO (small ubiquitin-like modifier) are less studied post-translational modifiers that are conjugated on lysine residues of histones. 3 different enzyme families are involved in the ubiquitination process. Firstly, ubiquitin is activated by E1 enzymes, and directed to E2s. Then, it is carried by E2 enzymes towards the substrate. E2s interact and complex with specific E3 ligases, and ubiquitin is bound to substrate by E3 enzymes [93]. Conversely, enzymes belong to a large protease family (DUBs) that are responsible for deubiquitination process. Lysine 119 residue of H2A and Lysine 120 residue of H2B histones are the known substrates for ubiquitination [94,95]. H2A-K119 ubiquitination is mediated by Ring2 enzyme in the hPRC1L complex and mainly associated with transcriptional repression, while H2B-K120 ubiquitination is mediated by UbcH6, RNF20/40 and hPAF complex, and associated with transcriptional activation [94,95]. SUMOs, which are ubiquitin-like proteins, are also conjugated to H2A, H2B or H4 histones, and associated with transcriptional repression. UBC9 is shown to

be the E2 enzyme, which is responsible for the known SUMOylation reactions with help of SUMO activating E1 enzymes and E3 ligases [96].

1.2.3 Chromatin remodeling complexes

Another group of proteins that regulate chromatin state, thus transcription, is called chromatin or nuclear remodeling complexes. These complexes have similar ATPase domains which provides energy from ATP hydrolysis for changing chromatin structure, either by moving nucleosomes, removing histones from nucleosomes, or replacing them with histone variants [97,98]. There are at least 4 protein families known for chromatin remodeling functions in humans; SWI/SNF family, ISWI family, NURD/Mi-2/CHD family and INO80 family. Even if all complex families share a high homology in terms of their ATPase domains, each have specific domains in their active regions. Therefore, each remodeling complex is associated with different cellular pathways such as development, differentiation, DNA repair, DNA replication, transcriptional regulation, etc.

1.2.4 Non-coding RNAs

Non-coding RNAs are another group that have important epigenetic effects on gene expression. These RNAs are the products of DNA transcription, but they do not encode proteins. They contain short non-coding RNAs (short ncRNAs) which are mostly around 20-25 bp length, and long non-coding RNAs (lncRNAs) which are longer than 200 bp length [99]. Short ncRNAs include micro RNAs (miRNAs) which can lead to degradation of target mRNAs by binding their 3' UTR, short interfering RNAs (siRNA) which can similarly leads to mRNA degradation or chromatin condensation together with a repression complex, and piwi-interacting RNAs (piRNA) which binds transposon transcripts and leads to their degradation by recruiting PIWI proteins [100]. Long ncRNAs which constitute most of the non-coding RNAs, are also associated with gene repression either in transcriptional or post-transcriptional level. It was shown that lncRNAs are able to prevent binding of transcription machinery, and recruit methyltransferases, nuclear remodeling complexes, or other regulatory proteins upon binding [101–103]. One important example is Xist lncRNA that bind to one of the whole X chromosomes in female and inactivate it by preventing binding of transcription complexes on it [104,105].

1.3 Epigenetics in glioma

As in most of the cancer types, aberrant epigenetic changes are very common in glioma. DNA methylation patterns vary between different grades and subtypes. In aggressive subtypes of glioma, there is mostly a global hypomethylation which leads to oncogene activations accompanied by specific hypermethylated regions mostly promoter of tumor suppressor genes (TSGs). Also, hypomethylation of long repetitive regions cause genomic instability which promote tumorigenesis [106]. On the other hand, since 2-HG, product of mutant IDH enzyme, interferes with DNA and histone demethylases, *IDH1/2*-mutant subtypes have a hypermethylation phenotype called glioma CpG island methylator phenotype (G-CIMP), which is accepted as a marker of prolonged survival [22]. Another well-known and one of the first identified clinical epigenetic marker is promoter methylation of *MGMT* gene. It encodes a DNA repair enzyme which can repair defects generated by DNA-damaging chemotherapy drugs such as temozolomide. If its promoter is methylated, so gene is silenced, DNA repair mechanism is disrupted, therefore, tumor cells give better response to temozolomide treatment [107]. In addition, it was shown that, in many glioma samples, there are mutations in some of the histone modifier genes such as HDAC2, HDAC9, JMJD1A, JMJD1B, MLL3, MLL4, etc. [15]. There are also many studies indicating significant changes in the expression level of histone modifiers, such as HDAC1 and HDAC2 upregulation in astrocytic glioma [108], or KDM6A and KDM6B upregulation in persister glioma stem cells (GSCs) [109]. Recently, mutations in *H3F3A* and *HIST1H3B* genes encoding H3.3 and H3.1, respectively, which are variants of histone 3 protein, were also identified in diffuse midline glioma [110,111]. These mutations cause a reduced methylation level in H3K27 residues which alter transcriptome dramatically and induce tumorigenesis. Mutations in *IDH1/2* and H3 variants, which lead to dramatic changes in epigenetic profile, are also evaluated as important diagnostic and prognostic markers by World Health Organization (WHO) and used in most recent WHO 2016 glioma classification [18]. Moreover, in a recent study, a direct DNA methylation-based classification was offered for the CNS tumors and shown that almost 12% of diagnosis based on conventional observations were corrected with this new method [112].

Based on these various epigenetic aberrations and considering that they can be reversed unlike genetic alterations, many inhibitors targeting epigenetic enzymes were

tested in *in vitro* and *in vivo* glioma studies in recent years, and even some of them have already entered clinical trials. These inhibitors targeting epigenetic pathways in glioma, mainly include DNMT inhibitors, HDAC inhibitors, KDM inhibitors, HMT inhibitors, BET inhibitors and mutant IDH inhibitors.

1.3.1 DNMT inhibitors

5-azacytidine and 5-aza-2'-deoxycytidine (decitabine) are the first DNMT inhibitors (DNMTi) which are synthesized more than 50 years ago [113]. They are cytidine analogs which can be incorporated into the new strands of DNA similiarly and inhibit DNMTs by binding them covalently. 5-azacytidine and decitabine were approved by the US Food and Drug Administration (FDA) in 2004 and 2006, respectively, for the treatment of myelodysplastic syndrome (MDS) [114,115]. Even though they were not approved by FDA for the acute myeloid leukemia (AML), they are mostly used off-label for these tumors as well. Considering their relatively short half-lives, a more stable drug, namely guadecitabine, was developed and entered phase III in a clinical trial for treatment of AML (Clinical trial identifier: NCT02920008).

Considering hypermethylated phenotype in IDH-mutant glioma, DNMTi were thought to be effective against these tumors by reversing this phenotype back. Both 5-azacytidine and decitabine were shown to induce tumor differentiation and growth inhibition by decreasing global methylation in xenografts derived from IDH1 mutant glioma patients [116,117]. There are ongoing clinical trials using DNMTi individually (Clinical trial identifier: NCT03666559) or in combination with either mutant IDH inhibitors (Clinical trial identifier: NCT02677922) or stabilizing agents (Clinical trial identifier: NCT03922555) for the treatment of glioma or other IDH-mutant tumors such as AML. There are also studies showing that decitabine induces the expression of tumor antigens in normally non-immunogenic GBM cells and sensitize them to T-cell mediated immunotherapies [118,119].

1.3.2 HDAC inhibitors

HDAC inhibitors (HDACi) are a large group of compounds which are discovered or developed to being used for treatment of many diseases, mainly cancer. Considering that all class I, II and IV HDACs have a similar catalytic site which should bind to zinc ion (Zn^{+2}) to work, small molecules that occupy this core can be used to inhibit their

catalytic activities [120]. Class III HDACs known as sirtuins, on the other hand, should bind to nicotinamide adenine dinucleotide (NAD) for their deacetylation activities. Based on their binding groups, HDACi are divided to 5 categories: hydroxamates, aliphatic acids, benzamides, cyclic tetrapeptides and sirtuin inhibitors [121]. Some HDACi such as TCA, belinostat, vorinostat or panobinostat can inhibit all class of HDACs which is known as pan-HDAC inhibitors, while others such as valproic acid, entinostat or rocilinostat act as selective against some classes [122]. In recent years, highly specific HDACi have been developed against one type of HDAC. For instance, CAY10603 is shown to be highly potent and selective inhibitor of HDAC6 [123]. It was also shown that most HDAC inhibitors may induce acetylation of non-histone proteins since the most HDACs, especially found in cytoplasm, may have non-histone targets as well [124].

Up to now, FDA has approved four HDAC inhibitors for different types of hematological tumors: vorinostat and romidepsin for cutaneous T-cell lymphoma (CTCL), belinostat for peripheral T-cell lymphoma (PTCL), and panobinostat for multiple myeloma (MM) [125–128]. In addition, valproic acid has been approved by FDA for seizures, bipolar disorder, epilepsy, and migraine, but not for any cancer type yet. For the solid tumors, including glioma, there is no approved HDACi yet, but there are many ongoing clinical trials testing different HDAC inhibitors either individually or in combination with other drugs. Even though many HDAC inhibitors have been shown to be effective in pre-clinical models of glioma, results from first clinical trials were not as expected. As the first HDACi to be clinically tested, vorinostat was shown to be well-tolerated and has modest effects as single agent [129]. However, following studies combining vorinostat with bortezomib, or standard chemoradiotherapies did not improve the patient survival further [130–132]. Similarly, romidepsin alone or panobinostat with bortezomib in phase II of clinical trials were shown to be ineffective and did not meet the criteria to pass to the phase III [133,134]. On the other hand, panobinostat in a phase I trial, and valproic acid in a phase II trial were shown to be effective as sensitizing agents when added to radiotherapy and chemoradiotherapy, respectively, and warranted for the next phases [135,136]. Belinostat is also thought as a promising drug for glioma treatment and now being tested in ongoing phase II clinical trial, as an adjuvant therapy to temozolomide and radiation (Clinical trial identifier: NCT02137759) [137].

1.3.3 KDM inhibitors

Since the first KDM, lysine specific demethylase 1 (LSD1/KDM1A) was discovered, KDMs were shown to have significant roles in many types of cancer [138,139]. Therefore, they have been thought as potential anti-tumor drugs and many KDM inhibitors were developed. First inhibitors were developed against KDM1, and most of them were targeting monoamine oxidase (MAO) activities by binding to flavin adenine dinucleotide (FAD) which is the cofactor of KDM1s [139,140]. These were mainly tranylcypromine or phenelzine derivatives which bind to FAD irreversibly/covalently. Then, inhibitors that bind reversibly have been developed since they were thought to have less side effects. ORY-1001 which is developed as tranylcypromine derivative was the first KDM inhibitor announced to be tested for treatment of acute myeloid leukemia (AML), extended-stage disease small cell lung cancer (ED SCLC), and refractory acute leukemia (AL) in clinical trials (EudraCT Numbers: 2013-002447-29, 2018-000469-35, 2018-000482-36) [141]. The results of this trial were not published yet. One of the reversibly binding KDM1 inhibitors, GSK2879552, has also entered clinical trials for treatment of small cell lung carcinoma (SLCL) and AML (Identifiers for clinical trials: NCT02034123, NCT02177812). However, both trials were terminated recently as the risk benefit did not favor continuation of the trials.

The second category of KDM inhibitors were small molecules that inhibit JmjC-KDMs. Most of these inhibitors are competitors of 2-oxoglutarate (2-OG) which is the co-substrate required by JmjC enzymes to work [142]. Recently, some allosteric inhibitors have also been discovered and shown to be effective for inhibition of JmjC-KDMs. IOX-1, 2,4-pyridinedicarboxylic acid (2,4-PDCA) and N-oxalylglycine (NOG) are some of the first JmjC-KDM inhibitors discovered and has broad-spectrum targets [143]. IOX-1 which acts 2-OG competitor and JIB-04 which is discovered later and shown to chelate iron in the catalytic site, were accepted as potent inhibitor of all JmjC-KDMs, known as pan-JmjC inhibitors [144]. Even though JmjC-KDMs have high homology at their catalytic sites, specific inhibitors for some types of them were developed recently. GSK-J1 was one of the first of these, which was shown to inhibit selectively KDM6 subfamily, although it was later shown to also have some potency against KDM5 enzymes [145,146]. Since its cell permeability was very poor, a pro-drug strategy which masks its polarity was used and GSK-J4 was developed. It has an ethyl ester group which is hydrolyzed

upon cell penetration and converts to the functional drug. More recently, selective inhibitors for KDM5 such as KDM5-C70 and KDOAM-25 were also developed and shown to be effective in pre-clinical studies [147–149].

Considering significant roles of KDMs in glioma, many KDM inhibitors were tested in pre-clinical studies. GSK-J4 was shown to be effective against pediatric brainstem glioma having H3K27M mutations in histone H3.3 variant gene [150]. Since this mutation prevents the methylation of 27th residue of H3.3 which is replaced with canonical H3 in some chromatin regions, inhibition of H3K27M demethylases, KDM6 subfamilies, via GSK-J4, reverted this hypomethylation and slowed down the tumor growth. This study was also important since it was the first to show that GSK-J4 can pass through blood brain barrier (BBB). After this study, GSK-J4 was tested on glioma cells in several other pre-clinical studies. In one study, it was shown that KDM6A and KDM6B were upregulated in therapy-resistant glioma stem cells, and these persister cells became dependent on these enzymes, so they are more sensitive to GSK-J4 treatment [109,151]. GSK-J4 was also suggested as a sensitizing agent to radiation therapy in diffuse intrinsic pontine glioma (DIPG, or diffuse midline glioma, according to WHO 2016 classification). Another study indicated that both JIB-04 which is a pan-JmjC inhibitor, and CPI-455 which is a specific KDM5 inhibitor strongly reduced viability of temozolomide (TMZ)-resistant GBM cells [152]. They also proved BBB permeability of JIB-04 by both mass spectrometric analysis and functional tumor growth analysis. The same group also showed that two KDM inhibitors, GSK-J4 and JIB-04 interestingly synergized and could be used for TMZ-resistant GBM [153].

1.3.4 Mutant IDH inhibitors

Since *IDH* mutations have been identified as driver mutations in various cancer types, a specific inhibitor of mutant IDH enzyme is offered as a potential treatment. First small molecules that inhibit mutant IDH1 or IDH2 enzymes were shown to be effective against glioma and luekemia cells, respectively [30,154]. They induced differentiation of tumor cells by inhibiting 2-HG accumulation in cells, and slowed down the cell growth. After these initial studies, many specific mutant IDH1 or IDH2 inhibitor, or pan-mutant IDH inhibitors were developed [32,155]. Some of these inhibitors were also shown to be effective in clinical trials for acute myeloid leukemia (AML) [156,157]. However, some studies had opposite results indicating that even if they prevent 2-HG accumulation,

mutant IDH inhibitors did not cause significant change in DNA or histone methylations, and have no significant effect on cell growth, especially on glioma cells [157,158]. Moreover, there are many studies showing vulnerabilities caused by mutant IDH, and potential therapeutic approaches targeting these vulnerabilities [36–39]. However, mutant IDH inhibitors may reverse these phenotypes and interfere with drugs targeting these weaknesses.

Controversial results may be related with the cellular dependence on IDH mutation. It is known that *IDH* mutations are critical for tumorigenesis in both glioma and AML [27–29]. However, it was shown that *IDH1* mutation is converted from driver to passenger mutation in glioma [159]. Therefore, proliferation of glioma cells were independent of mutant IDH. On the other hand, *IDH2* mutation is required for growth of leukemia cells and maintenance of the tumor [160] which may be the reason for mutant IDH inhibitor efficiency in AML. Still, for both *IDH* mutant glioma and other tumor types, there are ongoing clinical trials with mutant IDH inhibitors individually or in combination with other treatment options such as DNMT inhibitors (Identifiers for clinical trials: NCT02073994, NCT02481154, NCT03343197, NCT03030066, NCT02381886, NCT03684811, NCT02746081).

1.4 Cellular stress response

Many intrinsic or extrinsic signals may cause cellular stress that induce various molecular changes in the cell which is known as stress response pathways. Changes in extracellular conditions such as temperature, pH, nutrients, oxygen level, etc. or infection are examples for extrinsic stressors. On the other hand, unfolded or misfolded proteins, reactive oxygen species (ROS) accumulation, DNA damage, or disrupted cellular homeostasis are some of the intrinsic stressors. Cells have different sensor proteins that sense these stress conditions and activate appropriate response pathways. Stress responses may be in various ways, either to protect cells against stress or to activate senescence or cell death, according to stress level, duration, and other cell-specific factors [161].

1.4.1 Heat shock response

One of the first mechanisms discovered to be induced in stress conditions is the changes observed in *Drosophila* cells upon heat exposure which is named as heat shock

response [162–164]. After the initial studies, it was observed that many other signals such as heavy metals, oxidative or osmotic stress, or toxic chemicals have the ability to induce heat shock response as well [165–167]. Mainly, these conditions interfere with the protein folding which can be recognized by sensor proteins which is called heat shock proteins (HSPs). Richter et al. (2010) classified these stress inducible HSPs into seven universal categories [168]. The first category comprises the best-known HSPs assisting the correct folding of proteins which are now called as molecular chaperones. The second category contains proteases which are required for degrading misfolded proteins. Proteins involved in the repair mechanism of the stress-induced DNA or RNA modifications consist the third category. Metabolic enzymes which are responsible for maintaining cellular homeostasis are included in the fourth category. In the fifth category, there are transcription factors and cascade proteins to induce response pathways. Structural proteins important for cytoskeleton and organelle integrity are grouped as the sixth category. The last category includes proteins involved in the export mechanism for the removal of the stress source such as toxic chemicals.

Molecular chaperones are evolutionary highly conserved among species and can be classified with respect to their molecular weights as HSP100, HSP90, HSP70, HSP60 and small HSP (sHSP) families which are approximately 100 kDa, 90 kDa, 70 kDa, 60 kDa and less, respectively [169,170]. In the absence of stress, HSF1 which is the major transcription factor responsible for induction of heat shock response genes, is kept as inactive by the binding of HSPs such as HSP90 and HSP70 [171,172]. When cell is exposed to stress, accumulated misfolded proteins compete with HSF1 to bind HSPs, and released HSF1 transferred to the nucleus and activate stress response genes. These genes include other HSPs which correct misfolded proteins and inhibit many apoptotic pathways. Therefore, HSPs are thought as protection proteins and required for survival of cells under stress conditions [173].

1.4.2 Unfolded protein response

The endoplasmic reticulum (ER) is the principal site where correct folding and post-translational modifications of the proteins that will be secreted or directed to the membrane or other organelles [174,175]. There are lots of quality control mechanisms in the ER which regulate folding of newly synthesized proteins and degrade the misfolded ones via ER-associated degradation (ERAD) mechanism. Binding immunoglobulin protein

(BiP) which is also known as GRP78 and encoded from HSPA5 gene, belongs to HSP70 family, and accepted as major ER chaperone [176]. In normal conditions, it is located in the ER lumen as bound to transmembrane ER kinases: inositol-requiring enzyme 1 (IRE1), PKR-like ER kinase (PERK) and activating transcription factor 6 (ATF6) [177]. In a cell that is exposed to various stress conditions, misfolded or unfolded proteins accumulate in the ER lumen and compete for binding to BiP chaperone. Binding of BiP to unfolded proteins, releases IRE1, PERK and ATF6 which induces different arms of a response mechanism known as unfolded protein response (UPR) [178].

Released IRE1 functions as an endoribonuclease that cleaves the specific intron sequence in the XBP1 mRNA and leads to translation of functional XBP1 protein [179]. XBP1 is a transcription factor that upregulate stress-related survival genes, especially chaperones. ATF6 moves to the Golgi apparatus upon releasing from BiP and cleaved by SP1 and SP2 proteases found in the Golgi [180,181]. Cleaved form of ATF6 translocates to the nucleus and activate many genes involved in UPR. PERK is a kinase and phosphorylates eIF2α upon dissociation from BiP. eIF2α is the regulatory subunit of eukaryotic initiation factor 2 (eIF2) complex which is recruited to 5'methylguanine cap in mRNAs to initiate translation of almost all proteins in eukaryotes [182]. Phosphorylated eIF2α strongly bind to eIF2B which is guanidine exchange factor (GEF) for the eIF2 and inhibits its activity. Therefore, global cap-dependent protein translation is halted under stress conditions [182]. On the other hand, some specific mRNAs containing upstream open reading frames (uORFs) on their 5' end, are selectively translated [183]. ATF4 mRNA, for instance, has two uORFs of which the second one comprises the normal coding sequence as out of frame. In normal conditions, since active eIF2 complexes are highly available, translation starts from the first uORF which has only 3 codon and re-initiate on the second uORF which prevents translation of active ATF4 protein. Under the stress conditions, however, phosphorylated eIF2α blocks the activity of eIF2 complex. Since there is low amount of available eIF2 complexes, translation re-initiation on the uORF2 is inhibited. Therefore, translation starts on normal ORF, and level of active ATF4 translation increases unlike global translations [183]. ATF4 is a major transcription factor initially upregulating expression of necessary proteins to survive under mild stress conditions. In case of prolonged or severe stress conditions, it upregulates apoptotic genes [184].

By inhibiting global protein translation, cells alleviate unwanted accumulation of unfolded or misfolded proteins and use all its energy to cope with stress. Preferential translation of the stress-related proteins, on the other hand, is crucial for the protection of cells against stress conditions.

1.4.3 Integrated stress response

Integrated stress response (ISR) is a highly conserved pathway among eukaryotes which is triggered by various stimuli. It consists of four different signaling pathways including the PERK arm of the UPR, and similarly depends on phosphorylation of eukaryotic initiation factor 2 alpha (eIF2α) by one of the four well-described kinases [185]. These kinases have similar catalytic domains, but have specific regulatory domains which allow induction by different stress signals (**Figure 1.5**).

Protein kinase R (PKR) which is also known as double-stranded RNA-dependent protein kinase is the first of these enzymes and activated upon viral infection. Double-stranded RNAs longer than 30 bp which are markers for viral infection were shown to bind two PKR monomers and triggers autophosphorylation of the kinase [186]. Activated PKR phosphorylates eIF2α and induce global translation inhibition. By this way, cells try to prevent production of viral proteins. General control non-derepressible 2 (GCN2) is the second eIF2α kinase which is activated upon amino acid deprivation [187]. GCN2 was shown to be activated by binding uncharged, deacylated tRNAs which are normally bind amino acids during protein synthesis. When there is amino acid deprivation in cell, free tRNAs become available and activate GCN2 by binding and allowing autophosphorylation of it via dimerization [188]. Activated GCN2 phosphorylates eIF2α and inhibits global translation until more amino acids become available. Heme-regulated inhibitor (HRI) is the third eIF2α kinase which is activated upon heme deprivation mainly caused by iron deficiency. HRI is different from other eIF2α kinases as being tissue-specific and predominantly expressed in erythroid cells [189]. It has two heme-binding sites, one of which is stable and the other is reversible. Heme binding to the reversible site inhibits kinase activity of dimerized HRI. Therefore, in heme deprivation conditions, dimerized HRI is activated by autophosphorylation. Activated HRI inhibits global translation by phosphorylating eIF2α to protect red blood cells from globin aggregation which may be toxic for cell [190]. The fourth kinase which phosphorylates eIF2α is PKR-like ER kinase (PERK) which is activated upon ER stress caused mainly by unfolded

protein accumulations, but also by disruption of calcium balance or redox status in the ER. PERK is normally found on ER membrane as bound by BiP/GRP78. Upon accumulation of misfolded unfolded proteins in the ER, BiP binds these proteins as a molecular chaperone, and releases PERK. Released PERKs are dimerized, activated by autophosphorylation and phosphorylates eIF2α to inhibit global translation to prevent unfolded protein accumulation [191].

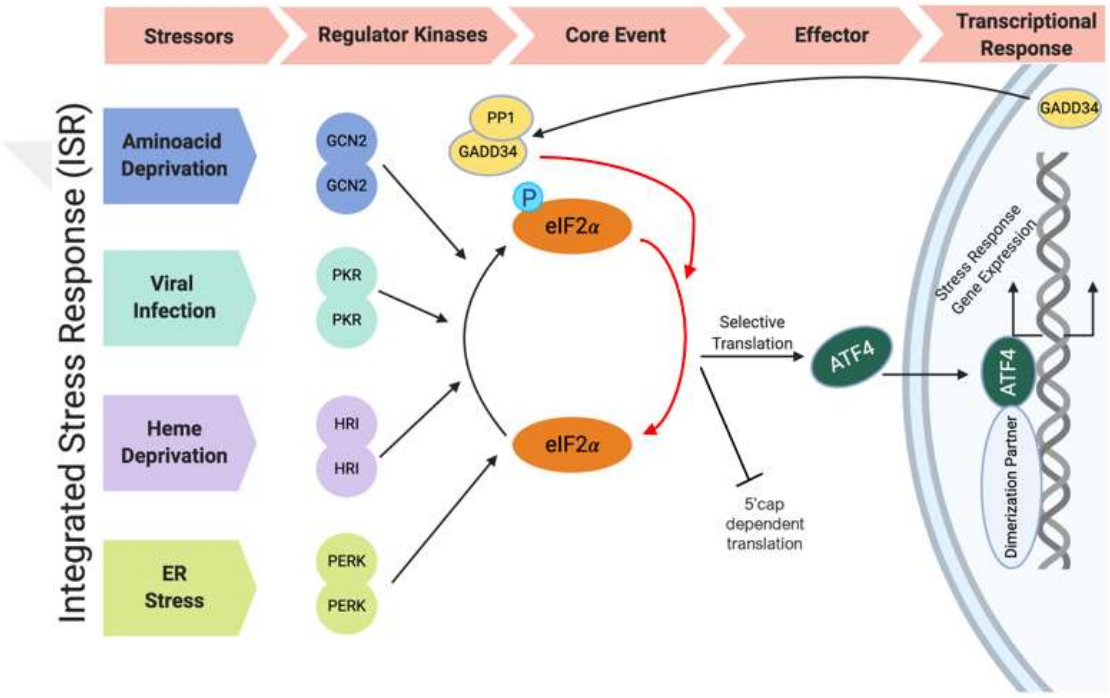

Figure 1.5 Integrated stress response (ISR) pathway. Figure adapted from [185].

In all four pathways, eIF2α is phosphorylated and global, 5' cap-dependent translation is inhibited (**Figure 1.5**). However, inhibition of global translation is not the only mechanism in ISR to cope with stress. Upon eIF2α phosphorylation, some 5' cap-independent mRNAs which are regulated by upstream open reading frame (uORF) sites and recruit ribosomes to their internal ribosome entry sites (IRES) instead of 5' cap, are preferentially translated under stress conditions [192]. Activating transcription factor 4 (ATF4) is one of these proteins and accepted as the master regulator of ISR (**Figure 1.5**). To survive under mild stress conditions, ATF4 upregulated many stress-related genes such as chaperones, amino acid transporters, heme oxygenases, etc. [193,194]. However, under severe or prolonged stress, ATF4 induced CHOP-mediated pro-apoptotic pathway by upregulating pro-apoptotic proteins such as Bim, Noxa, Puma, etc. and downregulating anti-apoptotic genes such as Bcl2, Bcl-xL and IAPs [195,196]. As a feedback

mechanism, ATF4 also activates GADD34 which bind to PP1 and induces dephosphorylation of eIF2α [197] (**Figure 1.5**).

2 MATERIALS AND METHODS

2.1 Reagents

The epigenetic chemical probe library was constructed in Oxford University by Dr. Udo Oppermann and kindly provided for screen and individual treatments. Bulk amounts of GSK-J4 and Belinostat were purchased from Adooq Bioscience (USA) for *in vivo* experiments. GSK864 was kindly provided by SGC Toronto. Z-VAD-FMK (general caspase inhibitor), Z-FA-FMK (negative control), LB broth and LB agar powders were purchased from BD Pharmingen (USA). ISRIB and PERKi was provided by Dr. Udo Oppermann. QNZ, Ferrostatin-1 and TMZ was purchased from Selleckchem (USA). Anti-IDH1 R132H (Hu) from mouse (clone: H09) antibody was purchased from Dianova (Germany). Anti-PARP, anti-ATF4 (D4B8), anti-p21 (12D1), anti-H3 (D1H2), anti-H3K4me3 (C42D8), anti-H3K9me3 (D4W1U), anti-H3K27me3 (C36B11), anti-H3K27ac (D5E4), and anti-acetyl-α-tubulin (D20G3) were purchased from Cell Signaling Technology (USA). Anti-GAPDH and anti-α-tubulin were purchased from Abcam (UK). Anti-puromycin (4G11) antibody was purchased from Merck Millipore (USA). GSK-J5, Thapsigargin and Cycloheximide were purchased from Cayman Chemical (USA). D-luciferin was purchased from Biotium (CA, USA). BsmBI enzyme, Cutsmart buffer, nuclease-free water, T4 PNK enzyme, T4 Ligase enzyme and T4 Ligase buffer were purchased from New England Biolabs (USA). M-MLV RT enzyme, 5X FS buffer, DTT, Random Hexamer, dNTP mix and Gateway LR Clonase II enzyme mix were purchased from Thermo Fischer Scientific (USA). DMEM 1X, FBS, Pen/Strep, PBS 1X, Neurobasal medium, L-Glutamine, FGF-basic, B-27 and N-2 supplements were purchased from Gibco (USA). Human EGF was purchased from PeproTech (USA). Heparin solution was purchased from Stemcell Technologies (Canada). D-2-Hydroxyglutarate (D2HG) Assay Kit, Polyethylene Glycol 8000, Puromycin dihydrochloride and Protamine sulfate were purchased from Sigma-Aldrich (USA). Blasticidin S HCl was purchased from GoldBio (USA). Fugene 6, Cell Titer-Glo (CTG) Luminescent Cell Viability Assay, Caspase Glo 3/7 assay and recombinant RNasin were purchased from Promega (USA). NucleoSpin Gel and PCR Clean-Up, NucleoSpin Plasmid miniprep, NucleoBond Xtra Midi and NucleoSpin RNA kits were purchased from Macherey-Nagel (Germany). LightCycler 480 SYBR Green I Master was purchased from Roche (Switzerland).

2.2 Plasmids

pCMV-VSV-G and pUMVC plasmids were gifts from Bob Weinberg (Addgene plasmid #8449 and #8454, respectively) [198]. psPAX2 plasmid was a gift from Didier Trono (Addgene plasmid #12260). pMIG Bcl-xL and pMIG Bcl-2 were gifts from Stanley Korsmeyer (Addgene plasmid #8790 and #8793, respectively) [199]. pLenti6.3/TO/V5 containing $IDH1^{R132H}$ was generated in Massachusetts General Hospital [36]. pLentiCRISPRv2 was a gift from Feng Zhang (Addgene plasmid #52961) [200]. HSPA5 overexpression vector was generated by cloning HSPA5 cDNA from donor vector pDONR221 (commercially supplied from DNASU, clone HsCD00041118) into pLEX307 (was a gift from David Root, Addgene plasmid # 41392) destination vector. pLEX-GFP plasmid was generated by Gateway cloning method, first cloning GFP cDNA into pENTR1A vector (was a gift from Eric Campeau & Paul Kaufman, Addgene plasmid #17398) [201], and then into pLEX307 destination vector using LR clonase II enzyme mix (NEB, USA). Pico2-Fluc.mCherry was a gift from Dr. Andrew Kung (Dana Farber Cancer Institute).

2.3 Cell culture

Human embryonic kidney 293T (HEK 293T) cells, and GBM cell lines A172 and LN18 were purchased from American Type Culture Collection (ATCC, USA). Human astrocytes (HAs) were purchased from ScienCell Research Laboratories (CA, USA). Fibroblast cell lines Fibro1 and Fibro2 were established at Koç University School of Medicine from skin biopsies of GBM patients operated at Koç University Hospital (Ethics approval no: 2013-5). They were cultured in DMEM (Gibco, USA), supplemented with 10% FBS (Gibco, USA) and 1% Pen/Strep (Gibco, USA) in a 37ºC incubator supplemented with 5% CO_2. HAs were cultured on Poly-L-Lysine coated plates. IDH1 mutant GBM cell lines MGG119 and MGG152 were established with patient-derived xenograft model by Dr. Hiroaki Wakimoto in Massachusetts General Hospital (MGH) [19]. They were cultured as neurospheres in GBM/EF medium consisting of neurobasal medium (Gibco, USA) with 7.5 ml L-Glutamine, 1X B-27 supplement (Gibco, USA), 0.5X N-2 supplement (Gibco, USA), 0.5 ml heparin solution (0.2%, Stemcell Technologies, Canada), 0.5% Pen/Strep, FGF (20 ng/ml), EGF (20 ng/ml).

2.4 Viral packaging and transduction

Retroviral particles from pMIG Bcl-xL and pMIG Bcl-2 and lentiviral particles from pLenti6.3/TO/V5 containing $IDH1^{R132H}$, pLentiCRISPRv2 containing gRNAs or pLEX307 containing HSPA5 cDNA, were produced in HEK 293T cells. Briefly, 293T cells were seeded on 10 cm-plates as $2.5x10^6$ cells/plate. The next day, with approximately 70-80% confluency, cells in each plate were transfected with required viral plasmids (2500 ng), and packaging plasmids; psPAX2 (2250 ng) or pUMVC (2250 ng), for lentiviral or retroviral packaging, respectively, and VSV-G (250 ng) by using 20 µl of Fugene 6 (Promega, USA). After overnight incubation, media were refreshed. Virus containing media from 48 and 72 hours post transfection were collected. Then, they were aliquoted either directly or after 100X concentrated with Polyethylene glycol (PEG 8000, Sigma-Aldrich, USA) overnight, and stored at -80°C.

Adherent GBM cells were seeded as 100.000 cells/well of 6-well plate, and transduced next day with virus containing media. Protamine sulfate (PS, 8 µg/ml) was also added to increase transduction efficiency. Primary GBM cells cultured as suspension, were transduced with spinfection method. Briefly, neurospheres were resuspended as individual cells in 2 mL of EF medium supplemented with PS (8 µg/ml) and seeded on 1 well of 6-well plates together with concentrated virus. Then, cells were centrifuged in a plate-centrifuge (Beckman Coulter, USA) at 800g for 90 minutes. Both adherent and suspension cells were incubated in virus containing media overnight in the cell culture incubator, and then, media were refreshed. 48 hours post-transduction, adherent and suspension cells infected with pLentiCRISPRv2 or pLEX307-HSPA5 were treated with 2 µg/ml or 1 µg/ml of puromycin, respectively, and selected for 3 days. A172 GBM cells infected with pLenti6.3/TO/V5 containing $IDH1^{R132H}$ were selected with blasticidin (10 µg/ml) for 5-7 days. Efficiency of pMIG BcL-xL and pMIG Bcl-2 infections was monitored via GFP expression under fluorescence microscope.

2.5 Cloning and CRISPR-mediated knock-out studies

gRNA sequences targeting exon regions of KDM6A and KDM6B genes were obtained from GeCKO library designed by Feng Zhang's laboratory at Broad Institute [200]. gRNAs targeting DDIT3 gene were designed using Chopchop gRNA design tool [202]. All gRNAs synthesized at Macrogen Europe Laboratories as top and bottom strands. They were annealed and cloned into lentiCRISPR v2 plasmid (Addgene #52961)

according to protocol published by Zhang Lab [200]. Briefly, 1 µl of resuspended top and bottom strand oligos (100 µM) were mixed with 0.5 µl of T4 PNK enzyme, 1 µl of T4 Ligase buffer, and 6.5 µl of nuclease-free water in a PCR tube. Annealing was performed by using following conditions: 30 min at 37ºC, 5 min at 95ºC and then ramp down to 25ºC with 5ºC/min rate. On the other hand, 5 µg of pLentiCRISPRv2 plasmid was digested in a 1.5 ml centrifuge tube containing 3 µl of BsmBI enzyme, 3 µl of Cutsmart buffer, and nuclease-free water up to total of 30 µl, by incubating at 55ºC for 3h. For ligation, 1 µl of annealed oligos (after 1:200 dilution) were mixed with 1 µl of digested and gel purified pLentiCRISPRv2 vector (from 50 ng/µl), 1 µl of T4 Ligase enzyme, 1 µl of T4 Ligase buffer, and 6 µl of nuclease-free water, and incubated overnight at 16ºC. 3 µl of ligation products were transformed into home-made competent bacteria, and liquid cultures were prepared from single colonies. Plasmids were isolated using either NucleoSpin Plasmid miniprep or NucloSpin Xtra Midi kit (Macherey-Nagel, Germany). All gRNA clonings were verified via Sanger sequencing. 3 gRNA plasmids targeting each gene were pooled and lentiviruses were produced from these pools for each gene. 2 gRNAs targeting nowhere in human genome were pooled and used as non-targeting control gRNAs (gNT) in further experiments. Cells were infected with ~MOI of 3. Then, growth analysis, viability assays after drug treatments and gene expression analysis were performed. Gene knockouts were validated via Sanger sequencing of targeted regions (**Figure 3.32 and 3.43**). gRNA sequences were given in **Table 2.1.**

Table 2.1 Sequences of gRNAs used in knockout experiments

gRNA	Sequence (5' to 3')
DDIT3 – gRNA1	GACTGATCCAACTGCAGAGA
DDIT3 – gRNA2	GGAAATCGAGCGCCTGACCA
DDIT3 – gRNA3	CCAGCTGGACAGTGTCCCGA
KDM6A – gRNA1	ACTGTAAACTGTAGTACCTC
KDM6A – gRNA2	CAGCATTATCTGCATACCAG
KDM6A – gRNA3	AAGTCGTAAATGAATTTCCT
KDM6B – gRNA1	TACCACAGCGCCCTTCGATA
KDM6B – gRNA2	CGAGTCAGAGCACGATAGTG
KDM6B – gRNA3	CCAGAACTACTGCCATGTGA
NT1	ACGGAGGCTAAGCGTCGCAA
NT2	CGCTTCCGCGGCCCGTTCAA

2.6 Cell Viability Assay

Cell viabilities after required treatments were measured via Cell Titer-Glo (CTG) Luminescent Cell Viability Assay (Promega, USA) according to manufacturer's instructions with some modifications. Briefly, cells were seeded to clear bottom black side 96-well plates (Corning Costar, USA) as 4000 cells/well and as triplicates for each condition. The next day, they were treated with corresponding chemicals of interest individually or in combination for defined period. At the end of the treatment period, media from each well were removed via multi-well pipette. 44 µl of CTG ready-to-use mix which is prepared as 1:10 dilution of CTG reagent with DMEM, were added on each well. For primary cells cultured as suspension, CTG reagent was directly added on cells at 1:10 amount of culture medium. After 2 minutes of shaking and 8 minutes of incubation, luminescence levels of each well were measured using a plate reader (BioTek's Synergy H1, Winooski, VT, USA). Relative cell viabilities were calculated by using luminescent values of untreated samples as control.

2.7 Chemical screen with epigenetic regulator inhibitors

MGG119 and MGG152 spheres were dissociated into individual cells and seeded in 96-well plates as 4000 cells/well. The next day, cells were treated with the chemical probe library consisting of 46 inhibitors targeting bromodomains (BRD), histone deacetylases (HDAC), histone methyltransferases (HMT), lysine demethylases (KDM), prolyl hydroxylases (PHD), methyl lysine binders, DNA methyltransferases (DNMT), poly ADP ribose polymerase (PARP), kinase inhibitors, and histone acetyltransferases (HAT) (Appendix A). Cell viabilities after 48h of treatment were determined via Cell Titer-Glo (CTG) Cell Viability Assay as described above. All treatments were studied as triplicate.

2.8 Individual and combinatorial treatment of screen hits

5-azacytidine, Chaetocin, GSK-J4 and Belinostat were applied individually in a dose dependent treatment on MGG119, MGG152, Fibro1 and Fibro2 cells and cell viability assays were performed after 72h of treatment. Both tumor and non-malignant cell lines were subjected to all possible dual combinations of these inhibitors. Human astrocytes (HA) were also treated with GSK-J4 (2.5 µM) and Belinostat (1 µM) individually and in combination. Combination index (CI) values were calculated using

CompuSyn software [203], for 5-azacytidine and Chaetocin or GSK-J4 and Belinostat combinations in MGG119 and MGG152 cells.

2.9 Sphere formation assay

Patient-derived IDH1 mutant MGG152 cells were seeded on 96-well plates at 150 cells/well. The next day, they were treated with different doses of 5-azacytidine, Chaetocin, GSK-J4 and Belinostat. After 7 days of drug treatment, number of spheres containing more than 1 cell were counted under microscope and recorded for each dose of treated drugs. 3 wells were counted for each condition as replicates.

2.10 Generation and validation of IDH1 mutant GBM cell lines

IDH1 mutant GBM cell lines were generated by lentiviral infection of pLenti6.3/TO/V5 containing IDH1 cDNA with R132H mutation [36]. Cells were cultured in parallel with parental wild type cells to obtain a paired cell line. Mutant IDH1 expression was analyzed with western blot and immunocytochemical staining by using $IDH1^{R132H}$ mutant specific antibody (DIA-H09, Dianova, Germany). D-2-Hydroxyglutarate production was assessed via D-2-Hydroxyglutarate (D2HG) Assay Kit (Sigma-Aldrich, USA) in the presence or absence of GSK864. Briefly, cellular extracts were obtained by lysing cell pellets in NP40 lysis buffer (1% NP40, 50 mM Tris buffer pH 7.4, 250 mM NaCl, 5mM EDTA, 50 mM NaF, 0.02% NaN_3) supplemented with 1X protease inhibitor cocktail set (cOmplete™ ULTRA Tablets, Roche, Germany) and 1mM PMSF prior to usage. Cell lysates were centrifuged at 13.000 rpm for 10 min at 4 ºC, and supernatants were collected. Then, deproteinization was performed for all samples by Trichloroacetic acid (TCA) precipitation. TCA was added to all samples with a final concentration of 1M. After vortexing briefly, samples were kept on ice for 5 minutes. They were centrifuged at 13.000 rpm for 2 min at 4ºC. Supernatants were transferred to a new tube and neutralized with 2M KOH. After vortexing, samples were centrifuged at 13.000 rpm for 15 minutes at 4ºC. 25 µl of undiluted samples, 1:5 diluted samples, and prepared standards were placed in a 96-well plate. After addition of 75 µl of D2HG complete reaction mixture into each well, plate was covered with aluminum foil and kept at 37ºC for 60 minutes. Fluorescence levels were detected with Synergy microplate reader, and D2HG levels were calculated based on the standard curve plotted with measured values of standards. After validations, paired GBM cell lines were treated with

hit inhibitors individually and in combination. Cell viabilities were determined after 72h of treatments via CTG assay.

2.11 Caspase Activity and Caspase Inhibition Assays

For Caspase 3/7 activity assay, A172 wild type and IDH1^{R132H} cells were seeded on 96-well plates as 4000 cells/well. The next day, cells were either untreated or treated with GSK-J4 (2.5 μM) alone, Belinostat (1 μM) alone or both in combination. After 48h of drug treatments, Caspase 3/7 activities in each well were measured via Caspase Glo 3/7 assay (Promega, USA), according to manufacturer's instructions.

For caspase inhibition assay, A172 wild type and IDH1^{R132H} cells were seeded on 96-well plates as 3000 cells/well. The next day, cells were pre-treated with Z-FA-FMK (Negative Control for Caspase Inhibitors) or Z-VAD-FMK (General Caspase Inhibitor) at 20 μM final concentration. After 24h of pre-treatments, cells were either untreated or treated with GSK-J4 (2.5 μM) alone, Belinostat (1 μM) alone or both in combination.

2.12 Inhibition of Cellular Stress Pathways

For inhibition assays, cells were seeded on 96-well plates as 3000 cells/well. The next day, corresponding pathway inhibitors were added on cells. PERKi (1 μM) was used for inhibition of PERK enzyme, or ISRIB (1 μM) for inhibition of eIF2α phosphorylation which both are responsible for stress response pathways. QNZ (10 nM) or Ferrostatin-1 (2 μM) was used for inhibition of NF-KB pathway or ferroptosis, respectively. After 24h of pre-treatments, cells were either untreated or treated with GSK-J4 alone, Belinostat alone or both in combination. After 72h of drug treatments, cell viabilities were measured via CTG assay.

For inhibition of reactive oxygen species (ROS) in cells, N-acetyl-L-cysteine (NAC) which is known as ROS scavenger was used. Similarly, cells were seeded on 96-well plates as 3000 cells/well and pre-treated with NAC (2 mM) for 24h. Then, 5-azacytidine, Chaetocin, GSK-J4 or Belinostat were added on cells individually. Cell viabilities were measured after 48h of drug treatment via CTG assay.

2.13 Inhibition of Mutant IDH1

For inhibition of mutant IDH1 enzyme, cells were pre-treated with GSK864 (2.5 μM), a selective IDH1^{R132H} inhibitor [32] for 3 days. Then, untreated and GSK864 pre-

treated cells were either directly collected for qRT-PCR, western blot, and RNA-seq analysis or re-seeded on 96-well plates to compare growth kinetics or drug responses. To generate growth curves, cells were seeded on 96-well plates as 3000 cells/well, and cell viabilities were measured via CTG assay at day 0, and then, each day for 96h. To compare drug responses, cells were seeded on 96-well plates as 4000 cells/well. After 24h of re-seeding, cells were either untreated or treated with GSK-J4 alone and Belinostat alone or both in combination. Cell viabilities were measured after 72h of drug treatments via CTG assay. Primary MGG119 and MGG152 cells were treated with GSK864 (2.5 μM) for 10 passages to observe long term effects.

2.14 Testing specificity of GSK-J4

To test the specificity of GSK-J4, MGG152 and A172 IDH1^{R132H} cells were treated with GSK-J5, an inactive form of GSK-J4, and other KDM inhibitors such as IOX-1, inhibitor of pan-2-OG dependent enzymes, KDOAM-25 and KDM5-C70, inhibitors of KDM5 enzymes, KDOAM-32, inactive form of KDOAM-25, and KDOBA67, inhibitor of KDM6 enzymes, in a dose-dependent manner. In addition, each of the inhibitors was co-treated with Belinostat (1 μM) to test their combination effect. Cell viabilities were performed after 72h of drug treatments via CTG viability assay.

2.15 Live cell imaging

Olympus Xcellence Pro inverted microscope with 10X air objective (Center Valley, PA, USA) was used for the live-cell imaging experiments in a 37ºC chamber supplied with 5% CO_2. A172 wild type and IDH1^{R132H} cells were seeded on 24-well plates at a density of 16.000 cells/well. Next day, they were treated with either GSK-J4 (2.5 μM) or Belinostat (1 μM), or in combination. Images of random positions from each well were captured with 8-10 min intervals during 96h after drug treatment. Cell numbers in 3 different frames for each condition was counted using ImageJ software (NIH Image, MD, USA) and viability curves were obtained for each condition.

2.16 Co-culture of fibroblasts with GBM cells

Fibro1 fibroblasts were labelled with GFP-expressing lentiviruses, and A172 IDH1^{R132H} cells were labelled with mCherry-expressing lentiviruses. Fibroblasts and A172 IDH1^{R132H} cells were seeded on same well of 6-well plates with 1:1 ratio. Co-culture wells were subjected to either no treatment, GSK-J4 alone (2.5 μM), Belinostat

alone (1 µM), or combination of them. After 72h of drug treatments, fluorescent images were taken under red and green fluorescent filters, and viable cells were quantified by counting 3 different frames for each condition.

2.17 Cell cycle analysis

A172 wild type, A172 IDH1^{R132H} and MGG152 cell pellets were collected after 24h or 48h of either without treatment or treatments with GSK-J4, Belinostat and their combination. They were washed with PBS and fixed with 200 µl of cold 70% ethanol via incubating for 30 min at 4ºC. Ethanol was added dropwise, and pellets were resuspended either with flicking tube or pipetting gently after each drop. After fixation, cells were centrifuged at 850g for 5 min, and washed 2 times with PBS. To remove RNA content, pellets were resuspended in 50 µl of 100 µg/ml RNase and incubated for 15 min at room temperature. Finally, 200 µl of 50 µg/ml propidium iodide (PI) solution was added on samples, and they were incubated for 30 min at room temperature. Samples were kept in the dark at 4ºC until analysis was performed. Quantification of PI staining were performed via flow cytometry (BD Accuri C6 Plus Flow Cytometry, BD Biosciences, USA), and cell cycle intervals were determined by assigning the n peak as G0/G1 phase, n to 2n interval as S phase and 2n peak as G2/M phase.

2.18 YO-PRO-1 staining

A172 wild type and IDH1^{R132H} cells were seeded on 24-well plates as 20.000 cells/well. The next day, cells were either kept untreated or treated with GSK-J4 (2.5 µM) and Belinostat (1 µM) in combination. After 48h of drug treatments, media were removed, and cells were kept in fresh media containing 0.1% (v/v) YO-PRO-1 stock solution. Plates were incubated at 37ºC for 15 min, and fluorescent images were taken directly, as soon as possible upon incubation.

2.19 Western blot and SUnSET assay

Cell pellets were collected after 24h or 48h of indicated drug treatments and stored at -80 ºC until the experiments were performed. Pellets were lysed in NP40 lysis buffer (1% NP40, 50 mM Tris buffer pH 7.4, 250 mM NaCl, 5mM EDTA, 50 mM NaF, 0.02% NaN_3) supplemented with 1X protease inhibitor cocktail set (cOmplete™ ULTRA Tablets, Roche, Germany) and 1mM PMSF prior to usage. Cell lysates were centrifuged at 13.000 rpm for 10 min at 4 ºC, and supernatants were collected.

For histone analysis, cell pellets were lysed in Triton Extraction Buffer (TEB), which consists of PBS with 0.5% Triton X 100 (v/v), 2 mM PMSF, 0.02% (w/v) NaN3 and 5 mM sodium butyrate, on ice for 10 min. Nuclei were precipitated via centrifuging at 6500 g for 10 min at 4 ºC, and washed again with TEB after discarding supernatants. Pellets were resuspended in 0.2N HCl as around 10^7 cells/ml and kept at 4 ºC overnight. Next day, lysates were neutralized by adding 1M of NaOH as 1/5 volume of HCl solution. They were centrifuged at 6500 g for 10 min at 4 ºC, and supernatants were stored as histone lysates at -20 ºC.

For SUnSET assay [204], MGG152 cells were treated with GSK-J4 and/or Belinostat for 24h or 48h. Thapsigargin (5 µM) or Cycloheximide (5 µM) were used as control treatments by incubation for 4h before puromycin treatment. Then, all cells were treated with puromycin (10 µM) for 30 min, pellets were collected and lysed in NP40 buffer as explained above. For the blotting part, anti-puromycin (4G11) antibody was used.

Protein concentration of lysates from all protocols were determined via Pierce's BCA protein assay kit (Thermo Fisher Scientific, USA). Lysates were mixed with 4X loading dye which is prepared by mixing 4X Laemmli Sample Buffer (Bio-Rad, USA) with 2-mercaptoethanol in 9:1 ratio, and boiled at 95 ºC for 10 min. Appropriate amount of samples and protein ladder (Precision Plus Protein, Bio-Rad, USA) were loaded into gradient SDS polyacrylamide gels (Mini-PROTEAN® TGX™ Precast Gels, Bio-Rad, USA), and run at 25 mA for 40 min. Then, protein transfer was performed via Trans-Blot® Turbo™ RTA Mini PVDF Transfer Kit (Bio-Rad, USA) with manufacturer's defined transfer protocol. Membrane was blocked with 5% non-fat dry milk for 1h with gentle shaking at room temperature. Then, blocking buffer was replaced with primary antibody diluted in PBST with 2% BSA and 0.02% NaN_3 by gently shaking overnight at 4 ºC. Next day, antibody solution was removed, and membrane was washed 3 times with PBST for 15 min each. Then, it was incubated with secondary antibody diluted in 5% milk solution for 1h at RT and washed 3 times with PBST for 15 min each. Membrane was incubated with Pierce™ ECL Western Blotting Substrate (Thermo Fisher Scientific, USA) for 5 min at dark, and visualized by Odyssey ® Fc Imaging System (LI-COR Biosciences, USA). Band intensities were quantified using ImageJ software (NIH Image, MD, USA) and normalized according to intensities of reference protein bands.

2.20 RNA sequencing

A172 wild type and IDH1^{R132H} overexpressing cells were cultured in the presence or absence of GSK864 (2.5 μM) for 3 days. Cell pellets were collected from each condition (**Figure 2.1A**). As the second set of samples, MGG152 patient derived IDH1 mutant cells were cultured without drugs as control, or with GSK-J4 alone, Belinostat alone or both in combination. Cell pellets were collected after 48h of drug treatments (**Figure 2.1B**). All samples were studied as duplicate. Total RNAs were extracted with Nucleospin RNA kit (Macherey-Nagel, Germany), according to manufacturer's protocol, and stored at -80 ºC until sending for RNA-seq analysis.

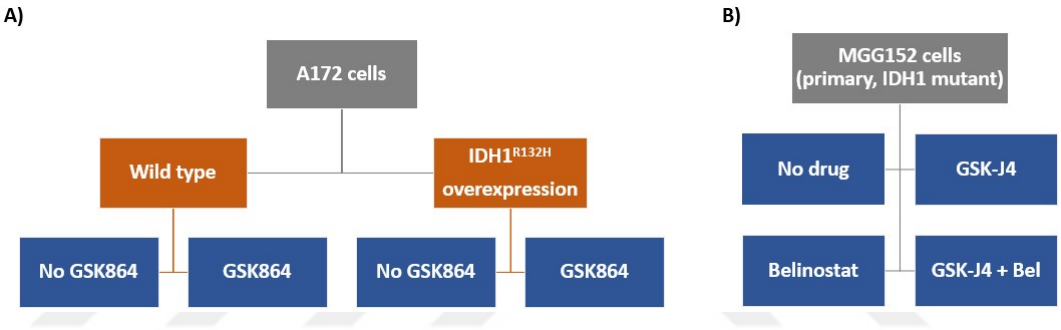

Figure 2.1 Samples collected for RNA sequencing.

Preparation of the RNA-seq libraries and data analyses were performed by Dr. Adam Cribbs in Oxford University. Briefly, the RNA-seq libraries were prepared using NEBNext Ultra Directional RNA library prep kit for Illumina (NEB, USA), according to manufacturer's instructions. Prior to the analysis, 42 bp paired-end reads were quality controlled using FastQC (version 0.11.4) [205], aligned using HISAT2 (version 2.1.0) [206], and assigned to annotated features using featureCounts (subread version 1.5.0-p2). The Fasta and GTF files for the human genome were obtained from the Ensembl FTP site release 75. Computational pipelines were used by calling scripts from the CGAT toolkit to analyze the next generation sequencing data (https://github.com/cgat-developers) [207,208]. Data have been deposited in NCBI's Gene Expression Omnibus (with the accession number of GSE134120). Differentially expressed genes (DEGs) were identified using DESeq2 [209]. Analysis of enriched pathways were performed using Gene Set Enrichment Analysis (GSEA) and eXploring Genomic Relations (XGR) softwares [210,211].

2.21 qRT-PCR experiments

Cell pellets were collected after specified treatments and stored at -80 ºC until the following experiments were performed. Total RNAs were isolated via Nucleospin RNA kit (Macherey-Nagel, Germany), according to manufacturer's instructions, and stored at -80 ºC. For cDNA production, 1000 ng of total RNA from each condition was mixed with 2.5 µl of dNTP mix (from 2 mM each), 1 µl of random hexamer, and nuclease-free water up to 16.5 µl total. This mixture was incubated at 65ºC for 5 minutes and transferred on ice. Then, 5 µl of 5X First Strand (FS) buffer, 2 µl of DTT (0.1M) and 0.5 µl of RNasin were added into each tube, and they were incubated at room temperature for 10 minutes. After addition of 1 µl of M-MLV RT enzyme into each tube, samples were incubated in a thermocycler with following conditions: 37ºC for 1 hour, 70ºC for 15 minutes, and 4ºC ∞. qRT-PCR was performed by using SYBR green mastermix (Roche, Switzerland), and LightCycler 480 instrument (Roche, Switzerland). Briefly, 2 µl of cDNAs from each condition were transferred into 3 wells of 96-well plate (LightCycler 480 Multiwell Plate 96, white, Roche, Switzerland). 10 µl of SYBR green mastermix, 7 µl of nuclease-free water, and 1 µl of primer mix (5 µM each) specific for required gene were added into each well. Plate was covered with sealing foil and centrifuged at 1300 rpm for 2 minutes in a plate centrifuge. qPCR reaction was performed in LightCycler 480 instrument with following conditions: 95ºC for 5 minutes, 45 cycles of (95ºC for 10 seconds, 60ºC for 30 seconds and 72ºC for 30 seconds), and 4ºC ∞. Relative gene expressions were calculated by using ΔΔCt method, and GAPDH as reference gene. Primers used in qRT-PCR experiments were given in **Table 2.2**.

Table 2.2 Sequences of primers used in qRT-PCR experiments

Gene	Forward Primer	Reverse Primer
ASNS	GGAAGACAGCCCGATTTACT	AGCACGAACTGTTGTAATGTCA
ATF4	ATGACCGAAATGAGCTTCCTG	GCTGGAGAACCCATGAGGT
ATF5	GGAGTGGCGACAGGATAGAGCT	CCTGTAGGATATGGGTCCCCTTC
BIRC5	GGACCACCGCATCTCTACAT	GACAGAAAGGAAAGCGCAAC
BCL2L1	GGTCGCATTGTGGCCTTTTTC	TGCTGCATTGTTCCCATAGAG
CDKN1A	TCAGAGGAGGTGAGAGAGCGG	CGCATGGGTTCTGACGGACA
COL1A2	GGCCCTCAAGGTTTCCAAGG	CACCCTTGTGGTCCAACAACTC
COL3A1	TGGTCCCCAAGGTGTCAAAG	GGGGGTCCTGGGTTACCATTA
DDIT3	ATGAACGGCTCAAGCAGGAA	GCAGATTCACCATTCGGTCAA
DDIT4	TCGGAGCATCACTACTGACCTGTTG	AACGCAGCTGCCAGGTGTAATTTT
DHRS2	CCTCTGGTAGGGAGCACTCT	CCAGCGCCACTACTGGATTA
GAPDH	AGCCACATCGCTCAGACAC	GCCCAATACGACCAAATC
IFI44L	AAGCCGTAGTGGGGTCTGAT	CATGCACAGTCCTGCTCCTT
IFIT1	GCTTACACCATTGGCTGCTG	CCATTTGTACTCATGGTTGCTGT
ITGA2	CTGCTGGTGTTAGCGCTCAGT	GGGTGAACCAACCAGTAACCAGT
NOXA	ACCAAGCCGGATTTGCGATT	ACTTGCACTTGTTCCTCGTGG
PSAT1	TGCCGCACTCAGTGTTGTTAG	GCAATTCCCGCACAAGATTCT
PUMA	GACCTCAACGCACAGTACGAG	AGGAGTCCCATGATGAGATTGT
RARRES2	AGAAACCCGAGTGCAAAGTCA	AGAACTTGGGTCTCTATGGGG
RSAD2	TTGGACATTCTCGCTATCTCCT	AGTGCTTTGATCTGTTCCGTC
WNT7B	TTTCTCTGCTTTGGCGTCCT	GGCCAGGAATCTTGTTGCAG

2.22 Hypoxia experiments

A172 wild type, A172 IDH1^{R132H}, MGG119 or MGG152 cells were seeded on two separate 96-well plates as 4000 cells/well. One of the plates for each cell type was incubated in normoxic conditions (21% O_2), while the other plate was incubated in hypoxic conditions (1% O_2). The next day, cells in both plates were treated with GSK-J4 or Belinostat individually or in combination, and some cells from each type were kept untreated to use as control and to analyze effect of oxygen level on cellular growth. Cell viabilities were measured after 72h of drug treatments via CTG cell viability assay.

2.23 *In vivo* studies

Non-obese diabetic/severe combined immunodeficiency (NOD/SCID) mice were used for generation of orthotopic tumor models. All experiments were performed in Koç University Animal Facility with appropriate conditions and all protocols were approved by the Koç University Ethics Committee. IDH1 mutant primary MGG152 cells were infected with lentiviruses containing both Firefly Luciferase and mCherry. 2x10^5 cells were injected intracranially using stereotaxic injection in 7 ul PBS at the coordinates anteroposterior (AP): -2 mm, mediolateral (ML): +1.5 mm, Dorsoventral (DV): +2 mm from bregma, which is accepted as a universal anatomical reference. To monitor tumor

formation and progression, D-Luciferin (50 mg/kg) was injected intraperitoneally and luminescence due to luciferase activity was measured via in vivo bioluminescence imaging system (IVIS Lumina III). After 17 days of tumor injection, mice were treated with either DMSO or GSK-J4 and Belinostat combination. Both drugs were injected intraperitoneally as 100 mg/kg, for 6 consecutive days. Tumor sizes were calculated as average radiance via Living Image software (PerkinElmer, USA). Kaplan-Meier survival plot was also generated via using GraphPad Prism version 8.0.2 for Windows, GraphPad Software, (CA, USA).

2.24 Statistical analysis

All charts were plotted using GraphPad Prism version 8.0 or Microsoft Excel 365 softwares. Two-way ANOVA analyses were performed in GraphPad Prism, and unpaired t-tests were performed in Microsoft Excel using pre-built functions. Combination indexes (CI) were calculated using CompuSyn software. Gene set enrichment scores, false discovery rate (FDR) values and p-values for enrichment analysis were calculated using GSEA version 4.0 software

3 RESULTS:

3.1 Epigenetic inhibitor screen identifies potent compounds targeting IDH1-mutant gliomas

To identify epigenetic compounds that can target IDH1 mutant gliomas, we conducted a chemical screen in two independent primary glioma cell lines that carry a R132H point mutation in IDH1, namely MGG119 and MGG152 cells [19]. We employed a library composed of 46 compounds targeting different classes of chromatin modifiers and assessed the overall viability of cells in response to treatment with a single dose of chemicals with ATP based cell viability assays (**Figure 3.1A).** DMSO-only treated and untreated cells served as negative controls. On average, most compounds had minimal effect on cell viability (92.4±15.3% for MGG119, and 86.7±21.7% for MGG152) (**Figure 3.1B**). We considered a compound a "hit" if it reduced cell viability 1 SD or lower (77.1% and 65.0%, respectively) in both cell lines. Accordingly, 4 compounds significantly decreased viability of both MGG119 and MGG152 cells (namely 5-azacytidine, Chaetocin, GSK-J4 and Belinostat). Treatment of glioma cells as well as non-malignant human fibroblasts, named Fibro1 and Fibro2, revealed dose-dependent effects of these compounds on both cell lines (**Figure 3.2**). Fibroblasts were not affected from these compounds to the same extent, attesting to the tumor specificity of the selected compounds.

We also performed sphere formation assay to see effects of hit drugs on sphere formation capabilities of primary IDH1 mutant MGG152 cells. Control cells formed large and mostly uniform spheres when cultured with serum-free media (**Figure 3.3A**). On the other hand, spheres from drug treated cells were much smaller and less in number. Number of spheres containing more than one cell decreased with the increasing doses of each drug (**Figure 3.3B**).

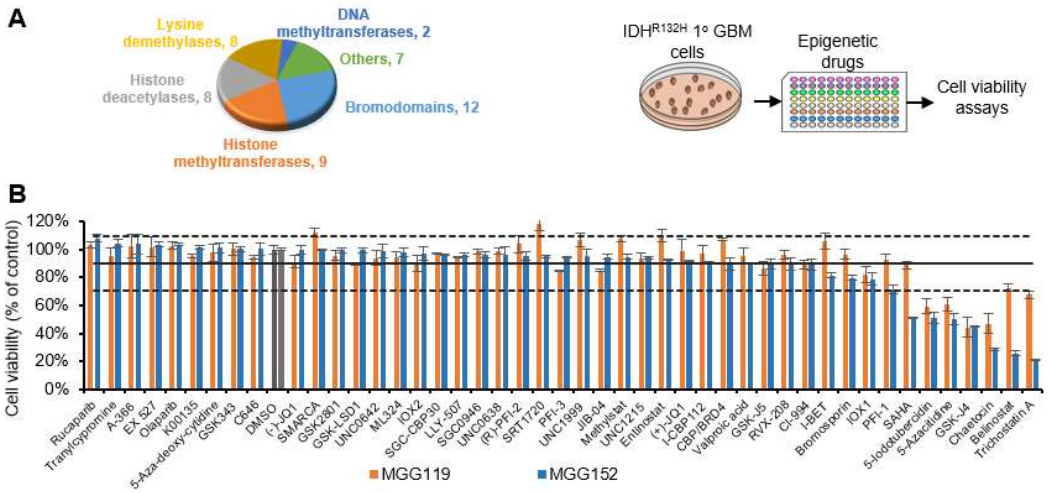

Figure 3.1 Epigenetic inhibitor screen. A) Pie chart shows total of 46 chemical probes targeting different classes of epigenetic enzymes. Drug screen was performed in 96-well plates as triplicates as shown in the scheme. **B)** Patient derived IDH mutant MGG119 and MGG152 cells were treated with chemical probe library for 48h. Black bar represents DMSO control. Horizontal black line represents viability mean; staggered lines denote SD=1.

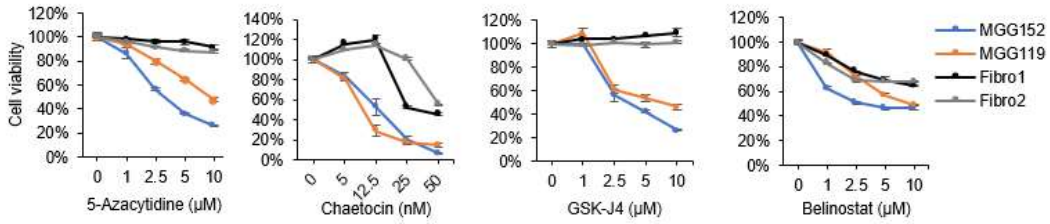

Figure 3.2 Individual treatment of screen hits. Patient-derived IDH mutant GBM cells and non-malignant fibroblasts were treated with screen hits individually at increasing doses for 72h; the tumor cells were markedly more sensitive to drug treatment.

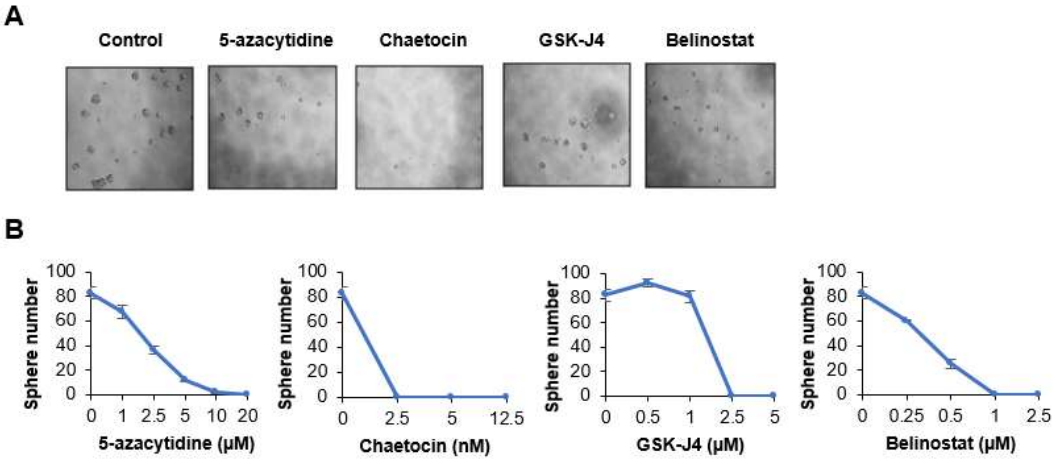

Figure 3.3 Sphere formation assay. A) Representative images showed that drugs have negative effects on sphere sizes and numbers. **B)** Patient derived GBM cells were seeded on 96-well plates at 150 cells/well. Sphere numbers after 7 days were recorded upon drug treatments at different doses.

In order to examine the combinatorial efficacy of the selected compounds, we applied all possible dual combinations of the 4 screen hits on IDH1 mutant cells or fibroblasts (**Figure 3.4A**). To this end, we chose compound concentrations that did not markedly reduce viability individually on tumor cells. Accordingly, fibroblasts were not affected from the treatment with compounds applied individually or in combination; however, glioma cells displayed significantly reduced viability upon combination treatments **(Figure 3.5),** as best illustrated as a heat map of the viability results (**Figure 3.4B**). Specifically, "5-azacytidine + Chaetocin" and "GSK-J4 + Belinostat" combinations showed dramatic effects on both IDH1 mutant cell lines, without majorly affecting fibroblasts. Indeed, the highest efficacy was demonstrated with the combination of GSK-J4, an HDM inhibitor, and Belinostat, an HDAC inhibitor. Their effects were synergistic on IDH1 mutant tumor cells, but not on fibroblasts **(Figure 3.6).**

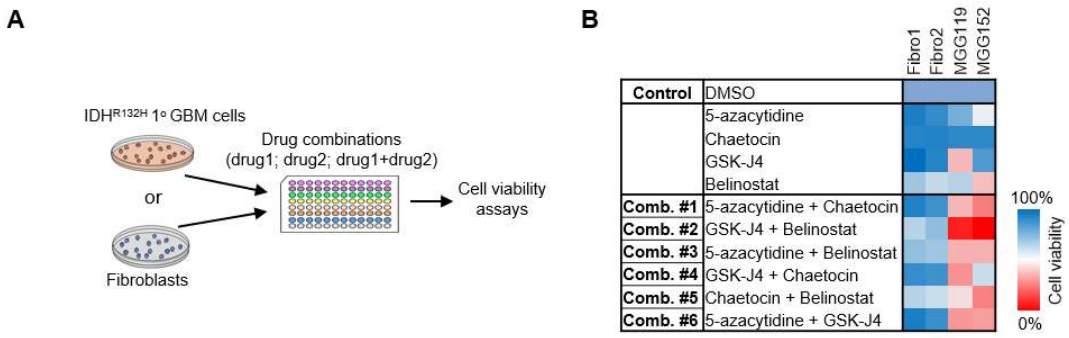

Figure 3.4 Combination of screen hits. A) Schematic view of drug combination strategy for IDH mutant primary GBM cells and patient-derived fibroblasts. **B)** GBM cells and fibroblasts were treated with all possible dual combinations of screen hits. Effects of individual and combinatorial treatments on viability are represented as heat map. Color scale indicates viability, increasing from red to blue.

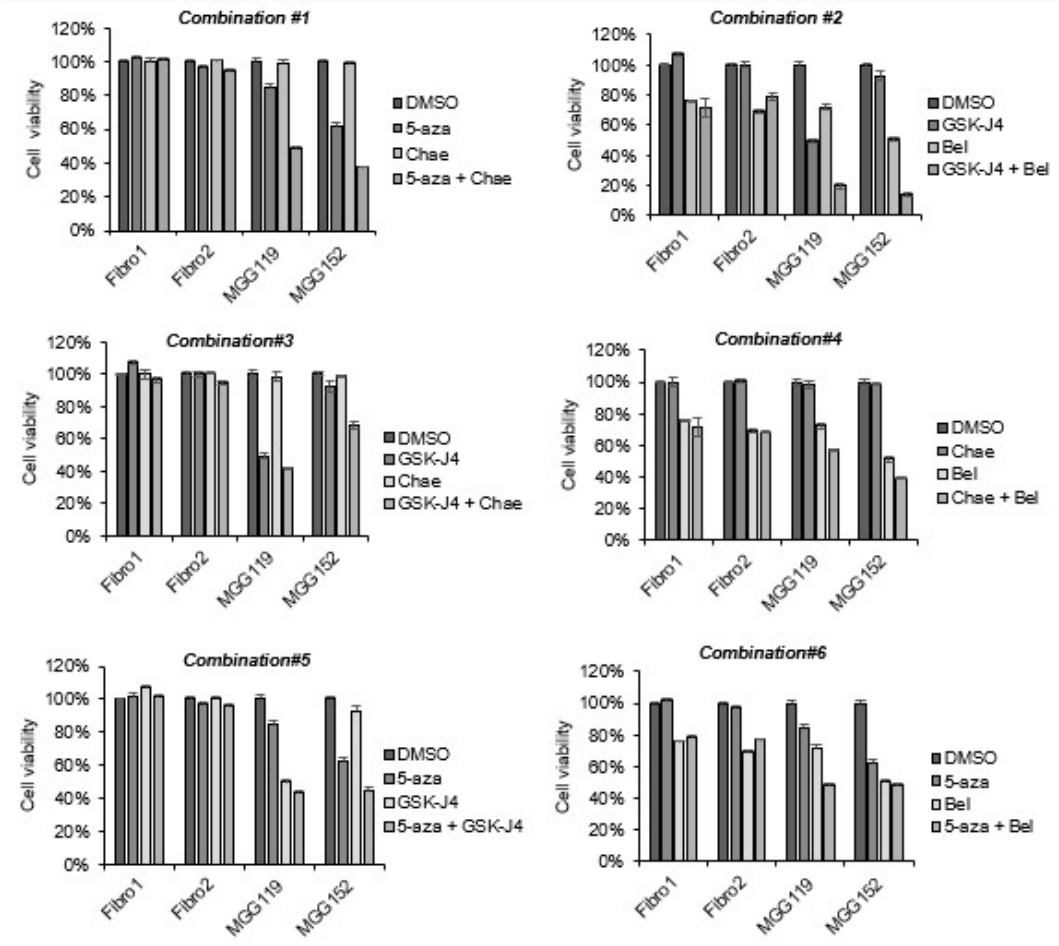

Figure 3.5 Viability results of each combination treatment. GBM cells and fibroblasts were treated with all possible dual combinations of screen hits: 5-azacytidine and

Chaetocin (#1), GSK-J4 and Belinostat (#2), GSK-J4 and Chatetocin (#3), Chaetocin and Belinostat (#4), 5-azacytidine and GSK-J4 (#5), 5-azacytidine and Belinostat (#6).

A

MGG119

CI Data for Non-Constant Combo: GJ4+Bel

Dose GJ4 (μM)	Dose Bel (μM)	Effect	CI
1.0	0.5	0.13	1.46827
1.0	1.25	0.30	1.46775
2.5	0.5	0.63	0.98627
2.5	1.25	0.80	0.85788

CI Data for Non-Constant Combo: 5-aza+Chae

Dose 5-aza (μM)	Dose Chae (nM)	Effect	CI
1.0	2.5	0.04	1.32691
1.0	5.0	0.22	0.68419
2.5	2.5	0.26	0.86384
2.5	5.0	0.51	0.60832

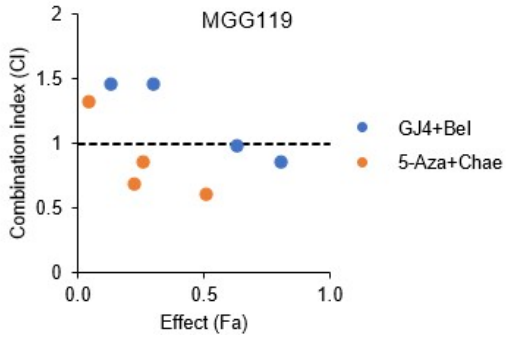

B

MGG152

CI Data for Non-Constant Combo: GJ4+Bel

Dose GJ4 (μM)	Dose Bel (μM)	Effect	CI
1.0	0.5	0.43	0.88419
1.0	1.25	0.53	0.9786
2.5	0.5	0.67	0.62316
2.5	1.25	0.86	0.44897

CI Data for Non-Constant Combo: 5-aza+Chae

Dose 5-aza (μM)	Dose Chae (nM)	Effect	CI
1.0	2.5	0.07	1.34387
1.0	5.0	0.15	1.14155
2.5	2.5	0.44	1.0255
2.5	5.0	0.62	0.84935

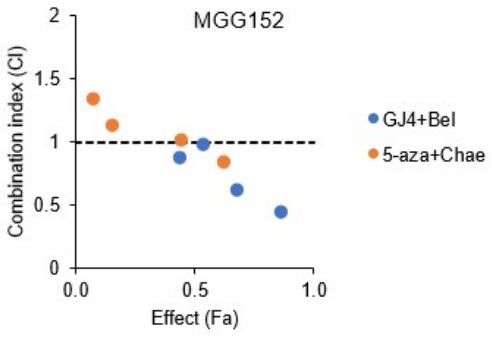

Figure 3.6 Combination index. Combination index for GSK-J4 and Belinostat or 5-azacytidine and Chaetocin co-treatments with different doses in MGG119 cells **(A)** and MGG152 cells **(B)** were calculated via CompuSyn software.

3.2 IDH1^{R132H} overexpression leads to global transcriptome alterations that are reversible with GSK864, an inhibitor of IDH^{R132H}

To examine the specific effects of IDH1 mutation on the response of IDH1 mutant glioma cells to epigenetic inhibitors, we generated a paired cell line via overexpression of mutant IDH1 (R132H point mutation) in A172 cells. Immunohistochemical staining and western blot analysis using an antibody specific to mutant IDH1 enzyme, confirmed the wild type and IDH1 mutant cells (**Figure 3.7A, 3.7B**). The production of 2-HG was pronounced in the A172 IDH1^{R132H} cells, which could be reversed with 3 days-long treatment of the IDH1 mutant cells with GSK864 an inhibitor of mutant IDH1 enzyme **(Figure 3.7C).** We observed that A172 IDH1^{R132H} cells grew slower than A172 wt cells, which was also reversible with GSK864 treatment (**Figure 3.7D**).

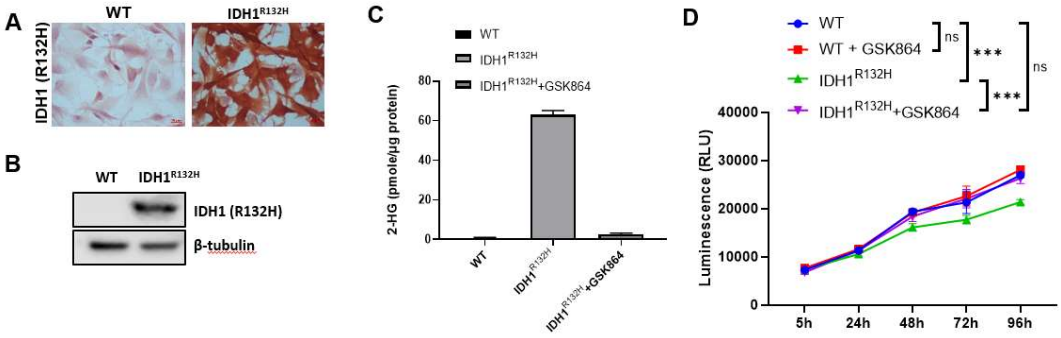

Figure 3.7 Generation of IDH-mutant glioma model via IDH1^{R132H} overexpression. Mutant IDH1 enzyme (IDH1^{R132H}) was overexpressed in A172 GBM cells to generate wild type and mutant cell pairs. Overexpression was validated via immunohistochemical staining **(A)** and western blot **(B)** using anti-IDH1 (R132H) antibody. **C)** The level of 2-HG was highly increased via IDH1^{R132H} overexpression, and blocked with GSK864 (2.5 µM), an inhibitor of mutant IDH1 enzyme. **D)** IDH1 mutation slowed down the growth of A172 cells, and this was recovered with GSK864. p-values were determined by 2-way ANOVA; ns, non-significant; *p < 0.05; **p < 0.01; ***p < 0.001.

To further examine the molecular differences between the A172 wt and A172 IDH1^{R132H} cells, we assessed the transcriptome differences in these cells by RNA sequencing. To this end, cells were grown with or without GSK864 prior to sequencing in order to dissect out mutant IDH1 driven differences between them **(Figure 3.8A).** Accordingly, A172 wt and A172 IDH1^{R132H} cells displayed high number of differentially expressed genes (DEGs), which was reduced in the presence of GSK864 **(Figure 3.8B)**. The MA plots showed that differential gene expression was most pronounced in the comparison of wt and IDH1^{R132H} cells and also in the comparison of IDH1^{R132H} cells treated or not treated with GSK864. However, there were not high number of DEGs in the comparison of wt cells that were treated or not treated with GSK864 (**Figure 3.8C**). In support of this finding, heat maps and cluster diagrams revealed that the highest change was between the wt and IDH1^{R132H} cells (**Figure 3.8D**). Accordingly, gene expression pattern was altered upon GSK864 treatment of IDH1^{R132H} cells and got closer to that of wt cells. qRT-PCR analysis confirmed the upregulation or downregulation of selected genes in the IDH1^{R132H} cells, which were also reversible with GSK864 treatment (**Figure 3.9**). Interestingly, Gene Set Enrichment Analysis (GSEA) [212] revealed that hallmark pathways that were activated in IDH1^{R132H} cells compared to wild type cells were inhibited in the presence of GSK864 in IDH1^{R132H} cells (**Figure 3.10).** These

pathways included several inflammation related networks such as "Interferon alpha response", "TNFa signaling via NFKB", "Interferon gamma response", "Inflammatory response", as well as cell stress related networks such as "Hypoxia", "P53 pathway", and "Unfolded protein response" (**Figure 3.10A)**. Enrichment plots for "Interferon alpha response" and "Unfolded protein response" showing that both pathways are significantly upregulated in IDH1^{R132H} cells and conversely, significantly downregulated with GSK864 treatment (**Figure 3.10B**).

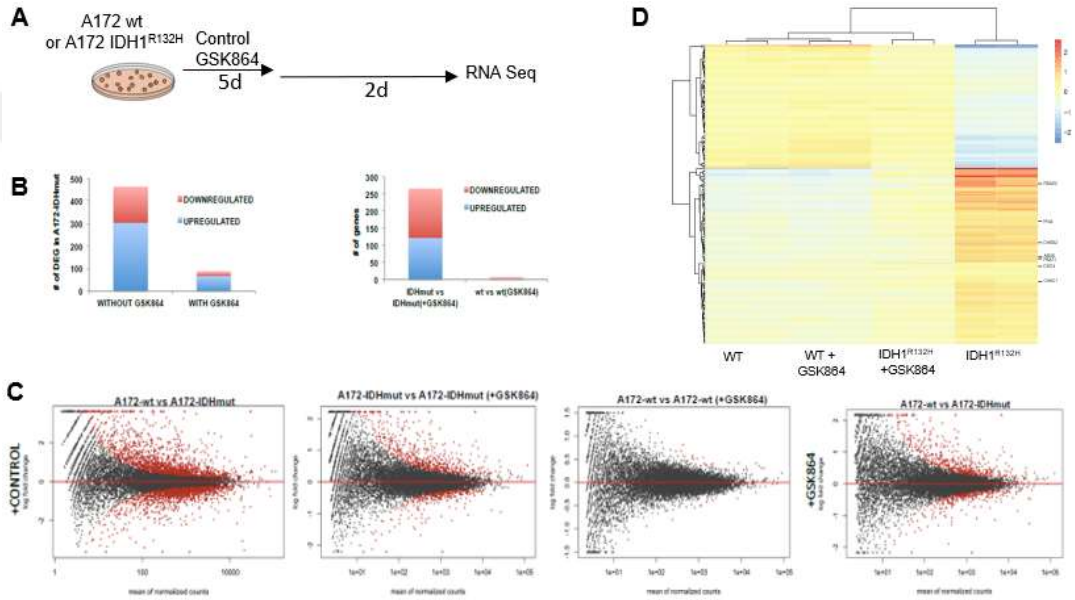

Figure 3.8 RNA sequencing of A172 wt and A172 mut cells. A) Scheme for treatment and sample collection for sequencing. **B)** Left graph showing drastic decrease in the numbers of differentially expressed genes (DEGs) in IDH1^{R132H} overexpressed A172 cells with GSK864 treatment. Right graph showing global effect of GSK864 on IDH1^{R132H} overexpressed cells while it has almost no effect on wild type cells. **C)** MA plots showing the DEGs upon IDH1^{R132H} overexpression in the absence or presence of GSK864. Significantly different counts were shown in red.

A

	Log2 fold changes in RNA-seq	
	WT vs IDH1^{R132H}	IDH1^{R132H} vs. IDH1^{R132H} with GSK864
IFI44L	5.17	-3.04
RSAD2	4.99	-3.16
WNT7B	3.80	-2.27
IFIT1	3.49	-3.01
DHRS2	3.46	-2.62
ITGA2	1.89	-2.07
RARRES2	-1.22	2.13
COL3A1	-3.04	2.85
COL1A2	-3.52	2.57

B

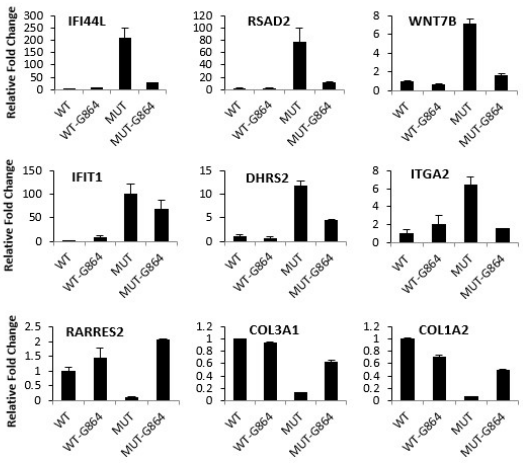

Figure 3.9 RNA-seq validations. The log2 fold changes of highest ranking DEGs in RNA-seq analysis of wild type and IDH1^{R132H} samples **(A)**, and their validation with qRT-PCR **(B)**.

A

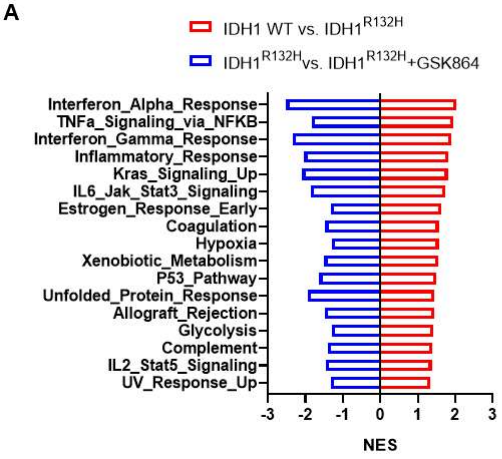

B

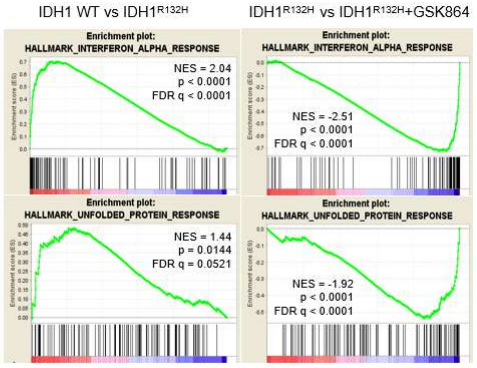

Figure 3.10 GSEA analysis. A) GSEA results showing hallmark pathways changing upon IDH1^{R132H} overexpression. All pathways upregulated with IDH1^{R132H} were downregulated with GSK864. NES, normalized enrichment score. **B)** Interpheron alpha response and unfolded protein response pathways were significantly activated with IDH1^{R132H} and inhibited with GSK864. FDR, false discovery rate. p-values were determined by 2-way ANOVA; ns, non-significant; *p < 0.05; **p < 0.01; ***p < 0.001.

Taken together, these results suggest that A172 wt and A172 IDH1^{R132H} cell line pair provided a comprehensive model to study the effects of IDH1 mutation in glioma. Testing the epigenetic inhibitors on this cell line pair, we observed that A172 IDH1^{R132H} cells were equally sensitive to 5-azacytidine or Chaetocin as A172 wt cells. However,

IDH1 mutant cells were significantly more sensitive to GSK-J4 or Belinostat then A172 wt cells **(Figure 3.11).** This was also evident in another cell line pair that we established similarly, namely LN18 wt and LN18 IDH1^{R132H} cells **(Figure 3.12).** Together, these results suggested that IDH1 mutant cells were more vulnerable to GSK-J4 or Belinostat treatment than wt or non-malignant cells.

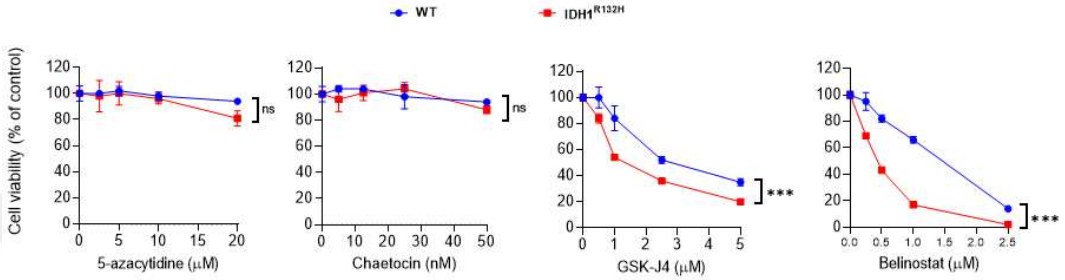

Figure 3.11 Individual drug treatment of generated wild type and IDH1^{R132H} cells. A172 wild type and IDH1^{R132H} overexpressed cells were treated with screen hits individually at different doses for 72h. IDH1^{R132H} cells were more sensitive to GSKJ4 and Belinostat than wild type cells. p-values were determined by 2-way ANOVA; ns, non-significant; *p < 0.05; **p < 0.01; ***p < 0.001.

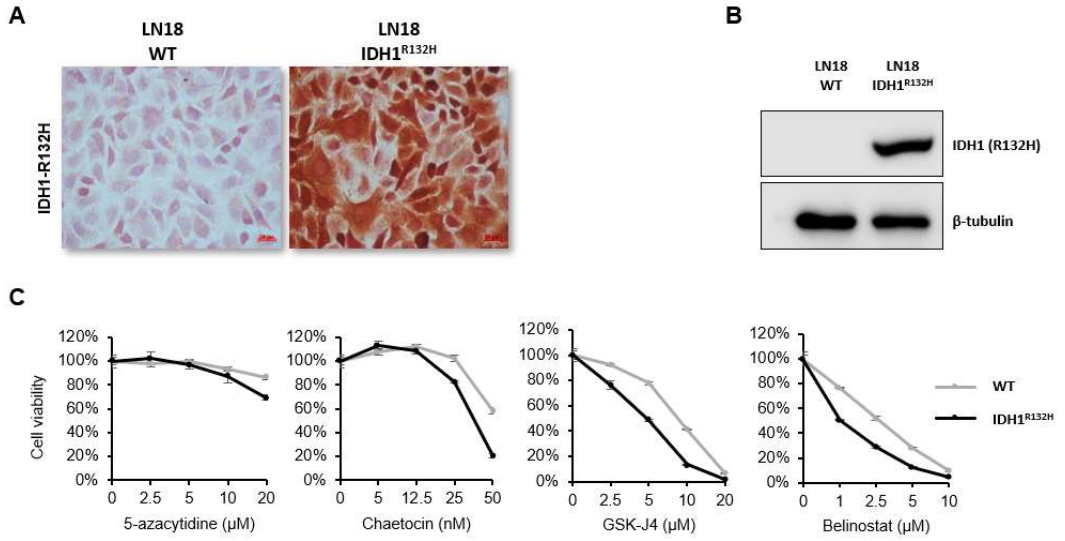

Figure 3.12 Generation of IDH-mutant LN18 cell line. Mutant IDH1 enzyme (IDH1^{R132H}) was overexpressed in LN18 GBM cells to generate wild type and mutant pairs. Overexpression was validated via immunohistochemical staining **(A)** and western blot **(B)** using anti-IDH1 (R132H) antibody. **C)** LN18 wild type and IDH mutant cells were treated with screen hits individually at different doses for 72h.

3.3 GSK-J4 and Belinostat combination selectively targets IDH1 mutant glioma cells

To assess the combinatorial efficacy of GSK-J4 and Belinostat in IDH1 mutant glioma cells, we applied each compound individually or in combination to the established cell line pairs and measured cell viability. Accordingly, GSK-J4 and Belinostat combination significantly reduced the viability of IDH1 mutant cells in a synergistic manner. On the contrary, the reduction in cell viability was not to the same extent in wt cells (**Figure 3.13)**. As a non-malignant control, viability of human astrocytes was not affected significantly from either individual or combination drug treatment (**Figure 3.14**).

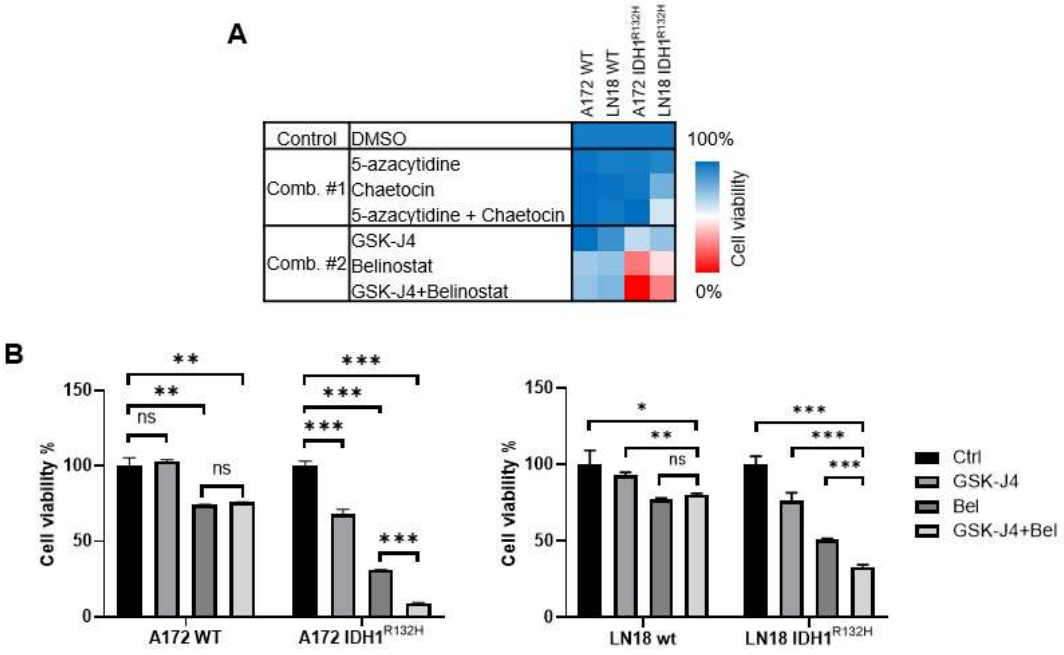

Figure 3.13 Combination treatment on A172 and LN18 cells. A) Heatmap of the effect of drug combinations on viability of A172 and LN18 wt and IDH1^{R132H} overexpressed cell pairs. **B)** GSK-J4 and Belinostat combination was highly effective on IDH1^{R132H} overexpressed A172 and LN18 cells, while it did not cause an additional effect on wild type cells. p-values were determined by unpaired t test; ns, non-significant; *p < 0.05; **p < 0.01; ***p < 0.001.

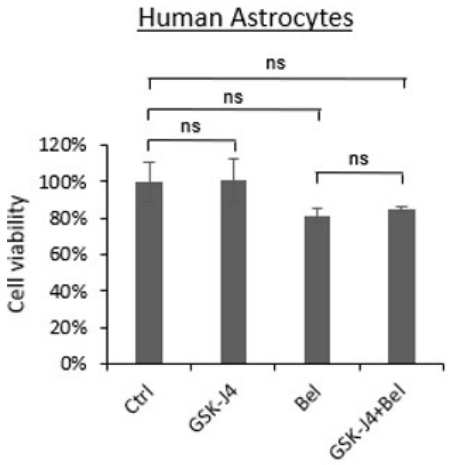

Figure 3.14 Effects of drugs on human astrocytes. Viability of normal human astrocytes (NHA) were not affected significantly from individual or combinational treatment of GSK-J4 (2.5 uM) and Belinostat (1 uM). For all panels, p-values were determined by unpaired t test; ns, non-significant; *p < 0.05; **p < 0.01; ***p < 0.001.

To further visualize the differential effects of GSK-J4 and Belinostat on wt and IDH1 mutant cells, we monitored cells with a live cell imaging system up to 96h after treatment (**Figure 3.15A)**. Quantification of the number of live cells at 0h, 24h, 48h, 72h and 96h for each condition demonstrated that IDH1 mutant cells were more vulnerable to GSK-J4 and/or Belinostat treatment than wt cells (**Figure 3.15B**). As evident in both the videos and the graphs, GSK-J4 and/or Belinostat treatment modestly affect the growth of wt cells, causing no detectable cell death. However, individual GSK-J4 treatment on IDH1 mutant cells slowed their growth, and individual Belinostat treatment led to death of few of these cells (**Figure 3.15).** Moreover, combination of GSK-J4 and Belinostat led to marked induction of cell death starting at 24 hours after treatment and complete eradication of tumor cells at 72 hours (**Figure 3.15**). These potent selective effects of GSK-J4 and/or Belinostat treatment on A172 IDH1^{R132H} cells were further investigated with co-culture experiments of tumor cells and fibroblasts (**Figure 3.16)**. A172 IDH1^{R132H} cells labelled with mCherry and Fibro2 cells labelled with GFP plasmids were admixed and then treated with compounds individually or in combination. After culturing these cells for 5 days, fibroblasts remained viable under all conditions, whereas A172 IDH1^{R132H} cells were significantly reduced in number after treatment (**Figure 3.16**). The selective sensitivity of A172 IDH1^{R132H} cells to GSK-J4 and Belinostat combination could be reversed with pre-treating cells with GSK864, while it

has no effect on drug response of wild type cells (**Figure 3.17)**. Together, these results suggest that IDH1 mutant glioma cells are more vulnerable to GSK-J4 and Belinostat treatment.

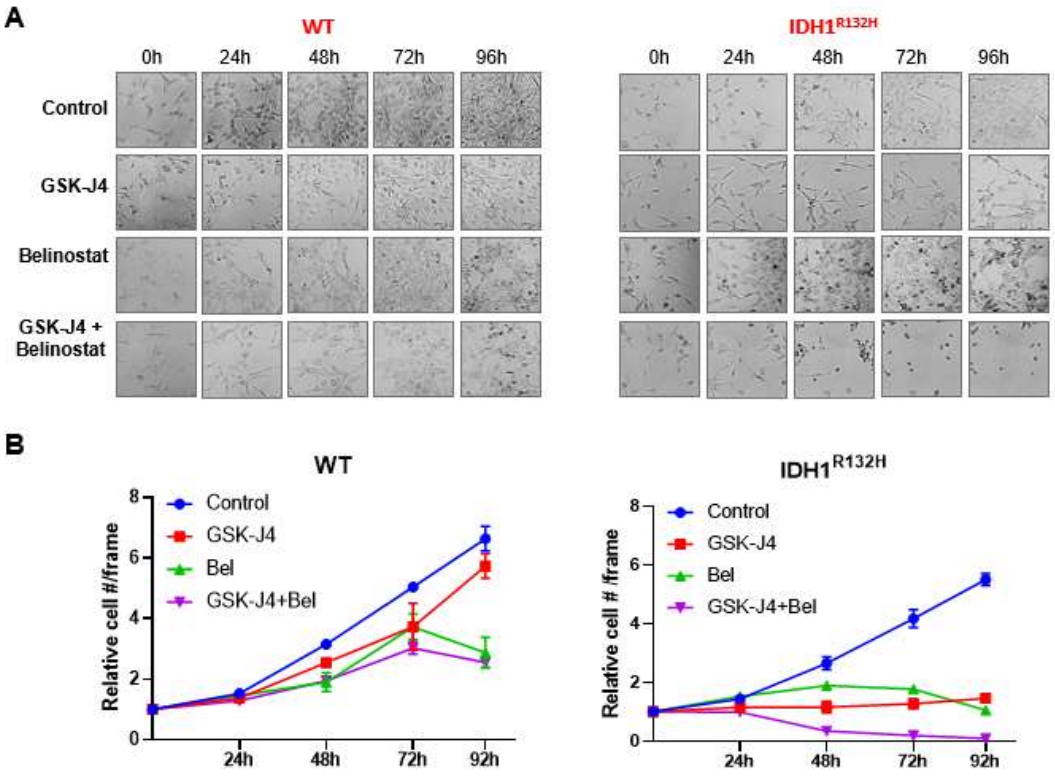

Figure 3.15 Live cell imaging. A) Live cell images of A172 wild type and IDH1^{R132H} mutant cells after 0h, 24h, 48h, 72h and 96h of control, GSK-J4 (2.5 µM), Belinostat (1 µM) or GSK-J4 + Belinostat combination treatments. **B)** Quantification of live cell images indicate that IDH1^{R132H} cells were completely eliminated with GSK-J4 + Belinostat combination, while few cells were dead in wild type cells.

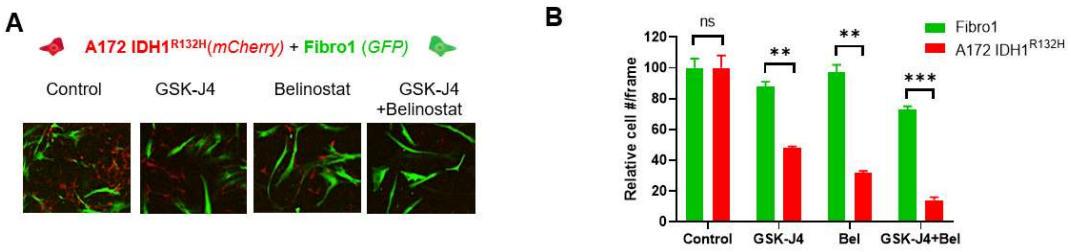

Figure 3.16 IDH-mutant GBM and fibroblast co-culture. A) mCherry-labelled IDH mutant A172 cells were co-cultured with GFP-labelled fibroblasts and treated with GSK-J4 and Belinostat individually and in combination. **B)** Quantification of co-culture images indicated that fibroblasts were not markedly affected by either GSK-J4, Belinostat or combination. However, A172 IDH mutant cells diminished after individual or combination treatments. p-values were determined by unpaired t test; ns, non-significant; *p < 0.05; **p < 0.01; ***p < 0.001.

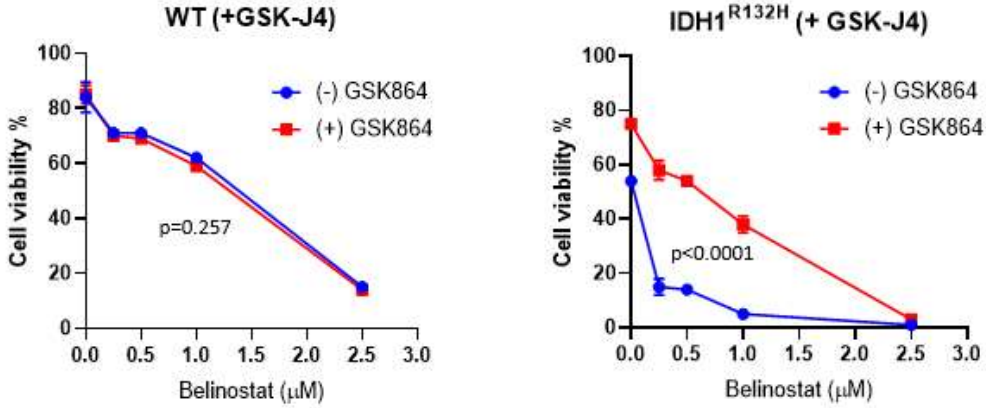

Figure 3.17 Effect of mutant IDH inhibitor (GSK864) on drug response. GSK864 (2.5 μM) pre-treatment recovered sensitivity of IDH mutant A172 cells against GSK-J4 and Belinostat treatments, while it has no effect on IDH wild type A172 cells. Horizontal axis represents increasing concentration of Belinostat in the presence of 2.5 μM of GSK-J4. p-values were determined by 2-way ANOVA test.

3.4 GSK-J4 and Belinostat combination leads to cell cycle arrest and apoptosis in IDH1 mutant glioma cells

To address the mechanism behind the observed reduction in cell viability upon combinatorial treatment, we first investigated the cell cycle distribution of glioma cells. Flow cytometric measurements with PI staining showed that both GSK-J4 and Belinostat

caused a cell cycle arrest in all IDH mutant cells (**Figure 3.18**). While GSK-J4 caused modest changes in cell cycle, Belinostat, caused a G2/M arrest in both the primary MGG119, MGG152 cells as well as A172 IDH1^{R132H} cells. We then investigated caspase activity of glioma cells. While GSK-J4 or Belinostat as single agents only moderately increased Casp3/7 activity, combinatorial treatment resulted in major elevation of Casp3/7 activity in A172 IDH1^{R132H} cells (**Figure 3.19A**). Application of general caspase inhibitor Z-VAD-FMK on tumor cells recovered the GSK-J4 and Belinostat induced decrease in cell viability (**Figure 3.19B).** Cleavage of Poly (ADP-ribose) polymerase-1 (PARP-1), an important hallmark of apoptosis, was also markedly enhanced upon combinatorial treatment in A172 IDH1^{R132H} cells but not in A172 wt cells (**Figure 3.20A**). This was also evident for MGG152 primary cells (**Figure 3.20B).** With a fluorescence dye-based "live/dead assay" utilizing YO-PRO-1 staining, we observed significant number of apoptotic cells upon combinatorial treatment in A172 IDH1^{R132H} cells (**Figure 3.21A).** Similarly, counting the number of live and dead cells in the media collected from treated cultures, we observed a significantly higher number of cells undergoing cell death upon combination of GSK-J4 and Belinostat in A172 IDH1^{R132H} cells (**Figure 3.21B)**. The number of the alive cells detached from surface to the medium which may be a marker for anoikis, were also higher in IDH1^{R132H} cells. To further investigate the changes in apoptotic machinery in glioma cells, we examined the expression levels of anti-apoptotic proteins Bcl-xL and XIAP. Accordingly, Belinostat decreased XIAP expression levels in all cells tested, and the Bcl-xL levels in the IDH1 mutant cells (**Figure 3.20**). Indeed, overexpression of Bcl2 or Bcl-xL partly recovered the GSK-J4 and Belinostat induced cell death in primary MGG152 cells (**Figure 3.22A**). Bcl-xL overexpression was slightly more effective for recovery. Even if up to lesser degree, A172 IDH1^{R132H} cells were also partly recovered from drug effects by overexpression of Bcl-xL (**Figure 3.22B**). Taken together, these results suggest that GSK-J4 and Belinostat induced reduction in cell viability involves the activation of apoptotic programs in IDH1 mutant cells.

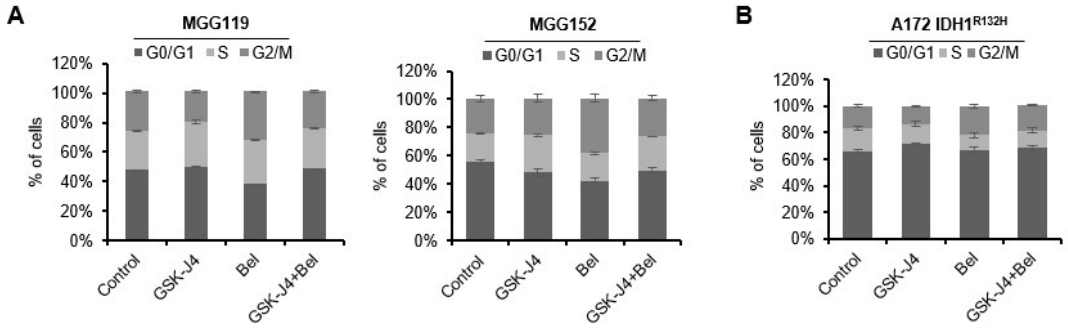

Figure 3.18 Cell cycle analysis. A) Cell cycle analysis of MGG119 and MGG152 primary cells indicated that GSK-J4 causes cell cycle arrest in S phase, and Belinostat causes a G2/M arrest after 24h of treatment. **B)** In IDH1^{R132H} overexpressed A172 cells, GSK-J4 causes cell cycle arrest in G0/G1 phase, and Belinostat causes an G2/M arrest after 24h of treatment.

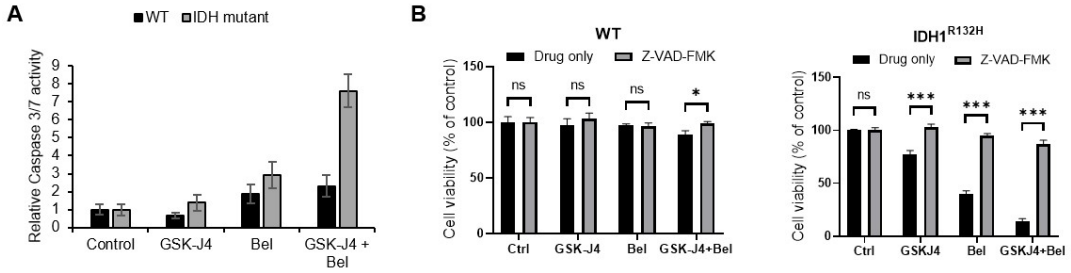

Figure 3.19 Caspase activity and inhibition assays. A) Caspase-Glo 3/7 activity assay showed that GSK-J4 and Belinostat combination treatment highly increased the Caspase 3/7 activity of IDH mutant A172 cells, compared to wild type cells. **B)** Z-VAD-FMK, a general caspase inhibitor, recovered the effects of GSK-J4 and Belinostat treatments on the viability of IDH mutant A172 cells. p-values were determined by unpaired t test; ns, non-significant; *p < 0.05; **p < 0.01; ***p < 0.001.

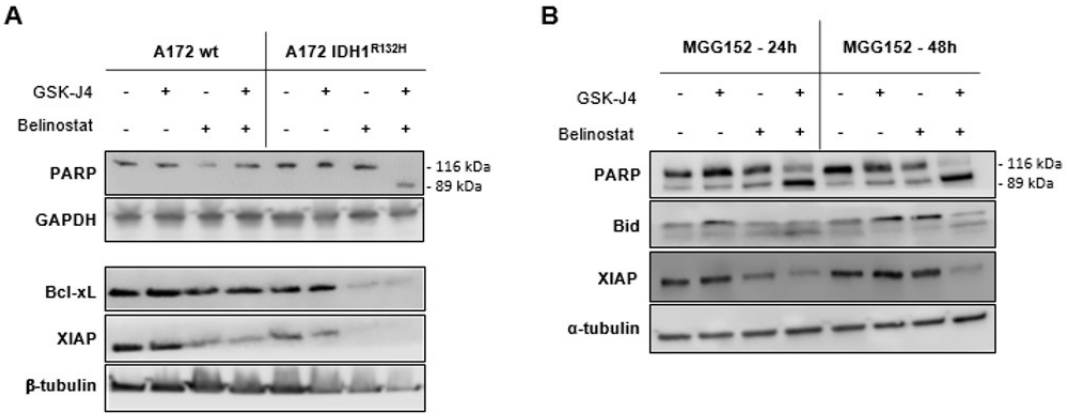

Figure 3.20 Western blot analysis for pro-apoptotic and anti-apoptotic markers. A) PARP cleavage was pronounced in western blots of IDH mutant A172 cells upon GSK-J4 and Belinostat co-treatment. Belinostat, individually or in combination, caused a decrease in level of anti-apoptotic Bcl-xL and XIAP proteins, especially in the IDH1^{R132H} cells. **B)** GSK-J4 and Belinostat combination induced PARP and Bid cleavage and reduced the XIAP level which are indicating the apoptosis in MGG152 cells. Cleavage and reduction level increased at 48h compared to 24h.

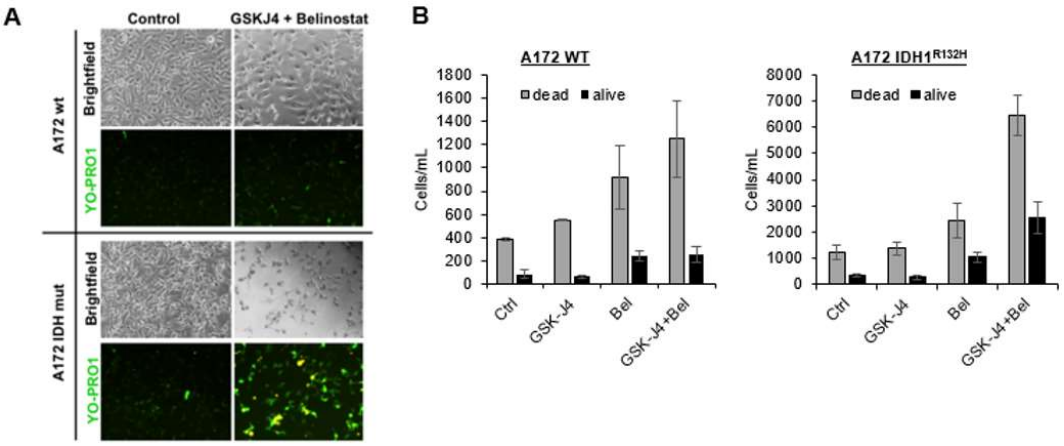

Figure 3.21 YO-PRO1 and anoikis assays. A) YO-PRO1 staining indicated cells undergoing apoptosis in A172 wt and A172 IDH mutant cells. A172 IDH mutant cells display more YO-PRO1 positive staining upon GSK-J4 and Belinostat treatment. **B)** As an indicator of anoikis, the number of both dead and alive cells were higher in the collected media of A172 IDH mutant cells after 24h of treatment with GSK-J4 and Belinostat combination.

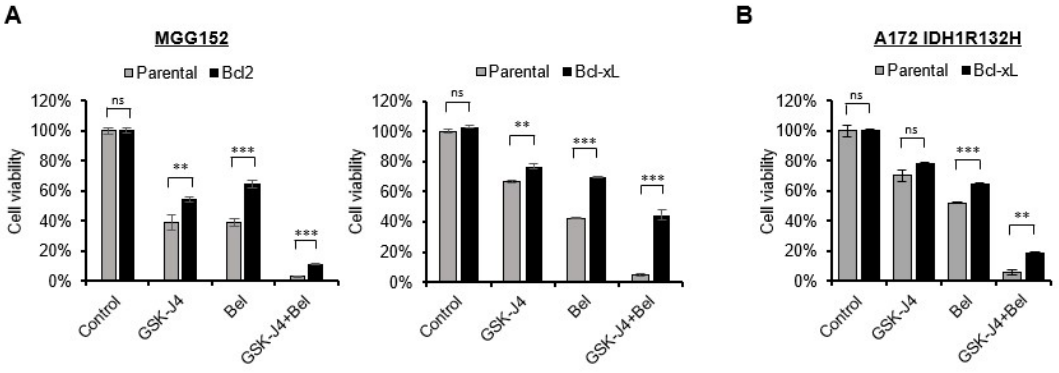

Figure 3.22 Recovery studies via Bcl-xL overexpression. A) Primary IDH1-mutant MGG152 cells were partially recovered from drug effects via overexpression of anti-apoptotic Bcl2 or Bcl-xL proteins. **B)** Similarly, drug effects on A172 IDH1^{R132H} cells were slightly recovered by Bcl-xL overexpression. p-values were determined by unpaired t test; ns, non-significant; *p < 0.05; **p < 0.01; ***p < 0.001.

3.5 RNA-seq analysis on 1°IDH1 mutant glioma cells reveals global changes and stress response activation upon GSK-J4 and Belinostat treatment.

In order to comprehensively assess the mechanism behind GSK-J4 and Belinostat induced cell death in IDH1 mutant cells, we performed global transcriptomic analysis in MGG152 cells upon treatment with compounds individually or in combination for 2 days (**Figure 3.23A)**. GSK-J4 and/or Belinostat treatment led to a high number of DEGs (**Figure 3.23B)**. There were overlapping genes between treatments (**Figure 3.23C)**. While individual treatments caused significant alterations in transcriptome, most changes were observed with the combination treatment. Principle component analysis (PCA) showed distinct clustering of samples from each condition (**Figure 3.23D**). qRT-PCR analysis validated the differential regulation of selected genes upon with individual or combined GSK-J4 and Belinostat treatment of MGG152 cells (**Figure 3.24**). GSEA analysis indicated many hallmark pathways deregulated with each treatment (**Figure 3.25)**. Interestingly, some pathways were distinct between GSK-J4 and Belinostat individual treatments (**Figure 3.26),** however some were commonly altered (**Figure 3.25).** The commonly altered networks included activation of "Epithelial-mesenchymal transition", "TNFa signaling by NFkB", "Hypoxia", "Xenobiotic metabolism", and "UV-response-dn"; and inhibition of "Myc targets, E2F targets", and "G2M checkpoint" among others. Major downstream changes were observed upon GSKJ4 exclusively,

including "Activation of genes by ATF4" and "Unfolded Protein Response". Given the numerous cell stress-related pathways observed, we further focused on characterizing stress-response as a candidate underlying mechanism for selective vulnerability of IDH1 mutant cells for GSKJ4 and Belinostat.

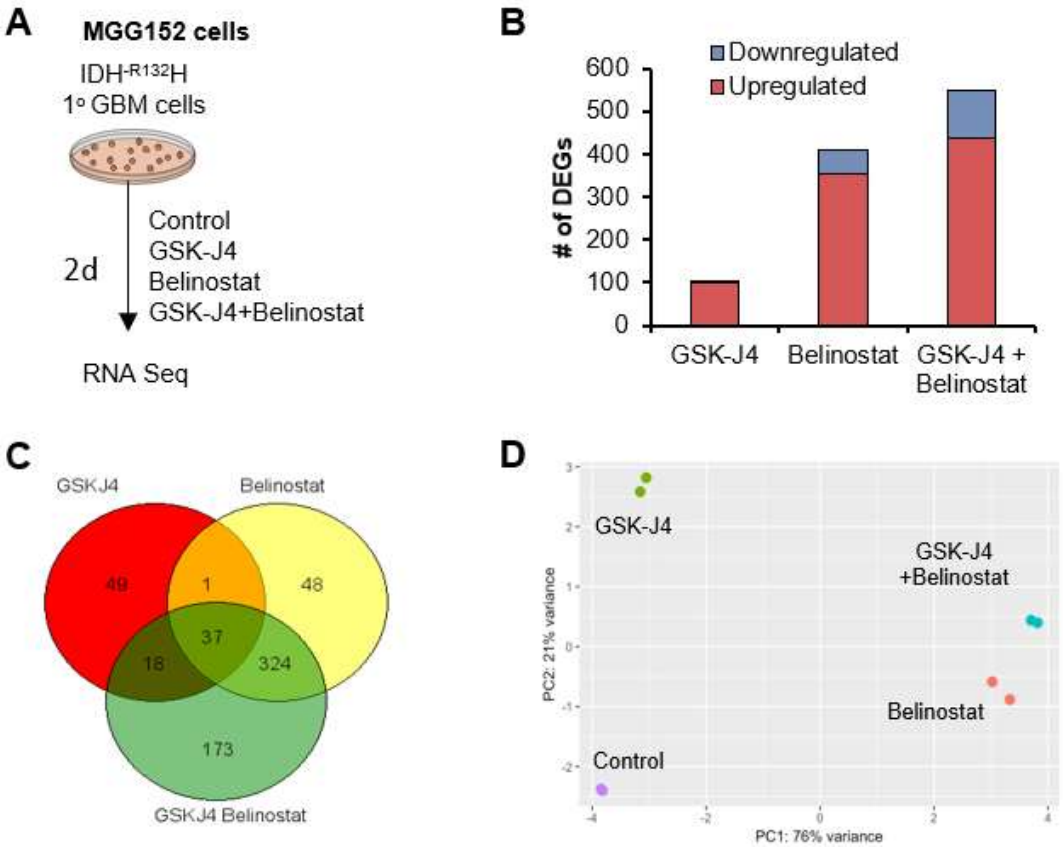

Figure 3.23 RNA-seq analysis on 1ºIDH mut GBM cells. A) Scheme for treatment and sample collection for sequencing. **B)** Graph showing the number of differentially regulated genes (DEGs). **C)** Venn Diagram showing the number of common genes altered in different treatment conditions. **D)** Principal component analysis of samples treated with GSKJ4 and/or Belinostat.

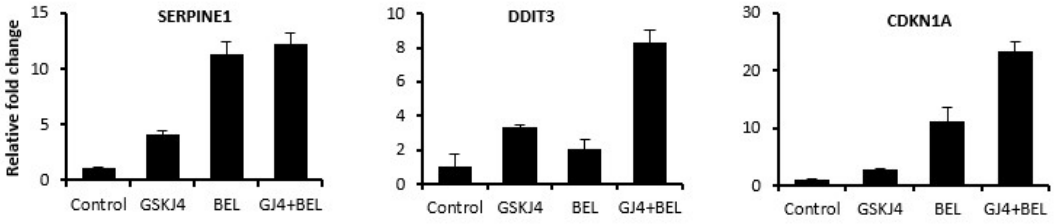

Figure 3.24 RNA-seq validations. qRT-PCR results of genes selected from different pathways for validation of RNA-seq analysis. Expression level of selected genes increased by individual treatments and further increased by combination treatment.

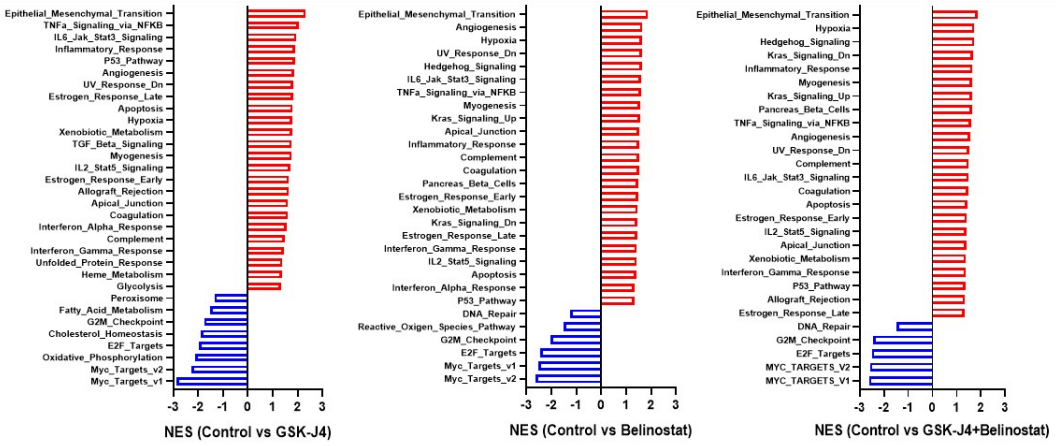

Figure 3.25 GSEA analysis. GSEA output showing the hallmarks that were specifically enriched in DEGs. Inset shows the GSEA hallmark pathways commonly deregulated in all 3 conditions. NES, normalized enrichment score.

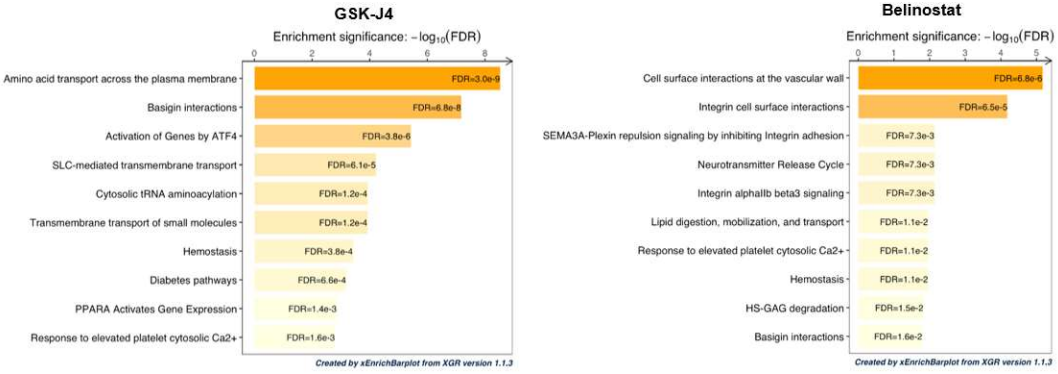

Figure 3.26 Reactome analysis. The bar graphs showing the top 10 enrichments in the reactome pathways database with GSK-J4 or Belinostat. The false discovery rate (FDR) is also displayed.

Given that ATF4 is a major transcription factor that upregulates survival pathways under stress conditions, or apoptotic pathways under severe stress [185], we first examined the changes in ATF4 signaling in IDH1 mutant cells treated with GSK-J4 and/or Belinostat. Accordingly, we observed ATF4 upregulation in both mRNA (**Figure 3.27A**) and protein level (**3.28A**) upon GSK-J4 treatment. Expression of known ATF4 targets such as *ASNS, DDIT4*, *PSAT1, ATF5 and DDIT3* was also upregulated upon GSK-J4 treatment (**Figure 3.27A**). The changes in ATF4 signaling components were majorly affected by GSK-J4, but not Belinostat treatment. On the contrary, the effects of Belinostat was pronounced on anti-apoptotic and cell-cycle related gene expression. Specifically, expression of the anti-apoptotic genes, such as *BCL2L1*/Bcl-XL and *BIRC5*/Survivin was decreased, and major cell cycle regulator *CDKN1A*/p21 was increased upon Belinostat treatment (**Figure 3.27B).** Interestingly, Belinostat also downregulated the *ATF5* gene which is shown to be responsible for survival under stress conditions [213] (**Figure 3.27B**). Increase in p21 protein levels was also evident upon Belinostat treatment in the western blots, where the hyperacetylation of α-tubulin served as positive control (**Figure 3.28A**). SUnSET assay also indicated significant decrease in global translation rate [204], which is a cell stress indicator, in primary GBM cells upon GSK-J4 treatment either individually or in combination. (**Figure 3.28B**). Together, these results suggested that while GSK-J4 activates ATF4 mediated stress response pathways, Belinostat activates cell cycle arrest and inhibits anti-apoptotic pathways, resulting in eradication of IDH1 mutant glioma cells.

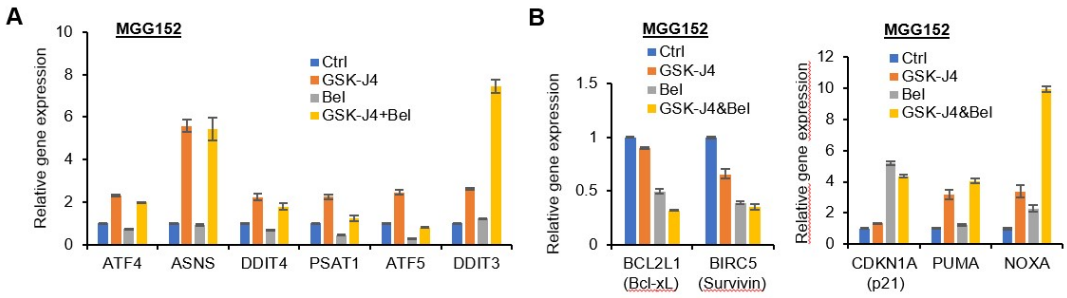

Figure 3.27 qRT-PCR validation for activation of stress response and apoptotic pathways. A) The genes involved in ATF4 mediated unfolded protein response (UPR) pathway were upregulated with GSK-J4 and combination treatment in MGG152 cells. **B)** The genes involved in apoptosis and cell cycle pathways were deregulated with GSK-J4 and Belinostat in MGG152 cells.

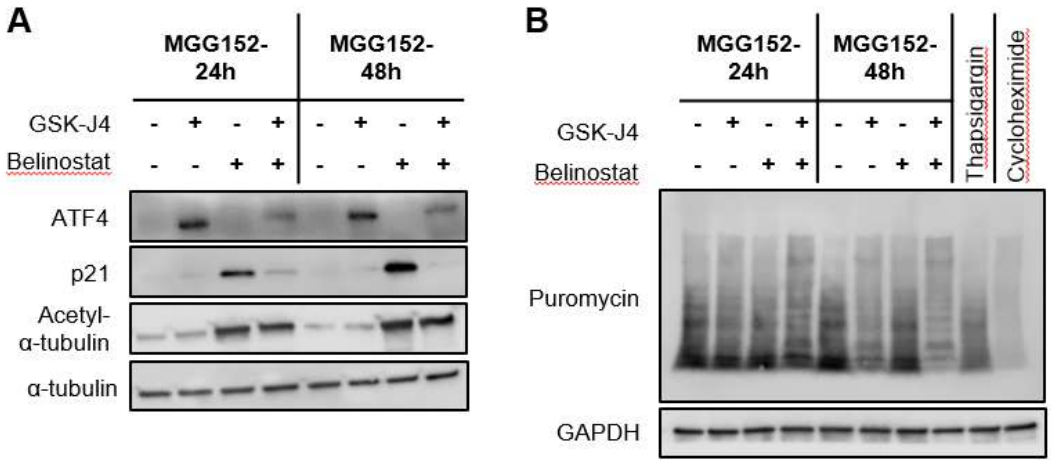

Figure 3.28 Western blot and SUnSET assays. A) Western blot images showing effects of GSK-J4 and Belinostat on ATF4, CDKN1A/p21 and acetyl-α-tubulin after 24h and 48h of treatments in MGG152 cells. **B)** SUnSET assay showing drug effects on global translation levels after 24h and 48h in MGG152 cells. GSK-J4 decreased global translation after 48h of treatment. Thapsigargin (5 μM) and cycloheximide (5 μM) were used as positive controls.

3.6 Blocking stress response protects IDH1 mutant glioma cell from GSK-J4 and Belinostat induced cell death

Given our finding that ISR is activated in IDH1 mutant cells because of the increased cellular stress conferred by epigenetic drug treatment, we sought to address the necessity of ISR in this vulnerability. To this end, we applied ISRIB, an inhibitor of integrated stress response, to IDH1 mutant glioma cells and observed significant protection of cells from GSK-J4 and Belinostat induced death (**Figure 3.29A**). PERKi, inhbitor of endoplasmic reticulum kinase PERK, which is activated during ER stress, provided only slight recovery upon drug treatment (**Figure 3.29B**). Similarly, ISRIB partially recovered $IDH1^{R132H}$ overexpressed cells especially from GSK-J4 induced death (**Figure 3.29C**). Similar with innately IDH1 mutant glioma cells, stress response genes were significantly upregulated in $IDH1^{R132H}$ overexpressed cells upon GSK-J4 and Belinostat treatment (**Figure 3.30**). On the other hand, these increases in gene expressions were blocked in the presence of GSK864. Compared to wild type cells, $IDH1^{R132H}$ overexpressed cells were also much more sensitive to Thapsigargin treatment which is recovered by GSK864 pre-treatment (**Figure 3.31**).

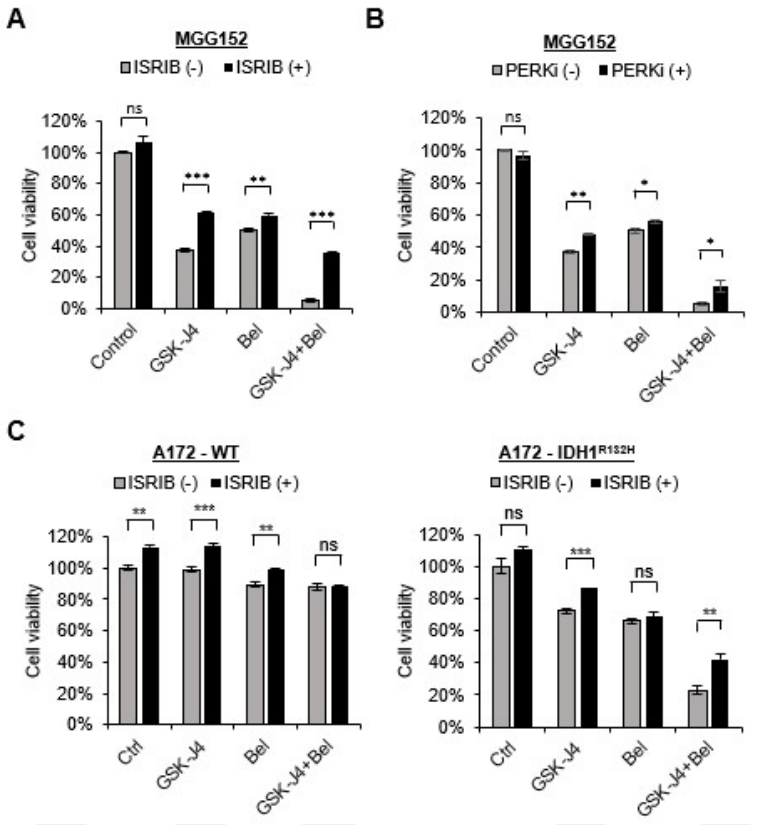

Figure 3.29 Recovery effects of ISRIB on drug response. A) ISRIB (1 μM), an inhibitor of integrated stress response pathway, partially prevented cytotoxic effects of GSK-J4 and Belinostat on MGG152 cells. **B)** PERKi (1 μM), inhibitor of PERK enzyme which activates UPR pathway, provided a slight recovery upon drug treatments on MGG152 primary cells. **C)** ISRIB (1 μM), significantly decreased cytotoxic effects of GSK-J4 individually and in combination on A172 IDH1^{R132H} cells. p-values were determined by unpaired t test; ns, non-significant; *p < 0.05; **p < 0.01; ***p < 0.001.

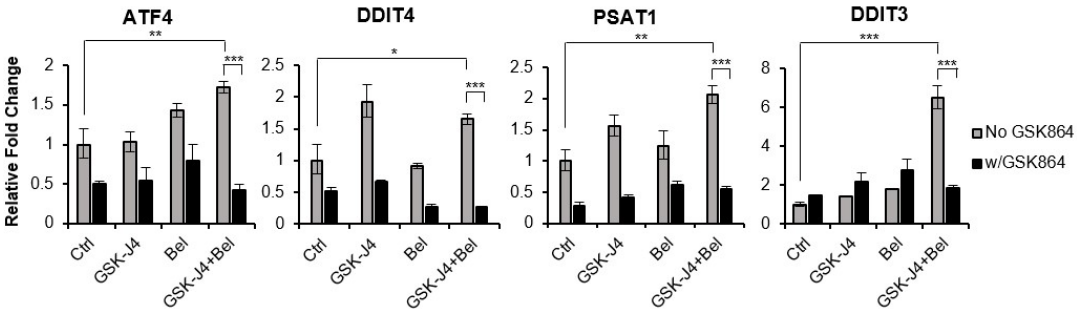

Figure 3.30 qRT-PCR analysis of stress response genes in A172 IDH1^{R132H} cells. The genes involved in ISR pathway were significantly upregulated with GSK-J4 and

Belinostat co-treatment upon IDH1^{R132H} overexpression, and they were significantly downregulated with GSK864 (2.5 μM) pre-treatment. p-values were determined by unpaired t test; ns, non-significant; *p < 0.05; **p < 0.01; ***p < 0.001.

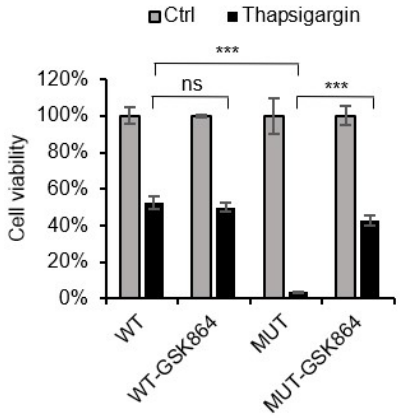

Figure 3.31 Thapsigargin treatment. IDH1^{R132H} overexpression significantly sensitized A172 cells against Thapsigargin, an ER stress inducer, and it was recovered with GSK864 treatment.

Given that *DDIT3*/CHOP is responsible for induction of apoptotic pathways under severe stress [214], we investigated its role in GSK-J4 and Belinostat induced apoptosis. To this end, we knocked out *DDIT3* gene via CRISPR/Cas9 method and validated with Sanger sequencing (**Figure 3.32**). *DDIT3* knockout did not affect the viability of cells, however it significantly protected IDH1^{R132H} cells from the both individual effect of GSK-J4 and combinatorial effect with Belinostat (**Figure 3.33**). Expression of pro-apoptotic proteins such as PUMA and NOXA, which are known to be induced during ER stress [215], did not change upon *DDIT3* knockout in the absence of drugs. On the other hand, induction of both genes was significantly inhibited upon combination treatment in *DDIT3* knockout cells (**Figure 3.34**).

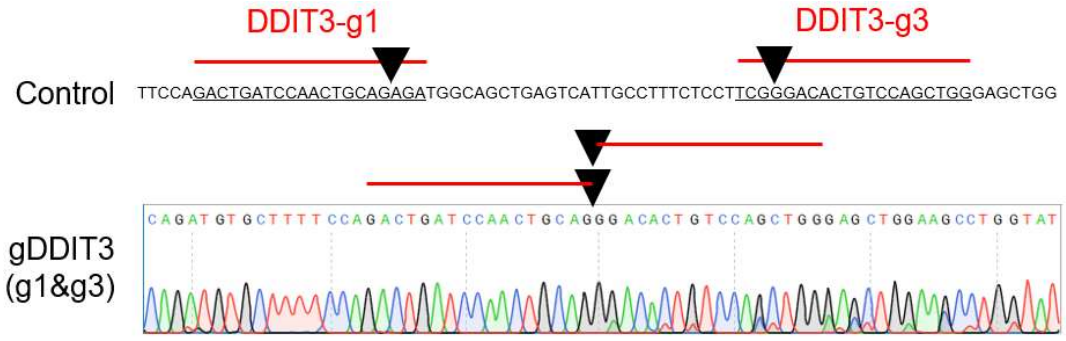

Figure 3.32 Validation of *DDIT3* knock-out. Sanger sequencing results to validate knock-out of *DDIT3* gene via CRISPR/Cas9. Red bars on the control sequence indicate regions targeted via gRNAs, and black triangles indicate the expected cleavage site. In the bottom parts, Sanger sequencing reveals deletions or frameshifts around the cleavage sites.

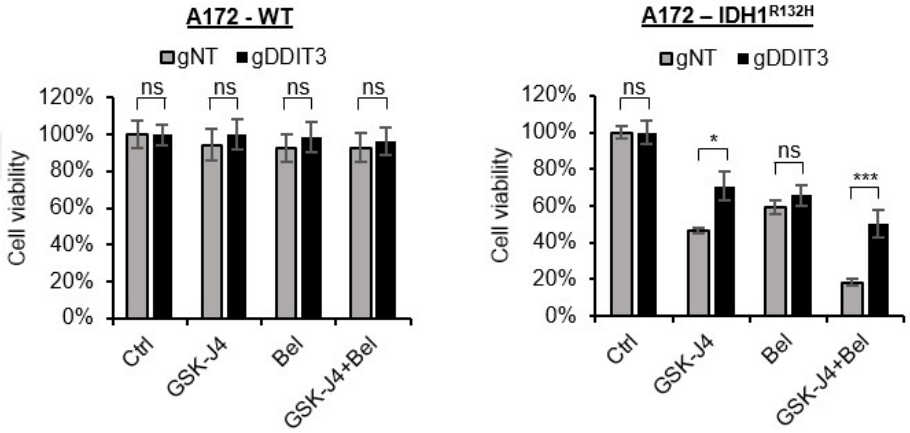

Figure 3.33 Effects of *DDIT3* knock-out on drug response. Sensitization of IDH1^{R132H} cells against GSK-J4 and combination treatment were significantly recovered upon inhibition of stress induced apoptosis via CRISPR/Cas9 mediated knock-out of *DDIT3* gene. p-values were determined by unpaired t test; ns, non-significant; *p < 0.05; **p < 0.01; ***p < 0.001.

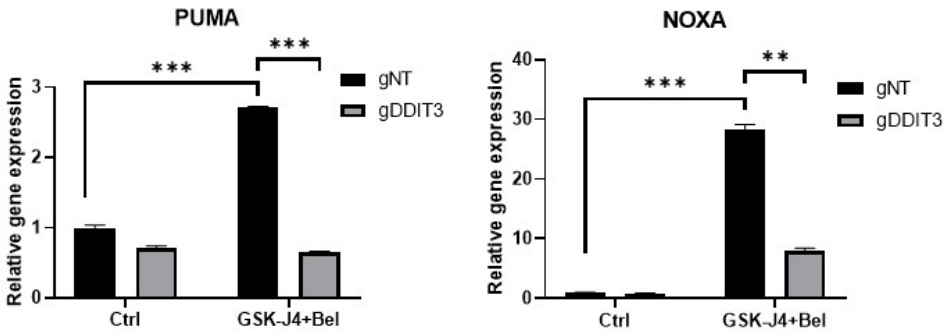

Figure 3.34 Effects of *DDIT3* knock-out on apoptotic gene activations. Knock-out of *DDIT3* gene significantly inhibited activation of pro-apoptotic genes, PUMA and NOXA, upon GSK-J4 and Belinostat combination treatment. p-values were determined by unpaired t test; ns, non-significant; *p < 0.05; **p < 0.01; ***p < 0.001.

Considering GSEA analysis indicating activated hypoxia response in $IDH1^{R132H}$ overexpressed cells (**Figure 3.10A**), we examined effects of hypoxic conditions on both wild type and IDH-mutant cells. The significant difference between growth rate (**Figure 3.35A**) and drug response (**Figure 3.35B**) of wild type and $IDH1^{R132H}$ cells became insignificant under hypoxic conditions. IDH-mutant primary cells were also grown in similar rate in hypoxia (**Figure 3.35C**). The cytotoxic effect of GSK-J4 was dissappeared under hypoxia. Belinostat, on the other hand, was more effective, especially on wild type cells under hypoxic conditions.

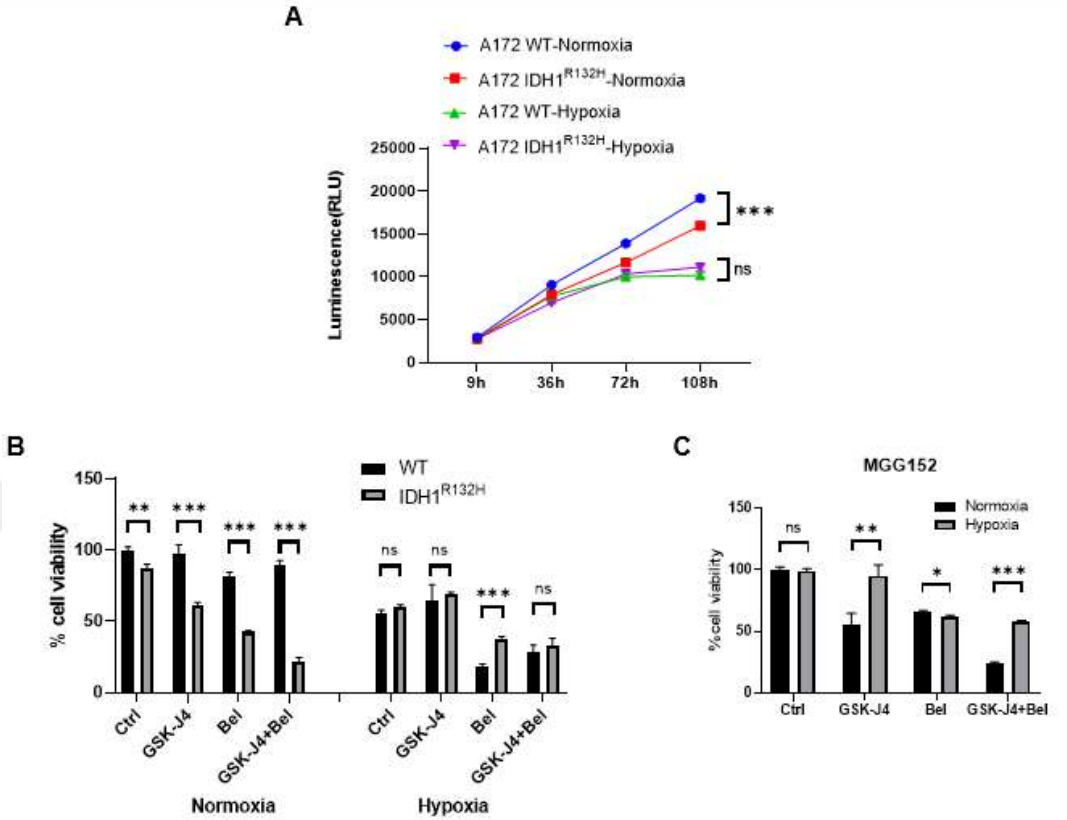

Figure 3.35 Effects of hypoxia on wild type and IDH1^{R132H} cells. A) Growth of IDH1^{R132H} overexpressed glioma cells is slower than wild type cells in normoxic conditions. However, their growth rates were similar under hypoxic conditions. **B)** IDH1^{R132H} cells were much more sensitive to GSK-J4 and Belinostat under normoxia, while their responses were similar with wild type cells in hypoxic conditions. **C)** GSK-J4 was not effective on IDH mutant primary MGG152 cells under hypoxic conditions, while Belinostat effect was similar. For panel A, p-values were determined by 2-way ANOVA test. For panels B and C, p-values were determined by unpaired t test; ns, non-significant; *p < 0.05; **p < 0.01; ***p < 0.001.

On the other hand, we checked how Temozolomide (TMZ), the frontline drug in GBM treatment, affects GSK-J4 and Belinostat treatment. IDH1 mutant cells were more sensitive to TMZ as expected [216], and effect of drugs, especially Belinostat, were more pronounced in the presence of TMZ (**Figure 3.36**). Based on GSEA results showing activation of NF-KB pathway in IDH1^{R132H} overexpressed cells (**Figure 3.10A**), we investigated the effect of QNZ, an NF-KB inhibitor on drug treatments. QNZ further sensitized IDH1^{R132H} overexpressed cells to GSK-J4 and Belinostat treatment (**Figure**

3.37A). We also checked if ferroptosis plays a role in cell death by drug treatments. Ferrostatin-1, an inhibitor of ferroptosis, did not cause any significant changes on drug sensitivity of IDH1^{R132H} overexpressed cells (**Figure 3.37B**). Considering that reactive oxygen species (ROS) is one of the well-known cellular stressors, we investigated effects of N-acetyl-L-cysteine (NAC) which is known as ROS scavenger. NAC was effective to recover Chaetocin-induced cell death, but cell response against none of the other drugs were recovered significantly via NAC (**Figure 3.38**). On the other hand, long-term treatment with GSK864, an inhibitor of mutant IDH1, caused a small but consistent acceleration in growth of primary IDH1 mutant GBM cells (**Figure 3.39A**). Moreover, drug sensitivity of MGG152 cells could be partly recovered with GSK864 (**Figure 3.39B**).

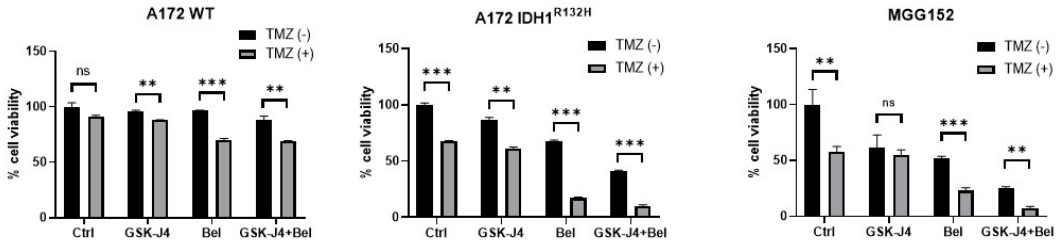

Figure 3.36 Effect of TMZ on IDH-mutant cells and their drug responses. A172 IDH1^{R132H} cells and MGG152 primary IDH mutant cells are more sensitive to Temozolomide (250 uM) when compared to A172 wild type cells. TMZ and GSK-J4 (2.5 uM) co-treatment did not show an additive effect on individual TMZ. On the other hand, Belinostat (0.5 uM) further sensitized cells, especially IDH mutant ones to Temozolomide. p-values were determined by unpaired t test; ns, non-significant; *p < 0.05; **p < 0.01; ***p < 0.001.

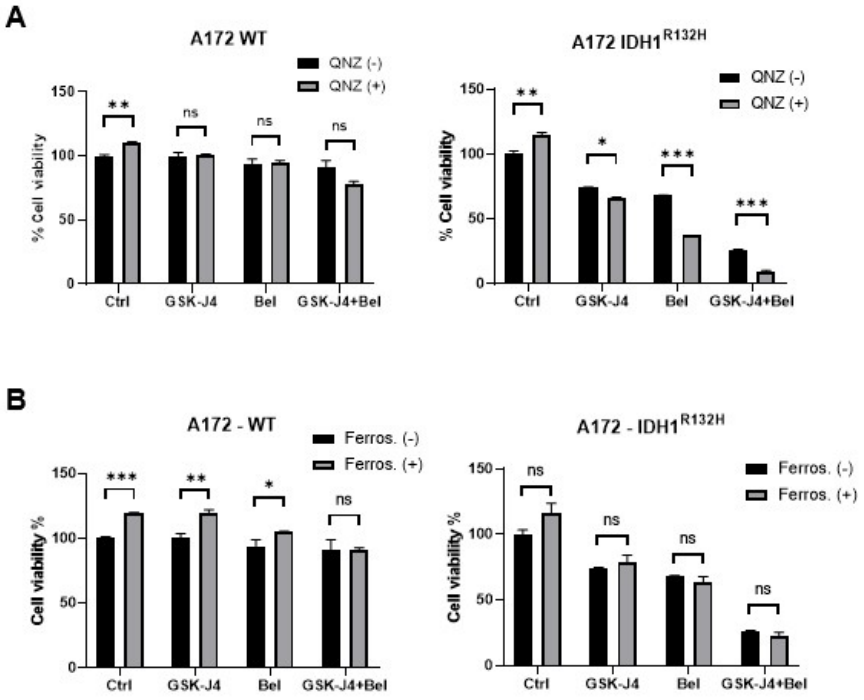

Figure 3.37 Effect of QNZ and PERKi on drug responses. A) An NF-KB inhibitor, QNZ (10 nM), increased sensitization of IDH1^{R132H} mutant cells against drugs. **B)** Ferrostatin-1 (2 μM), a ferroptosis inhibitor, did not change drug responses on IDH1^{R132H} mutant cells. p-values were determined by unpaired t test; ns, non-significant; *p < 0.05; **p < 0.01; ***p < 0.001.

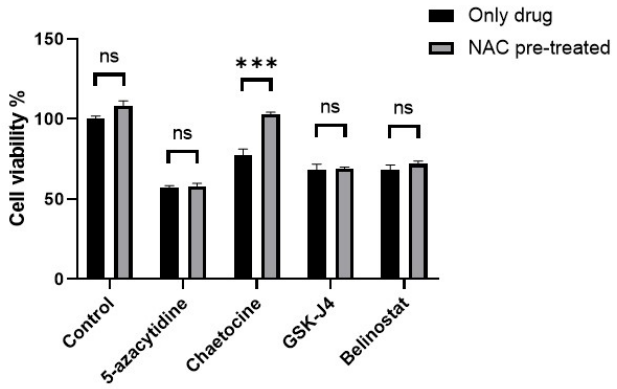

Figure 3.38 Effect of NAC on drug responses. Pre-treatment with NAC (0.2 mM) which is a ROS scavenger, recovered only Chaetocin effects on IDH1-mutant primary MGG152 cells. Responses against other drugs did not change significantly by NAC pre-treatment. p-values were determined by unpaired t test; ns, non-significant; *p < 0.05; **p < 0.01; ***p < 0.001.

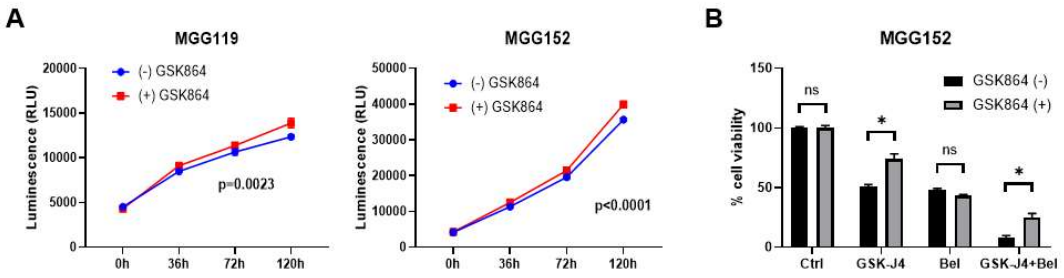

Figure 3.39 Effect of GSK864 on innately IDH-mutant primary cells. A) Mutant IDH inhibitor, GSK864 (2.5 µM), slightly increases growth rate of IDH mutant primary cells. **B)** Sensitivity of primary MGG152 cells against GSK-J4 and Belinostat treatment was slightly recovered via long-term passaging *in vitro*, in the presence of GSK864, mutant IDH inhibitor. For panel A, p-values were determined by 2-way ANOVA test. For panel B, p-values were determined by unpaired t test; ns, non-significant; *p < 0.05; **p < 0.01; ***p < 0.001.

3.7 KDM6A and KDM6B inhibition phenocopies the effects observed with GSK-J4 in IDH- mutant cells

Given the epigenetic vulnerability of IDH1 mutant cells, we assessed the major global changes in chromatin marks in cells treated with GSK-J4 and/or Belinostat. To this end, H3K4me3, H3K9me3, H3K27me3 and H3K27ac histone modifications in A172 wild type and IDH1^{R132H} cells, and MGG152 IDH1 mutant primary cells were analyzed via western blot (**Figure 3.40**). All analyzed histone methylations were increased in IDH1 mutant A172 cells compared to wild type cells. GSK-J4 slightly increased total H3K27me3 level in IDH1 mutant cells. Belinostat increased both H3K4me3 and H3K27ac levels in all cell types, i.e. A172 wild type, A172 IDH1^{R132H} and MGG152 cells after 48h.

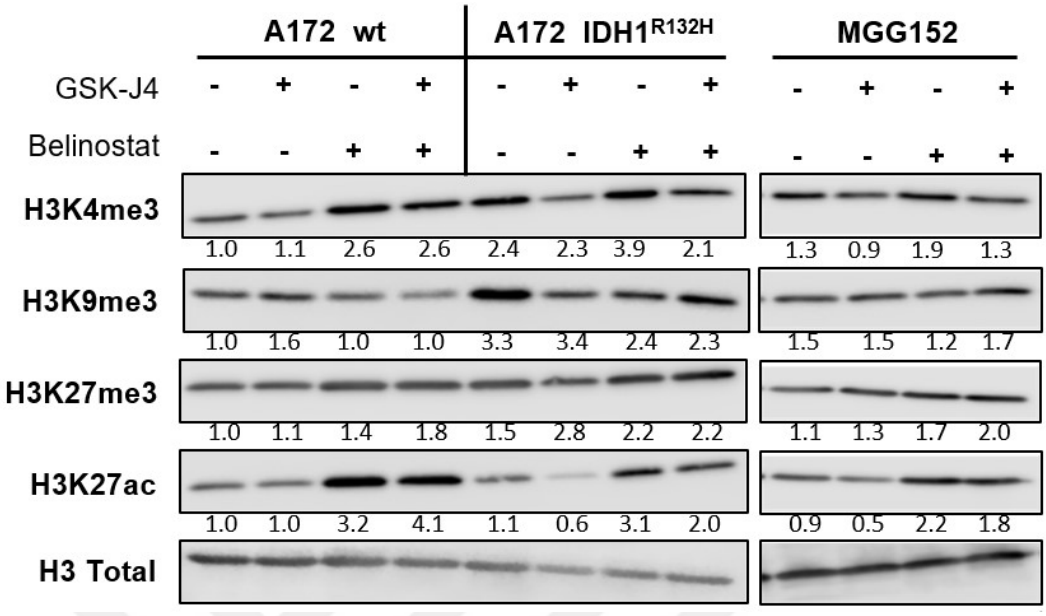

Figure 3.40 Western blot analysis for histone modifications. Western blot images of A172 wild type, A172 IDH mutant and MGG152 cells after 48h of drug treatment showed that epigenetic modifications occured with IDH1^{R132H} overexpression, and they were further modified with GSK-J4 and Belinostat treatments.

A172 IDH1^{R132H} cells (**Figure 3.41A**) and MGG152 cells (**Figure 3.41B**) were treated with GSK-J5, inactive form of GSK-J4. Their viabilities were not affected from inactive form, and GSK-J5 did not generate any additivity with Belinostat treatment. Some other KDM inhibitors, namely IOX-1 (pan 2-OG inhibitor), KDOBA67 (GSKJ1 analog), KDOAM-25a (JARID inhibitor), KDOAM32, KDM5-C70 (JARID1 inhibitor) were also tested. None of them, except KDOBA67 which also targets KDM6A and KDM6B, affected MGG152 cell viability, either individually or in combination with Belinostat (**Figure 3.42**).

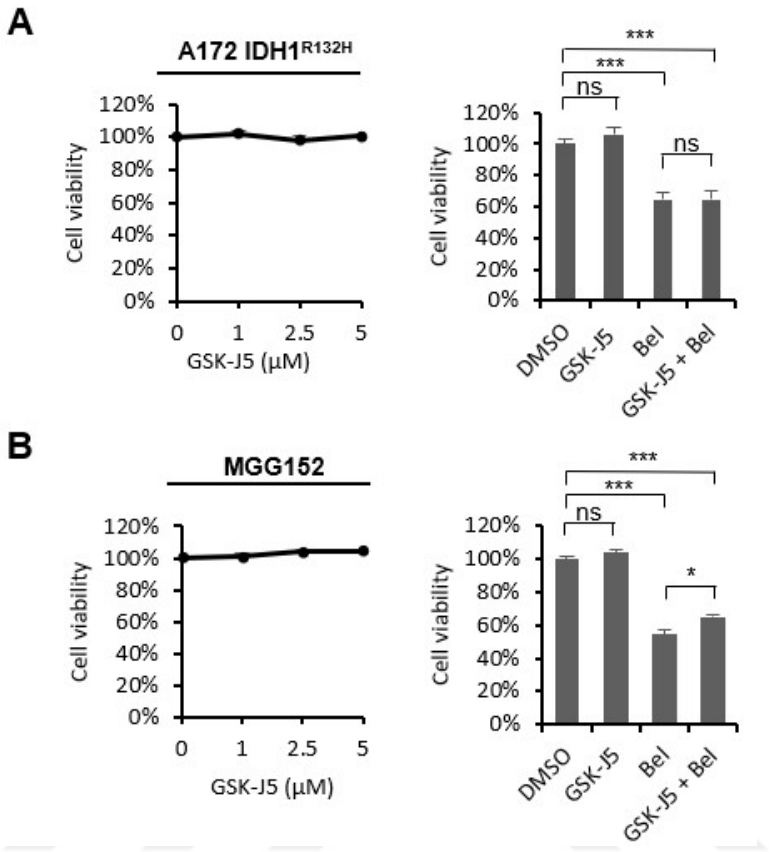

Figure 3.41 Effect of GSK-J5 on IDH-mutant cells. GSK-J5, inactive form of GSK-J4, did not affect the viability of IDH1^{R132H} mutant A172 cells **(A)** or primary MGG152 cells **(B)** individually, and its combination with Belinostat did not cause further cytotoxicity. p-values were determined by unpaired t test; ns, non-significant; *p < 0.05; **p < 0.01; ***p < 0.001.

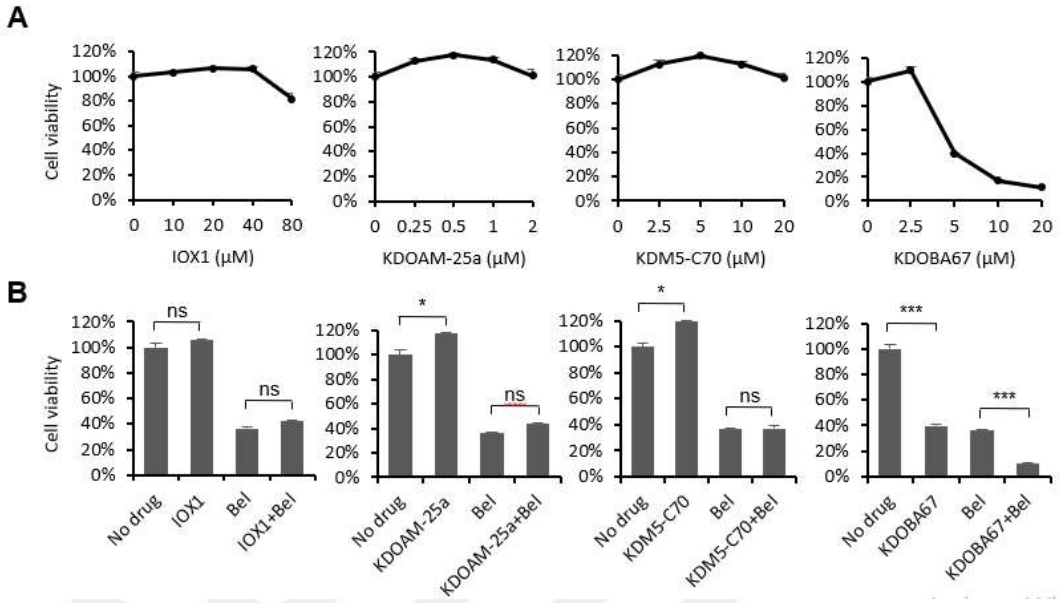

Figure 3.42 Effect of other KDM inhibitors on IDH-mutant cells. Treatments of other KDM inhibitors, IOX1, KDOBA67, KDOAM-25a and KDM5-C70, on primary IDH mutant GBM cells showed that only KDOBA67 which has very similar structure to GSK-J4, affected cell viability individually **(A)** or in combination with Belinostat **(B)**. p-values were determined by unpaired t test; ns, non-significant; *p < 0.05; **p < 0.01; ***p < 0.001.

KDM6A and *KDM6B* genes were knocked out either individually or together in A172 wild type, A172 IDH1^{R132H} and MGG152 cells via CRISPR/Cas9 method. Knockouts were validated by analyzing the results of Sanger sequencing (**Figure 3.43**). Individual knockout of either gene has only slight negative effects on cell growth in IDH1 mutant cells, while double knockout suppressed cell growth significantly in all cell types (**Figure 3.44**). The growth inhibition effect was more drastic in IDH1 mutant cells. Growth of *KDM6A* and *KDM6B* double knockout cells were also further inhibited by Belinostat treatment (**Figure 3.45A**), similar with GSK-J4 and Belinostat combination treatment. Double knockout was also induced stress response genes similar with GSK-J4 (**Figure 3.45B**).

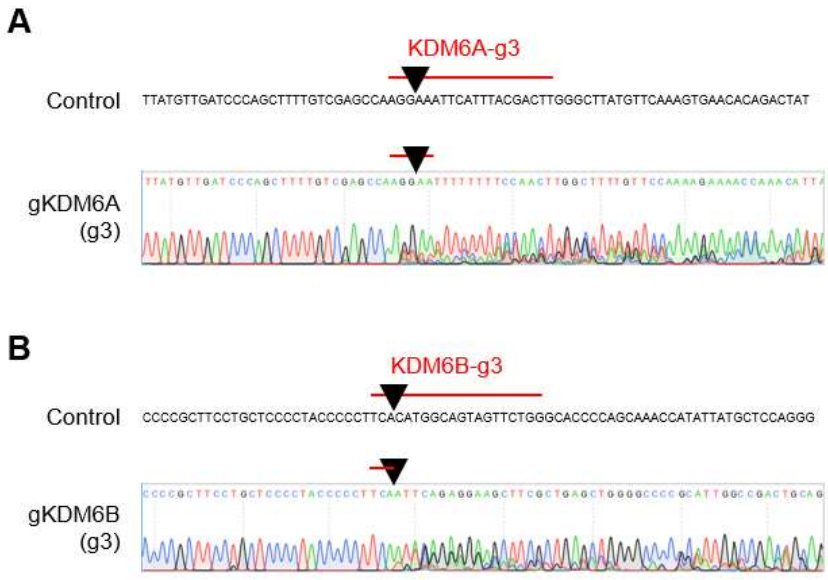

Figure 3.43 Validation of *KDM6A* and *KDM6B* knock-outs. Sanger sequencing results to validate knock-out of *DKDM6A* **(A)** and *KDM6B* **(B)** genes via CRISPR/Cas9. Red bars on the control sequence indicate regions targeted via gRNAs, and black triangles indicate the expected cleavage site. In the bottom parts, Sanger sequencing reveals deletions or frameshifts around the cleavage sites.

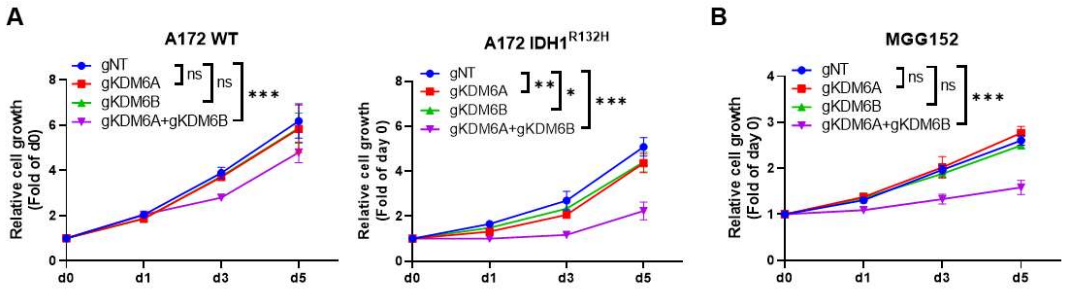

Figure 3.44 Effect of *KDM6A* and *KDM6B* knock-outs on cell viability. A) Individual knock-out of *KDM6A* or *KDM6B* slightly affected growth of IDH mutant A172 cells, not of WT cells, while knocking-out both *KDM6A* and *KDM6B* together suppressed the cell growth significantly when compared to non-targeting gRNAs (gNT) in both cell types. **B)** Similarly, double knock-out of *KDM6A* and *KDM6B* suppressed the cell growth in patient-derived MGG152 cells. p-values were determined by 2-way ANOVA test.

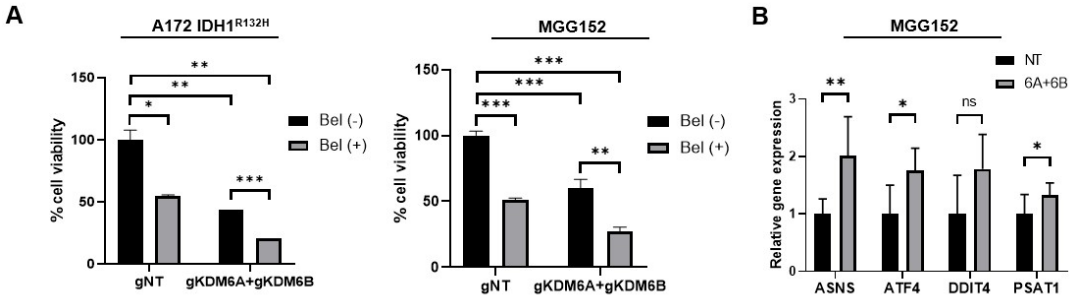

Figure 3.45 Effect of *KDM6A* and *KDM6B* knock-outs on belinostat treatment and stress response. A) Double knock-out of *KDM6A* and *KDM6B* increased the cytotoxic effect of belinostat in IDH mutant A172 cells and primary MGG152 cells. **B)** Double knock-out of *KDM6A* and *KDM6B* induced expression of stress response genes in MGG152 cells. p-values were determined by unpaired t test; ns, non-significant; *p < 0.05; **p < 0.01; ***p < 0.001.

3.8 GSK-J4 and Belinostat combination has inhibitory effect on *in vivo* growth of IDH-mutant glioma

In vivo effects of GSK-J4 and Belinostat were tested in intracranial GBM model by treating animals with drugs for 6 days after tumor formations were observed (**Figure 3.46**). Animal experiments showed that GSK-J4 and Belinostat co-treatment decreased tumor volume comparing to DMSO control group (**Figure 3.47A**). Before the drug treatment, in day 15, average tumor volumes were almost equal in both groups. As quick as 4 days after beginning of drug treatment, in day 22, average tumor volume was significantly lower in the drug treated group. Significant difference was protected on day 25, and day 28 as well (**Figure 3.47B**). Kaplan-Meier survival plot also indicated that drug treated animals had significantly longer survival (**Figure 3.47C**).

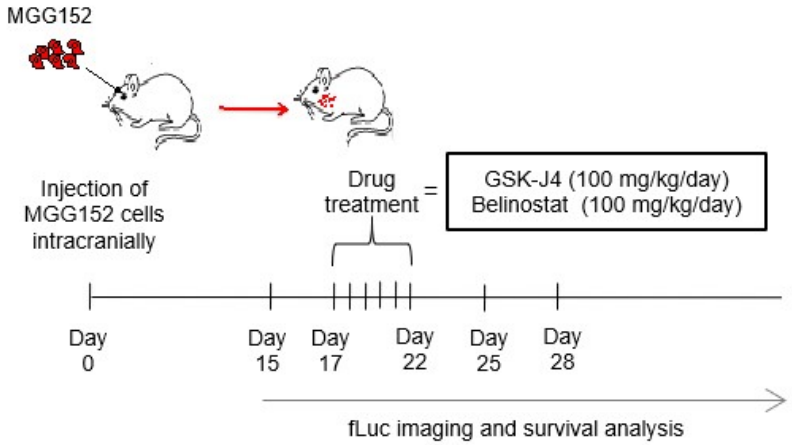

Figure 3.46 *In vivo* experimental plan. Schematic representation of timeline for *in vivo* experiments conducted with MGG152 cells.

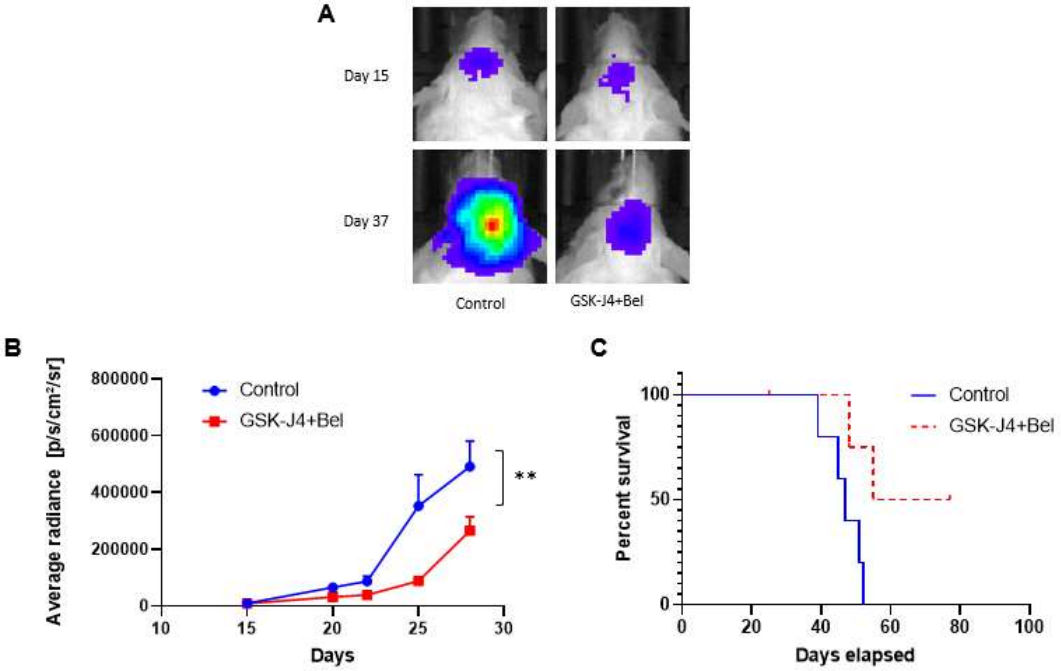

Figure 3.47 Effects of drug combination on *in vivo* tumor development A) Representative images of intracranial tumors on days 15 and 37. **B)** Average radiances [p/s/cm²/sr] of control and drug treated tumors. p-value was calculated via two-way ANOVA test, *p < 0.05; **p < 0.01; ***p < 0.001. **C)** Kaplan-Meier survival plot for control and drug treated mice (n=5). p-value was calculated via Log-rank test (p=0.0318).

4 DISCUSSION:

In this study, we interrogated the epigenetic vulnerabilities of IDH1 mutant glioma cells, based on their distinct epigenetic phenotype. From a chemical screen targeting several chromatin modifiers, we established that combination of GSK-J4, a histone demethylase inhibitor, and Belinostat, a histone deacetylase inhibitor, was highly effective on IDH1 mutant glioma cells. This selective vulnerability of IDH1 mutant glioma cells involved the activation of integrated stress response and apoptosis, which were reversible with the mutant IDH enzyme inhibitor GSK864. Together, our findings reveal a novel combinatorial approach for IDH1 mutant gliomas by exploiting their vulnerability.

IDH1 mutation is very common in low grade glioma and secondary GBM. It is accepted as a biomarker for favorable prognosis compared to IDH-wild type glioma. However, it may become aggressive as it harbors new mutations during tumor progression or recurrence. It is also so important diagnostic marker that new classification of WHO for glioma, published in 2016, divides each glioma subgroup into IDH wildtype or IDH mutant subtypes [18]. However, there is still no approved drug specific to these subtypes. Based on distinct hypermethylator phenotype of IDH-mutant gliomas [21,22], we decided to use a chemical library consisting of inhibitors of epigenetic enzymes to find potential drugs for these tumor cells. Considering heterogeneity problems in GBM, and negative effects of drugs on non-malignant cells in high doses, we decided to combine screen hits to obtain an additive/synergistic effect. GSK-J4 and Belinostat combination showed the strongest effect on IDH1 mutant GBM cells while they had minimal effects on non-malignant cells.

4.1 Epigenetic inhibitor screen to identify new drugs against IDH mutant GBM

Although it is well-known that IDH mutation induces hypermethylation in both histones and DNA, as far as we know, there is no study performed with chemical or genetic screen targeting epigenetic enzymes in IDH mutant gliomas. Therefore, we applied a library including many epigenetic enzyme inhibitors on 2 different IDH1-mutant patient-derived GBM cell lines. This library consists of chemical probes which were shown before to inhibit epigenetic enzymes from various categories including HDACs, KDMs, HMTs, DNMTs, BETs, etc. Some of these probes have targets in a

broad range, and some of them were developed to inhibit specific enzymes. We selected 5-azacytidine, Chaetocin, GSK-J4 and Belinostat as common hits for further experiments. Among them, only 5-azacytidine which is a DNMT inhibitor was shown before to be effective against IDH mutant glioma in pre-clinical studies [116,117]. Considering DNA hypermethylation in IDH-mutant tumors, 5-azacytidine is a good candidate to reverse this phenotype by inhibiting DNMTs. There are ongoing clinical trials for individual 5-azacytidine treatment or combination with mutant IDH inhibitors (Identifiers for clinical trials: NCT03666559, NCT02677922). However, other 3 inhibitors were not studied on IDH mutant tumors yet and may be important to find new potential targets for these tumors. Chaetocin which is an inhibitor of SUV39H1 enzyme [217] responsible for methylation of lysine 9 of histone 3 (H3K9), was shown to be effective on GBM cells either individually or as a sensitizer for other drugs [218,219]. GSK-J4 is an inhibitor of KDM6A and KDM6B [145] which are responsible for H3K27 methylation. There are several studies showing its cytotoxic effects on diffuse midline glioma and TMZ-resistant GBM cells [150,153]. Finally, Belinostat is a pan-HDAC inhibitor for class I, II and IV HDACs [220]. It was also shown to be effective on GBM cells in a pre-clinical study [221].

4.2 Drug combination against IDH mutant GBM

GBM cells are highly heterogeneous, and this is one of the main reasons of therapeutic resistance. One drug may be effective against large proportion of bulk tumor, but the rest of the cells, even if they are low in number, can continue to proliferate and lead to recurrence. Increasing the drug concentration may not be sufficient to kill whole tumor cells, but it may harm healthy cells in body. Combinations of different drugs in low concentrations can be a good approach to overcome this issue. This strategy is thought to be more efficient and commonly used in clinical trials in recent years [222,223].

Individual drug treatments, even if they are highly specific and effective, mostly lead to derivation of resistant population. Drug combination is offered as a promising strategy for cancer treatment to overcome resistance against single drug and reduce high-dose leading toxicity [224]. As we checked effects of these screen hits on non-malignant fibroblasts, we observed that even if at lesser degree, high doses of Chaetocin and Belinostat have cytotoxic effects on them as well. To eliminate cytotoxic effects on non-malignant cells, we performed all possible dual combination of these 4 hits in low doses.

Some combinations did not increase the individual effects of single drug, while some of them generates additive or synergistic effects. Combinations of 5-azacytidine with Chaetocin, and GSK-J4 with Belinostat were the most effective combinations in terms of drug synergy and selective cytotoxicity against IDH1 mutant GBM cells. Further experiments showed that mutant IDH1 causes a high sensitivity to GSK-J4 and Belinostat combination. Viability of non-malignant fibroblasts were only slightly affected from low dose of Belinostat and this effect did not increase with GSK-J4 combination. To see drug effects on normal brain tissue cells, we used human astrocytes and observed no significant effect on their viability either. Landry et al. indicated that interaction between tumor cells and stromal cells such as fibroblasts may have dramatic influences on drug response [225]. Based on this observation, we cocultured mCherry-labelled IDH1^{R132H} overexpressed cells with GFP-labelled non-malignant fibroblasts. IDH1-mutant cells were much more sensitive against GSK-J4 and Belinostat combination treatment, and fibroblast viability was only slightly affected. This result is important to show the safety of this combination by selective killing of GBM cells, for potential clinical applications.

4.3 Inhibitors of mutant IDH enzyme: a good therapeutic strategy?

Since *IDH1* mutation is accepted as initial event in tumorigenesis of low-grade glioma, it is preserved in most of the recurrences as well. Therefore, it was thought as a perfect candidate to target, many inhibitors specific to mutant IDH enzymes were developed [30,32,154,155] and most of them are now in clinical trials. However, we found that GSK864, a specific inhibitor of mutant IDH1, rescued *IDH1* mutant cells from slow growth and sensitivity against GSK-J4 and Belinostat treatments. This recovery effect of mutant IDH inhibitors was also seen in several recent studies [36–39]. Wakimoto et al. indicated that IDH1 mutation is initial alteration in IDH1-mutant tumors, and it is followed by secondary mutations such as *TERT* mutation and 1p/19q co-deletion for oligodendroglioma, or *TP53* and *ATRX* mutations for astrocytoma [19]. However, tertiary mutations such as *PDGFRA* or *MYC* amplifications, or *PIK3CA* mutation are required for tumor progression, especially in an aggressive manner. We suggest that even if *IDH1* mutation is critical for tumorigenesis, tumor progression may be independent of it after gaining of tertiary mutations. On the other hand, *IDH1* mutation, by 2-HG production, creates vulnerabilities to cells via disrupted mechanisms discussed above, and these weaknesses exist as *IDH1* mutation is protected in the tumor. Mutant IDH1 inhibitors may restore these disrupted mechanisms by depleting 2-HG production. Therefore, using

these inhibitors may not be safe in all cases to treat IDH1 mutant tumors, and may interfere with additional drugs targeting known vulnerabilities.

4.4 *In vitro* GBM cell culture models for IDH mutant GBM

Piaskowski et al. indicated that it is highly difficult to propagate IDH mutant glioma cells in standard *in vitro* cell culture conditions [226]. They emphasized the need for new cell culturing models for glioma cells which simulate *in vivo* conditions better.

In our study, we cultured patient-derived primary GBM cells as spheres in EGF/FGF containing serum-free media. Lee et al. clearly showed that cells obtained from primary human GBM samples more closely reflect the primary tumor characteristics when cultured in EGF and FGF containing serum-free media, compared to conventional serum-containing monolayer cultures [227]. This culture conditions were commonly accepted as a more reliable model than traditional cell lines for understanding tumor biology. Sphere-formation ability is also thought as a marker of cancer stem-like cells for many cancer types including GBM [228,229]. Therefore, our sphere cultures were highly valuable to mimic natural environments of GBM and to find efficient treatments for cancer stem-like cells which are thought to be more therapy-resistant [230]. To check the effects of hit drugs on sphere-forming ability of primary GBM cells, we performed a sphere-formation assay. All four drugs were shown to be reduce the sphere sizes and number of spheres. Therefore, they have potential to target IDH1-mutant glioma stem cells. However, since they don't have IDH wild type counterparts we couldn't check if there is causality between IDH mutation and drug sensitivity. Even if we observed sensitivity of two different patient-derived IDH-mutant GBM cells against hit drugs, there are lots of variables that may affect drug response of cells in that way. To this end, we established a paired cell line via ectopic overexpression of $IDH1^{R132H}$ in A172 GBM cell line which has normally wild type IDH1. It is well-known that IDH1 mutation is found as heterozygous since mutant IDH1 uses α-KG produced by wild type IDH1 enzyme as substrate [20]. Therefore, our model is convenient to see the effects of 2-HG production by mutant IDH1. Since we observed a clear sensitivity of established $IDH1^{R132H}$ cell line against GSK-J4 and Belinostat and considering the sensitivity of 2 different IDH1 mutant primary GBM cells, we concluded that mutant IDH1 generates a sensitivity to GSK-J4 and Belinostat. Reversibility of this sensitive phenotype by mutant

IDH1 inhibitor eliminated non-specific effects of overexpression and consolidated our hypothesis.

4.5 Integrated Stress Response (ISR) is involved in GSK-J4 and Belinostat effects

Based on both our experimental results and computational analyses, we hypothesized that integrated stress response (ISR) is activated in IDH1 mutant cells because of the increased cellular stress. This is compatible with recent studies showing 2-HG, product of the mutant IDH enzyme, inhibits many 2-OG dependent dioxygenases. PHD enzymes are one of these dioxygenase families and it was recently shown that inhibition of collagen hydroxylases which belong to PHD family, causes ER stress via immature collagen accumulation in IDH1 mutant tumor cells [48]. Another study indicated that 2-HG also inhibits cytochrome c oxidase (COX) enzyme in electron transport chain and increased mitochondrial stress [231]. Based on that, authors offered Bcl2 inhibition as a synthetic lethality approach in IDH1/2-mutant acute myeloid leukemia (AML). In addition, Turcan et al. showed that immune response pathways and genome instability were upregulated in IDH-mutant cells, as a result of deregulated DNA and histone methylation and activation of endogenous retroviruses (ERVs) which are normally quiescent [232]. ERV activation was independently shown to induce ER stress and unfolded protein response (UPR) in previous studies [233–235]. We also observed similar results in GSEA analysis after RNA-seq; Interferon (IFN)-α, IFN-γ, NF-KB, inflammatory response pathways and UPR were upregulated in IDH1^{R132H} overexpressed cells when compared to their wild type counterparts. Contrarily, all of these pathways were downregulated when the IDH1^{R132H} overexpressed cells were treated with mutant IDH1 inhibitor, GSK864. We validated these results via qRT-PCR and observed significantly increased expression of genes involved in viral response and UPR pathways in IDH1^{R132H} overexpressed cells, while all of these genes were downregulated in the presence of GSK864 (**Figure 3.8**). Therefore, it is clear that IDH1 mutant cells have an increased basal cellular stress because of disrupted metabolic and epigenetic mechanisms. However, stress response pathways and survival pathways such as NF-KB can protect cells from death since stress level is below a threshold. GSK-J4 and Belinostat treatments increase cell stress above this threshold, so activate apoptotic pathways and cell death occurs.

Enrichment analysis for Reactome pathways after RNA-seq indicated that GSK-J4 induced ATF4-mediated stress response pathways in IDH1 mutant primary cells. ATF4 is a major transcription factor that upregulates survival pathways under mild stress conditions, or apoptotic pathways under severe stress. Different stress conditions such as amino acid deprivation, viral infection, ER stress, oxidative stress, etc. trigger phosphorylation of eIF2α as part of integrated stress response (ISR) [185]. This results in suppression of global cap-dependent translation, while induction of specific cap-independent translations such as ATF4. We validated ATF4 upregulation in both mRNA and protein level upon GSK-J4 treatment. Expression of its known targets such as ASNS, DDIT4 and PSAT1 were also upregulated in GSK-J4 treated, or *KDM6A* and *KDM6B* double-knockout cells. As expected, pre-treatment with mutant IDH inhibitor, GSK864, alleviated activation of stress-response genes in IDH1^{R132H} overexpressed cells upon combination drug treatment. This supports the hypothesis of that IDH-mutant cells have high basal stress level that make them more sensitive against stress inducer GSK-J4 individually or in combination treatment. Moreover, via SUnSET assay, a remarkable decrease in global protein translation which is known to be cellular response mechanism under stress, was observed in GSK-J4 treated primary IDH-mutant cells.

ISRIB, an inhibitor of integrated stress response (ISR) [236] protected IDH1 mutant cells partially against GSK-J4 and Belinostat treatment. Since it is known that stress response pathways lead to apoptosis under chronic or harsh stress conditions, it is an expected result. An inhibitor of PERK enzyme, PERKi, was also partially recovered drug-induced cell death, but in lesser degree. Considering the kinases other than PERK which are responsible for eIF2α phosphorylation in ISR, we may conclude that ER-stress is not the only stress source in GSK-J4 and Belinostat treated IDH-mutant cells. It was shown before that CHOP which is the protein encoded by *DDIT3* gene is responsible for the apoptotic arm of the ISR [195]. It was activated by ATF4 under severe stress. Therefore, we investigated its effects by knocking-out via CRISPR/Cas9 method and observed significant recovery in viability of *DDIT3* knocked-out IDH1^{R132H} cells upon individual GSK-J4 treatment and in combination treatment. Belinostat-mediated cell death was not recovered by *DDIT3* knock-out indicating that Belinostat individually activated an alternative pathway in IDH-mutant cells. These results indicate that GSK-J4 individually or in combination with Belinostat increases cellular stress, which is already high in IDH1 mutant cell, and leads to apoptosis through ATF4 mediated *DDIT3*/CHOP induction.

However, since we observed partial recovery both with ISRIB and *DDIT3* knock-out, it is understood that stress response pathway is not the only reason of the cell death. Integrated stress response leads cells to death when stress level is over a threshold since cells cannot handle that much stress. Even if we inhibited the ISR-mediated cell death by chemical or genetic ways, stress sources are still present in the cell. They may continue to impair critical cellular activities and induce alternative death mechanisms. More detailed mechanistic studies should be performed to reveal all mechanisms leading to cell death.

4.6 Mechanism of action of drugs

Considering that GSK-J4 increases H3K27me3 which is a repressive epigenetic marker, and Belinostat increases histone acetylation, which is an activation marker, a neutralization effect may be expected when they are used in combination. In contrast, we observed an additive/synergistic effect which may be related with different targets of each drugs. It is known, and we showed that histone methylations are already increased in IDH1 mutant cells. Therefore, remaining unmethylated regions might include crucial genes for cell proliferation, and GSK-J4 may inhibit proliferation by increasing methylation of these regions. On the other hand, Belinostat may induce open chromatin structure in regions including tumor suppressor genes, cell cycle regulators, or pro-apoptotic genes. We observed a clear increase of p21, which may be responsible for cell cycle arrest, in both mRNA and protein level upon Belinostat treatment. Combination treatment, on the other hand, reduced p21 protein to basal levels. It was shown that p21 has anti-apoptotic effects beside its growth inhibitory effects, and it is downregulated by CHOP during increased stress conditions [237]. In our study, CHOP was highly increased upon combination treatment, and might be responsible for apoptosis via downregulation of p21, and upregulation of NOXA and PUMA. All in all, GSK-J4 and Belinostat boost their individual effect, increases cellular stress which is already increased in IDH1 mutant cells above the threshold that response pathways can handle, and lead to cell death through apoptosis.

GSK-J4 was developed to selectively inhibit *KDM6A*/UTX and *KDM6B*/JMJD3 which are H3K27 demethylases [145]. However, it was shown that it has some activity towards KDM5B and KDM5C as well [146]. To check if the effect of GSK-J4 is an on-target effect or not, we used GSK-J5, which is an inactive form of GSK-J4, and KDM5

specific inhibitors, KDOAM25a and KDM5-C70, and observed no effect individually or upon Belinostat treatment. Finally, we tested KDOBA67, which is a very similar chemical with GSK-J4 that inhibits KDM6 enzymes, and we observed similar individual effects and synergy with Belinostat. We also observed dramatically decreased cell growth and increased expression of stress related genes upon double-knockout of *KDM6A* and *KDM6B* genes. Growth of double-knockout cells were also further inhibited with Belinostat treatment. Recent studies showed KDM6A and KDM6B upregulation in therapy-resistant glioma stem cells, and efficient sensitization by GSK-J4 [153]. However, to our knowledge, there is no study showing effect of GSK-J4 and inhibition of KDM6 enzymes in IDH1 mutant glioma. Our results indicate that GSK-J4 is highly effective on IDH1 mutant glioma cells and its effects is coming from inhibition of KDM6A and KDM6B enzymes together.

Previous studies showed that GSK-J4 induced cellular stress response, differentiation, cell cycle arrest, and apoptosis [238–241]. We found that GSK-J4 decreases proliferation but did not induce cell death individually in low doses. There was also no significant increase in Caspase 3/7 activities, PARP cleavage or YO-PRO1 staining with GSK-J4 alone. Instead, it causes a cell cycle arrest accompanying with change in cell morphology which was clearly observed in live cell images and videos. We confirmed that by observing an increase in S and G0/G1 phase, in MGG152 and A172 IDH mutant cells, respectively. Considering the clear increase in stress response upon GSK-J4 treatment, it may be assumed that GSK-J4 leads to a mild stress in low doses individually which can be tolerated by stress response pathways, and causes a slight increase in senescence and cell cycle arrest instead of cell death.

Belinostat is a pan-HDAC inhibitor [220]. Therefore, it is difficult to say that its effect is derived from inhibition of a specific enzyme. We confirmed increased acetylation of histones (H3K27ac) and non-histone proteins such as α-tubulin upon Belinostat treatment either individually or in combination with GSK-J4. There are many studies showing different mechanisms of action for HDACi, such as upregulating pro-apoptotic genes, downregulating anti-apoptotic proteins, induction of ER stress because of hyperacetylated non-histone proteins, cell cycle arrest and apoptosis [221,242–244]. We found that expression of anti-apoptotic genes, such as *BCL2L1*/Bcl-XL and *BIRC5*/Survivin and level of anti-apoptotic proteins, Bcl-XL and XIAP, were decreased upon Belinostat

treatment. It also downregulated the *ATF5* gene which is induced by ATF4 and responsible for survival pathways under stress conditions [213]. Belinostat also clearly caused a G2/M arrest in both innately and engineered IDH1^{R132H} GBM cells. This may be a result of induction of p21, which was shown to be an important target of many HDAC inhibitors [245–247]. Assay for anoikis which is a type of apoptosis because of detachment from the solid surface also indicated that Belinostat treatment induces anoikis. Since cells die after detached from the surface in this type of apoptosis, the media should contain more viable cells which is the case most clearly in Belinostat treated cells. It is also compatible with Reactome enrichment analysis showing activation of cell surface and ECM-related pathways upon Belinostat treatment. Acetylation of cytoskeletal proteins such as α-tubuline by Belinostat as shown in our study may be responsible for this situation. Live cell images and videos also indicated cell detachment instead of a classical apoptosis blebbing. Increases in Caspase 3/7 activity and live cell images and videos showed that even individual Belinostat treatment also leads to cell death through apoptosis.

4.7 Effects of hypoxia

An interesting result of our study was related with hypoxia. There are controversial studies about the effect of *IDH1* mutation on hypoxic response. Some studies showed that 2-HG which is produced by mutant IDH enzyme, inhibits enzymes containing prolyl hydroxylase domains (PHD), also known as EGLN enzymes [24,248]. PHD enzymes are 2-OG-dependent enzymes, and one of their canonical targets to mark for degradation is HIF-1α which is responsible for activation of hypoxia response genes [249,250]. It is initially thought that 2-HG competes with 2-OG to bind and inhibit PHD enzymes, like in TET and JmjC-KDM enzymes. Therefore, HIF-1α hydroxylation and so degradation is inhibited, and hypoxic response is activated in IDH-mutant cells even if in normoxic conditions. However, some further studies demonstrated that 2-HG activates PHD enzymes rather than inhibit its activity. Therefore, HIF-1α is degraded and IDH-mutant cells are more sensitive to hypoxic conditions [26,251]. In our study, we observed a phenotype more similar to initial studies. Growth of primary IDH1-mutant cells were not affected in hypoxic conditions significantly. Moreover, growth rate of IDH1^{R132H} overexpressed cells were similar to IDH1 wild type cells in hypoxia while they were growing slower than wild type cells in normoxia. Interestingly, drug responses of wild type and IDH1^{R132H} cells were also similar under hypoxic conditions. In parallel with

these results, GSEA analysis also indicated activation of hypoxia response in IDH1^{R132H} overexpressed cells which was downregulated with mutant IDH inhibitor. These are compatible with the hypothesis of already hypoxic state of IDH-mutant cells based on HIF-1α stabilization. However, more detailed hypoxia studies should be performed to prove this hypothesis.

4.8 *In vivo* studies

Animal studies confirmed that, even if they were used only for 6 days, GSK-J4 and Belinostat have cytotoxic effect on tumor cells *in vivo* as well and provided longer survival. Some important limitations in our *in vivo* studies were low number of animals and short period of drug treatment. Since especially GSK-J4 has low stability in physiological conditions, bulk amounts of it were required for treating longer and high number of animals. If more stable KDM6 inhibitors could be developed, lower concentrations of drugs might be used for longer times. By this way, they may have a potential to be used in more detailed *in vivo* studies or clinical trials in the future. Hashizume et al. (2014) showed therapeutic effects of GSK-J4 on pediatric brainstem glioma and concluded that it can pass through blood-brain barrier [150]. Many HDAC inhibitors such as SAHA [252] and VPA [253] were also shown to penetrate blood-brain barrier (BBB). Gurbani et al. (2019) recently reported that Belinostat can cross the BBB [137]. As parallel with literature, our results may also be thought as an indirect evidence for the ability of GSK-J4 and Belinostat for penetrating BBB. However, spectrometric analysis should also be performed as direct evidence. It would also be useful to measure the ratio of the drugs that can pass throughout the BBB.

4.9 Conclusion

To sum up our study, we generated a model explaining the effects of mutant IDH1 and mechanisms behind the drug treatments (**Figure 4.1**). Collectively, mutant IDH1 enzyme generates a distinct epigenome with hypermethylated DNA and histone profile. On the other hand, it leads to activation of cellular stress response pathways, such as inflammatory response, UPR and NF-KB which are reversible with GSK864 treatment. By means of the response pathways, cells survive under stress conditions. GSK-J4 treatment increase this cellular stress and induce ATF4 mediated ISR, while Belinostat downregulates anti-apoptotic proteins and induce cell cycle arrest. Together, they further

modify epigenome and cause severe stress leading to *DDIT3*/CHOP mediated induction of PUMA and NOXA, and eventually caspase 3/7-dependent apoptosis.

Our study suggests that specific targeting of epigenetic enzymes might be a good option for the treatment of IDH mutant gliomas, based on their distinct epigenetic phenotypes. Together with combination strategies, such as GSK-J4 and Belinostat combination in our study, drug effects could be amplifed without harming healthy cells.

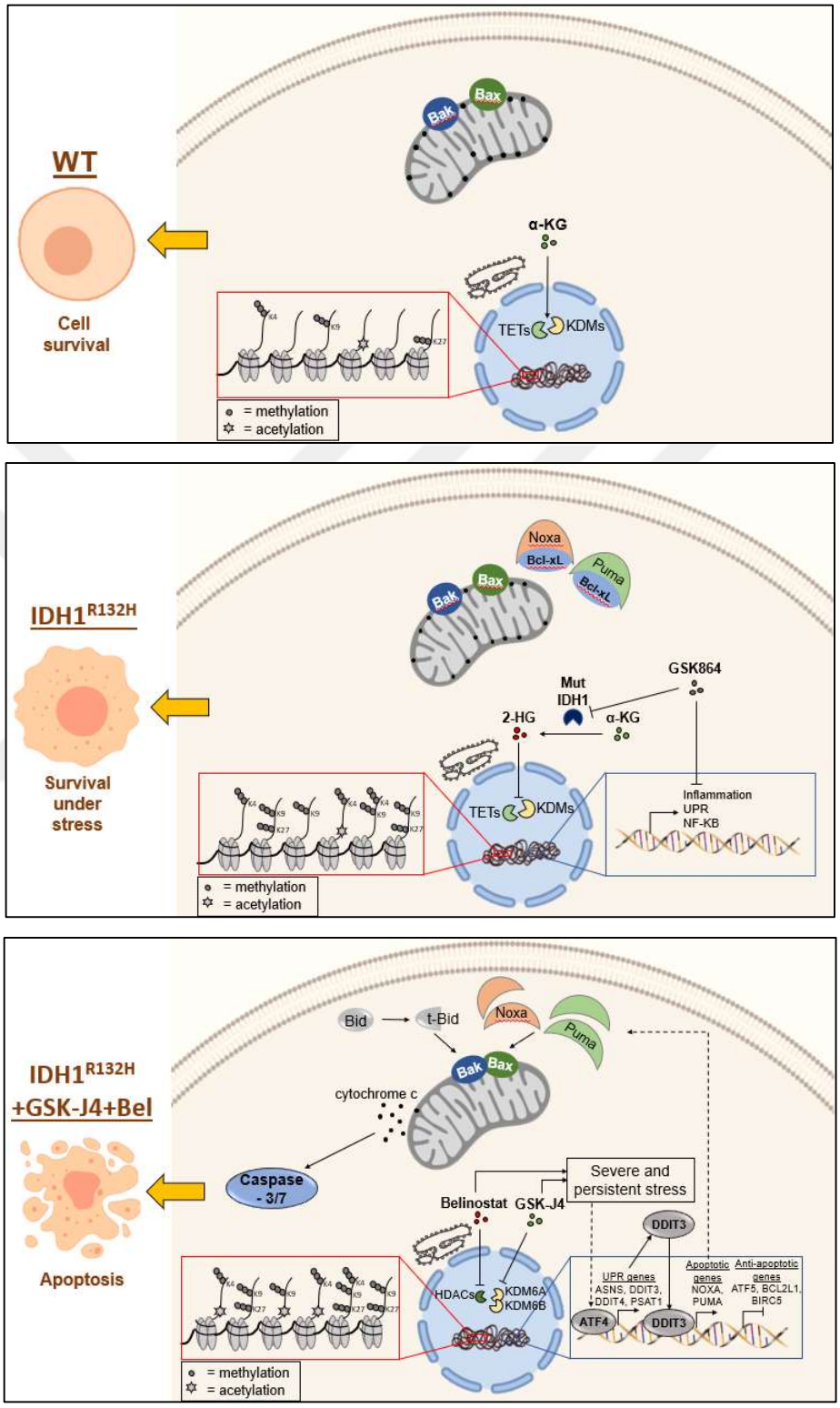

Figure 4.1 Model of the study. Upper panel shows wild type cells as surviving with less stress. Middle panel indicates survival of IDH1^{R132H} mutant cells under 2-HG-dependent stress conditions. Lower panel shows effects of GSK-J4 and Belinostat combination on IDH1^{R132H} cells, leading to apoptosis.

5 APPENDIX A – LIST OF INHIBITORS AND SCREEN RESULTS

Table 5.1 Epigenetic probes in the drug screen with their potential targets, and viability of MGG119 and MGG152 primary IDH mutant cells

Class/Target	Source Name	MGG119 viability	MGG152 vability
Bromodomains - BRD2, BRD3, BRD4, BRDT (BET)	(+)-JQ1	99±8%	92±0%
Bromodomains - Negative control	(-)-JQ1 (inactive)	91±5%	100±3%
Bromodomains - BRD2, BRD3, BRD4, BRDT (BET)	PFI-1	93±3%	72±3%
Bromodomains - BRD2/3/4	I-BET	106±6%	81±2%
Bromodomains - pan-Bromodomain	Bromosporin	97±4%	80±2%
Bromodomains - CBP, BRD4(1)	CBP/BRD4 (0383)	107±1%	90±5%
Bromodomains - CREBBP, EP300	SGC-CBP30	97±0%	97±0%
Bromodomains - CREBBP, EP300	I-CBP112	97±6%	90±1%
Bromodomains - BRD2, BRD3, BRD4, BRDT (BET, BD2)	RVX-208	96±3%	89±4%
Bromodomains - SMARCA, PB1	SMARCA	112±3%	100±1%
Bromodomains - SMARCA2/4, PB1(5)	PFI-3	85±0%	95±0%
Bromodomains - BAZ2A, BAZ2B	GSK2801	96±4%	99±2%
HDAC - hydroxamic acids	Belinostat	73±3%	26±2%
HDAC - aliphatic acid compounds	Valproic acid	95±6%	90+0%
HDAC - ortho-amino anilides	Entinostat	110±5%	93±0%
HDAC - hydroxamic acids	SAHA	89±2%	51±0%
HDAC - hydroxamic acids - Class I & II	Trichostatin A	68±2%	22±0%
HDAC - SIRT1 (indirect?) activator	SRT1720	118±5%	95±1%
HDAC - SIRT1	EX 527	102±7%	104±2%
HDAC - 1,2,3,(8)	CI-994	89±3%	89±4%
Histone methyltransferase - G9a, GLP	UNC0638	99±2%	96±6%
Histone methyltransferase - G9a, GLP	UNC0642	94±5%	99±5%
Histone methyltransferase - G9a, GLP	A-366	102±8%	104±7%
Histone methyltransferase - SUV39H1	Chaetocin	47±7%	29±1%
Histone methyltransferase - SETD7	PFI-2	104±6%	95±3%
Histone methyltransferase - DOT1L	SGC0946	98±2%	96±2%
Histone methyltransferase - EZH2	GSK343	100±5%	100±2%
Histone methyltransferase - EZH2	UNC1999	107±5%	95±5%
Histone methyltransferase - SMYD2	LLY-507	94±0%	96±1%
Lysine demethylases - LSD1	Tranylcypromine	96±5%	104±3%
Lysine demethylases - LSD1	GSK-LSD1	89±0%	99±2%
Lysine demethylases - JMJD3, UTX, JARID1B	GSK J4	44±7%	45±0%
Lysine demethylases - Negative control	GSK J5 (inactive)	86±5%	90±4%
Lysine demethylases - pan-2-OG	IOX1 (5-carboxy-8HQ)	82±6%	79±4%
Histone demethylase	Methylstat (Ester)	107±2%	95±2%
Histone demethylase - Pan JmjC	(E)-JIB-04	85±1%	95±2%
Histone demethylase - JMJD2E	ML324	94±4%	98±3%
Prolyl-Hydroxylases - PHD2 (EGLN1)	IOX2	90±6%	97±5%
Methyl Lysine Binder - L3MBTL3	UNC1215	93±4%	94±1%
DNA methyltransferase (DNMT) -	5-Azacitidine	61±5%	51±4%
DNA methyltransferase (DNMT) - DNMT1/3	5-Azadeoxycitidine	98±6%	101±3%
Poly ADP ribose polymerase (PARP)	Olaparib	103±3%	103±1%
Poly ADP ribose polymerase (PARP)	Rucaparib	103±2%	108±2%

6 BIBLIOGRAPHY

1. Ostrom, Q. T. *et al.* CBTRUS statistical report: Primary brain and other central nervous system tumors diagnosed in the United States in 2009-2013. *Neuro. Oncol.* **18**, v1–v75 (2016).
2. Louis, D. N. *et al.* The 2007 WHO classification of tumours of the central nervous system. *Acta Neuropathol.* **114**, 97–109 (2007).
3. Stupp, R. *et al.* Radiotherapy plus Concomitant and Adjuvant Temozolomide for Glioblastoma. *N. Engl. J. Med.* **352**, 987–996 (2005).
4. Gilbert, M. R. *et al.* A randomized trial of bevacizumab for newly diagnosed glioblastoma. *N. Engl. J. Med.* **370**, 699–708 (2014).
5. Claus, E. B. *et al.* Survival and low-grade glioma: the emergence of genetic information. *Neurosurg. Focus* **38**, E6 (2015).
6. Snuderl, M. *et al.* Mosaic amplification of multiple receptor tyrosine kinase genes in glioblastoma. *Cancer Cell* **20**, 810–817 (2011).
7. Shrieve, D. C. Basic Principles of Radiobiology Applied to Radiotherapy of Benign Intracranial Tumors. *Neurosurg. Clin. N. Am.* **17**, 67–78 (2006).
8. Cohen, M. H., Johnson, J. R. & Pazdur, R. Food and drug administration drug approval summary: Temozolomide plus radiation therapy for the treatment of newly diagnosed glioblastoma multiforme. *Clin. Cancer Res.* **11**, 6767–6771 (2005).
9. Westphal, M. *et al.* A phase 3 trial of local chemotherapy with biodegradable carmustine (BCNU) wafers (Gliadel wafers) in patients with primary malignant glioma. *Neuro. Oncol.* **5**, 79–88 (2003).
10. Mariani, L. *et al.* MGMT Gene Silencing and Benefit from Temozolomide in Glioblastoma . *N. Engl. J. Med.* **352**, 997–1003 (2005).
11. Wick, W. *et al.* Lomustine and bevacizumab in progressive glioblastoma. *N. Engl. J. Med.* **377**, 1954–1963 (2017).
12. Ferrara, N., Hillan, K. J. & Novotny, W. Bevacizumab (Avastin), a humanized anti-VEGF monoclonal antibody for cancer therapy. *Biochem. Biophys. Res. Commun.* **333**, 328–335 (2005).
13. Westphal, M. *et al.* A phase 3 trial of local chemotherapy with biodegradable carmustine (BCNU) wafers (Gliadel wafers) in patients with primary malignant glioma. *Neuro. Oncol.* **5**, 79–88 (2003).
14. Buckner, J. C. *et al.* Phase III trial of carmustine and cisplatin compared with carmustine alone and standard radiation therapy or accelerated radiation therapy in patients with glioblastoma multiforme: North Central Cancer Treatment Group 93-72-52 and Southwest Oncology Group. *J. Clin. Oncol.* **24**, 3871–3879 (2006).
15. Parsons, D. W. *et al.* An integrated genomic analysis of human glioblastoma multiforme. *Science (80-.).* **321**, 1807–1812 (2008).
16. Yan, H. *et al.* IDH1 and IDH2 Mutations in Gliomas. *N. Engl. J. Med.* **360**, 765–773 (2009).
17. Xu, X. *et al.* Structures of human cytosolic NADP-dependent isocitrate dehydrogenase reveal a novel self-regulatory mechanism of activity. *J. Biol. Chem.* **279**, 33946–33957 (2004).
18. Louis, D. N. *et al.* The 2016 World Health Organization Classification of Tumors of the Central Nervous System: a summary. *Acta Neuropathol.* **131**, 803–820 (2016).

19. Wakimoto, H. *et al.* Targetable signaling pathway mutations are associated with malignant phenotype in IDH-mutant gliomas. *Clin. Cancer Res.* **20**, 2898–2909 (2014).
20. Losman, J. A. & Kaelin, W. G. What a difference a hydroxyl makes: Mutant IDH, (R)-2-hydroxyglutarate, and cancer. *Genes Dev.* **27**, 836–852 (2013).
21. Ye, D., Xiong, Y. & Guan, K. L. The mechanisms of IDH mutations in tumorigenesis. *Cell Res.* **22**, 1102–1104 (2012).
22. Turcan, S. *et al.* IDH1 mutation is sufficient to establish the glioma hypermethylator phenotype. *Nature* **483**, 479–483 (2012).
23. O'Rourke, D. M. *et al.* IDH mutation impairs histone demethylation and results in a block to cell differentiation. *Nature* **483**, 474–478 (2012).
24. Xu, W. *et al.* Oncometabolite 2-hydroxyglutarate is a competitive inhibitor of α-ketoglutarate-dependent dioxygenases. *Cancer Cell* **19**, 17–30 (2011).
25. Chowdhury, R. *et al.* The oncometabolite 2-hydroxyglutarate inhibits histone lysine demethylases. *EMBO Rep.* **12**, 463–469 (2011).
26. Koivunen, P. *et al.* Transformation by the (R)-enantiomer of 2-hydroxyglutarate linked to EGLN activation. *Nature* **483**, 484–488 (2012).
27. Johnson, B. E. *et al.* Mutational Analysis Reveals the Origin and Therapy-Driven Evolution of Recurrent Glioma. *Science (80-.).* **343**, 189–193 (2014).
28. Watanabe, T., Nobusawa, S., Kleihues, P. & Ohgaki, H. IDH1 mutations are early events in the development of astrocytomas and oligodendrogliomas. *Am. J. Pathol.* **174**, 1149–1153 (2009).
29. Lai, A. *et al.* Evidence for sequenced molecular evolution of IDH1 mutant glioblastoma from a distinct cell of origin. *J. Clin. Oncol.* **29**, 4482–4490 (2011).
30. Rohle, D. *et al.* An inhibitor of mutant IDH1 delays growth and promotes differentiation of glioma cells. *Science (80-.).* **340**, 626–630 (2013).
31. Wang, F. *et al.* Targeted Inhibition of Mutant. *Science (80-.).* **622**, 622–627 (2013).
32. Okoye-Okafor, U. C. *et al.* New IDH1 mutant inhibitors for treatment of acute myeloid leukemia. *Nat. Chem. Biol.* **11**, 878–886 (2015).
33. Grassian, A. R. *et al.* IDH1 mutations alter citric acid cycle metabolism and increase dependence on oxidative mitochondrial metabolism. *Cancer Res.* **74**, 3317–3331 (2014).
34. Vertino, P. M. *et al.* Characterization of a Linked Jumonji Domain of the KDM5/JARID1 Family of Histone H3 Lysine 4 Demethylases. *J. Biol. Chem.* **291**, 2631–2646 (2015).
35. Chesnelong, C. *et al.* Lactate dehydrogenase A silencing in IDH mutant gliomas. *Neuro. Oncol.* **16**, 686–695 (2014).
36. Tateishi, K. *et al.* Extreme Vulnerability of IDH1 Mutant Cancers to NAD+ Depletion. *Cancer Cell* **28**, 773–784 (2015).
37. Molenaar, R. J. *et al.* Radioprotection of IDH1-mutated cancer cells by the IDH1-mutant inhibitor AGI-5198. *Cancer Res.* **75**, 4790–4802 (2015).
38. Sulkowski, P. L. *et al.* 2-Hydroxyglutarate produced by neomorphic IDH mutations suppresses homologous recombination and induces PARP inhibitor sensitivity. *Sci. Transl. Med.* **9**, (2017).
39. Molenaar, R. J. *et al.* Idh1/2 mutations sensitize acute myeloid leukemia to parp inhibition and this is reversed by idh1/2-mutant inhibitors. *Clin. Cancer Res.* **24**, 1705–1715 (2018).
40. Schumacher, T. *et al.* A vaccine targeting mutant IDH1 induces antitumour immunity. *Nature* **512**, 324–327 (2014).

41. Pellegatta, S. *et al.* Effective immuno-targeting of the IDH1 mutation R132H in a murine model of intracranial glioma. *Acta Neuropathol. Commun.* **3**, 4 (2015).
42. Kohanbash, G. *et al.* Isocitrate dehydrogenase mutations suppress STAT1 and CD8+ T cell accumulation in gliomas. *J. Clin. Invest.* **127**, 1425–1437 (2017).
43. Bird, A. P. & Wolffe, A. P. Methylation-Induced Repression-Minireview Belts, Braces, and Chromatin. **99**, 451–454 (1999).
44. Carnell, A. N. & Goodman, J. I. The long (LINEs) and the short (SINEs) of it: Altered methylation as a precursor to toxicity. *Toxicol. Sci.* **75**, 229–235 (2003).
45. Chen, Z. X. & Riggs, A. D. DNA methylation and demethylation in mammal. *J. Biol. Chem.* **286**, 18347–18353 (2011).
46. Tahiliani, M. *et al.* Conversion of 5-methylcytosine to 5-hydroxymethylcytosine in mammalian DNA by MLL partner TET1. *Science (80-.).* **324**, 930–935 (2009).
47. Ito, S. *et al.* Role of Tet proteins in 5mC to 5hmC conversion, ES-cell self-renewal and inner cell mass specification. *Nature* **466**, 1129–1133 (2010).
48. Guengerich, F. P. Introduction: Metals in Biology: α-Ketoglutarate/Iron-Dependent Dioxygenases. *J. Biol. Chem.* **290**, 20700–20701 (2015).
49. Nicholson, T. B., Veland, N. & Chen, T. *Writers, Readers, and Erasers of Epigenetic Marks*. *Epigenetic Cancer Therapy* (Elsevier Inc., 2015). doi:10.1016/B978-0-12-800206-3.00003-3
50. Luger, K., Mäder, A. W., Richmond, R. K., Sargent, D. F. & Richmond, T. J. Crystal structure of the nucleosome core particle at 2.8 Å resolution. *Nature* **389**, 251–260 (1997).
51. Jenuwein, T. & Allis, C. D. Translating the histone code. *Science (80-.).* **293**, 1074–1080 (2001).
52. Bannister, A. J. & Kouzarides, T. Regulation of chromatin by histone modifications. *Cell Res.* **21**, 381–395 (2011).
53. Li, X., Egervari, G., Wang, Y., Berger, S. L. & Lu, Z. Regulation of chromatin and gene expression by metabolic enzymes and metabolites. *Nat. Rev. Mol. Cell Biol.* **19**, 563–578 (2018).
54. Sun, X. J., Man, N., Tan, Y., Nimer, S. D. & Wang, L. The role of histone acetyltransferases in normal and malignant hematopoiesis. *Front. Oncol.* **5**, 1–11 (2015).
55. Seto, E. & Yoshida, M. Erasers of Histone Acetylation: The Histone Deacetylase Enzymes. *Cold Spring Harb. Perspect. Biol.* **6**, a018713–a018713 (2014).
56. Sanchez, R., Meslamani, J. & Zhou, M. M. The bromodomain: From epigenome reader to druggable target. *Biochim. Biophys. Acta - Gene Regul. Mech.* **1839**, 676–685 (2014).
57. Wood, A. & Shilatifard, A. Posttranslational modifications of histones by methylation. *Adv. Protein Chem.* **67**, 201–222 (2004).
58. Zhang, Y. & Reinberg, D. Transcription regulation by histone methylation: Interplay between different covalent modifications of the core histone tails. *Genes Dev.* **15**, 2343–2360 (2001).
59. Bedford, M. T. & Richard, S. Arginine methylation: An emerging regulator of protein function. *Mol. Cell* **18**, 263–272 (2005).
60. Pedersen, M. T. & Helin, K. Histone demethylases in development and disease. *Trends Cell Biol.* **20**, 662–671 (2010).
61. Shi, Y. *et al.* Histone Demethylation Mediated by the Nuclear Amine Oxidase Homolog LSD1 instance, histone H3 K9 (H3-K9) methylation is associ-ated with heterochromatin formation (Nakayama et al and also. *Sidney Kimmel*

Compr. Cancer Cent. **119**, 941–953 (2004).
62. Tsukada, Y. I. *et al.* Histone demethylation by a family of JmjC domain-containing proteins. *Nature* **439**, 811–816 (2006).
63. Cuthbert, G. L. *et al.* Histone Deimination Antagonizes Arginine Methylation. *Cell* **118**, 545–553 (2004).
64. Zhang, X. *et al.* Peptidylarginine deiminase 2-catalyzed histone H3 arginine 26 citrullination facilitates estrogen receptor α target gene activation. *Proc. Natl. Acad. Sci. U. S. A.* **109**, 13331–13336 (2012).
65. Wang, Y. *et al.* Human PAD4 regulates histone arginine methylation levels via demethylimination. *Science (80-.).* **306**, 279–283 (2004).
66. Walport, L. J. *et al.* Arginine demethylation is catalysed by a subset of JmjC histone lysine demethylases. *Nat. Commun.* **7**, 1–12 (2016).
67. Chang, B., Chen, Y., Zhao, Y. & Bruick, R. K. JMJD6 Is a Histone Arginine Demethylase. *Science (80-.).* **318**, 444–447 (2007).
68. Bottomley, M. J. Structures of protein domains that create or recognize histone modifications. *EMBO Rep.* **5**, 464–469 (2004).
69. Gayatri, S. & Bedford, M. T. Readers of histone methylarginine marks. *Biochim. Biophys. Acta - Gene Regul. Mech.* **1839**, 702–710 (2014).
70. Kirmizis, A. *et al.* Arginine methylation at histone H3R2 controls deposition of H3K4 trimethylation. *Nature* **449**, 928–932 (2007).
71. Sims, R. J., Nishioka, K. & Reinberg, D. Histone lysine methylation: A signature for chromatin function. *Trends Genet.* **19**, 629–639 (2003).
72. Rea, S. *et al.* Regulation of chromatin structure by site-specific histone H3 methyltransferases. *Nature* **406**, 593–599 (2000).
73. Su, X. *et al.* Molecular basis underlying histone H3 lysine-arginine methylation pattern readout by Spin/Ssty repeats of Spindlin1. *Genes Dev.* **28**, 622–636 (2014).
74. Yamane, K. *et al.* JHDM2A, a JmjC-Containing H3K9 Demethylase, Facilitates Transcription Activation by Androgen Receptor. *Cell* **125**, 483–495 (2006).
75. Bauer, U. M., Daujat, S., Nielsen, S. J., Nightingale, K. & Kouzarides, T. Methylation at arginine 17 of histone H3 is linked to gene activation. *EMBO Rep.* **3**, 39–44 (2002).
76. Schurter, B. T. *et al.* Methylation of histone H3 by coactivator-associated arginine methyltransferase 1. *Biochemistry* **40**, 5747–5756 (2001).
77. Cao, R. *et al.* Role of Histone H3 Lysine 27 Methylation in Polycomb-Group Silencing. *Science (80-.).* **298**, 1039–1043 (2002).
78. Agger, K. *et al.* UTX and JMJD3 are histone H3K27 demethylases involved in HOX gene regulation and development. *Nature* **449**, 731–734 (2007).
79. Krogan, N. J. *et al.* Methylation of histone H3 by Set2 in Saccharomyces cerevisiae is linked to transcriptional elongation by RNA polymerase II. *Mol. Cell. Biol.* **23**, 4207–18 (2003).
80. Klose, R. J. *et al.* Demethylation of Histone H3K36 and H3K9 by Rph1: a Vestige of an H3K9 Methylation System in Saccharomyces cerevisiae? *Mol. Cell. Biol.* **27**, 3951–3961 (2007).
81. Steger, D. J. *et al.* DOT1L/KMT4 Recruitment and H3K79 Methylation Are Ubiquitously Coupled with Gene Transcription in Mammalian Cells. *Mol. Cell. Biol.* **28**, 2825–2839 (2008).
82. Kang, J. Y. *et al.* KDM2B is a histone H3K79 demethylase and induces transcriptional repression via sirtuin-1–mediated chromatin silencing. *FASEB J.* **32**, 5737–5750 (2018).

83. Strahl, B. D. *et al.* Methylation of histone H4 at arginine 3 occurs in vivo and is mediated by the nuclear receptor coactivator PRMT1. *Curr. Biol.* **11**, 996–1000 (2001).
84. Mazur, P. K., Gozani, O., Sage, J. & Reynoird, N. Novel insights into the oncogenic function of the SMYD3 lysine methyltransferase. *Transl. Cancer Res.* **5**, 330–333 (2016).
85. Nishioka, K. *et al.* PR-Set7 is a nucleosome-specific methyltransferase that modifies lysine 20 of histone H4 and is associated with silent Chromatin. *Mol. Cell* **9**, 1201–1213 (2002).
86. Liu, W. *et al.* PHF8 mediates histone H4 lysine 20 demethylation events involved in cell cycle progression. *Nature* **466**, 508–512 (2010).
87. Rossetto, D., Avvakumov, N. & Côté, J. Histone phosphorylation. *Epigenetics* **7**, 1098–1108 (2012).
88. Healy, S., Khan, P., He, S. & Davie, J. R. Histone H3 phosphorylation, immediate-early gene expression, and the nucleosomal response: A historical perspective. *Biochem. Cell Biol.* **90**, 39–54 (2012).
89. Van Attikum, H. & Gasser, S. M. The histone code at DNA breaks: A guide to repair? *Nat. Rev. Mol. Cell Biol.* **6**, 757–765 (2005).
90. Cheung, P. *et al.* Synergistic coupling of histone H3 phosphorylation and acetylation in response to epidermal growth factor stimulation. *Mol. Cell* **5**, 905–915 (2000).
91. Hendzel, M. J. *et al.* Mitosis-specific phosphorylation of histone H3 initiates primarily within pericentromeric heterochromatin during G2 and spreads in an ordered fashion coincident with mitotic chromosome condensation. *Chromosoma* **106**, 348–360 (1997).
92. Goto, H., Yasui, Y., Nigg, E. A. & Inagaki, M. Aurora-B phosphorylates Histone H3 at serine28 with regard to the mitotic chromosome condensation. *Genes to Cells* **7**, 11–17 (2002).
93. Nath, D. & Shadan, S. The ubiquitin system. *Nature* **458**, 421 (2009).
94. Wang, H. *et al.* Role of histone H2A ubiquitination in Polycomb silencing. *Nature* **431**, 873–878 (2004).
95. Zhu, B. *et al.* Monoubiquitination of human histone H2B: The factors involved and their roles in HOX gene regulation. *Mol. Cell* **20**, 601–611 (2005).
96. Shiio, Y. & Eisenman, R. N. Histone sumoylation is associated with transcriptional repression. *Proc. Natl. Acad. Sci. U. S. A.* **100**, 13225–13230 (2003).
97. Vignali, M., Hassan, A. H., Neely, K. E. & Workman, J. L. ATP-Dependent Chromatin-Remodeling Complexes. *Mol. Cell. Biol.* **20**, 1899–1910 (2000).
98. Wang, G. G., Allis, C. D. & Chi, P. Chromatin remodeling and cancer, part II: ATP-dependent chromatin remodeling. *Trends Mol. Med.* **13**, 373–380 (2007).
99. Kapranov, P. *et al.* RNA maps reveal new RNA classes and a possible function for pervasive transcription. *Science (80-.).* **316**, 1484–1488 (2007).
100. Thomson, T. & Lin, H. The Biogenesis and Function of PIWI Proteins and piRNAs: Progress and Prospect. *Annu. Rev. Cell Dev. Biol.* **25**, 355–376 (2009).
101. Guttman, M. *et al.* Chromatin signature reveals over a thousand highly conserved large non-coding RNAs in mammals. *Nature* **458**, 223–227 (2009).
102. Rinn, J. L. *et al.* Functional Demarcation of Active and Silent Chromatin Domains in Human HOX Loci by Noncoding RNAs. *Cell* **129**, 1311–1323 (2007).
103. Khalil, A. M. *et al.* Many human large intergenic noncoding RNAs associate

with chromatin-modifying complexes and affect gene expression. *Proc. Natl. Acad. Sci. U. S. A.* **106**, 11667–11672 (2009).
104. Penny, G. D., Kay, G. F., Sheardown, S. A., Rastan, S. & Brockdorff, N. Requirement for Xist in X chromosome inactivation. *Nature* **379**, 131–137 (1996).
105. Plath, K., Mlynarczyk-Evans, S., Nusinow, D. A. & Panning, B. Xist RNA and the Mechanism of X Chromosome Inactivation . *Annu. Rev. Genet.* **36**, 233–278 (2002).
106. Cadieux, B., Ching, T. T., VandenBerg, S. R. & Costello, J. F. Genome-wide hypomethylation in human glioblastomas associated with specific copy number alteration, methylenetetrahydrofolate reductase allele status, and increased proliferation. *Cancer Res.* **66**, 8469–8476 (2006).
107. Wick, W. *et al.* NOA-04 randomized phase III trial of sequential radiochemotherapy of anaplastic glioma with Procarbazine, Lomustine, and Vincristine or Temozolomide. *J. Clin. Oncol.* **27**, 5874–5880 (2009).
108. Campos, B. *et al.* Expression of nuclear receptor corepressors and class I histone deacetylases in astrocytic gliomas. *Cancer Sci.* **102**, 387–392 (2011).
109. Liau, B. B. *et al.* Adaptive Chromatin Remodeling Drives Glioblastoma Stem Cell Plasticity and Drug Tolerance. *Cell Stem Cell* **20**, 233-246.e7 (2017).
110. Wu, G. *et al.* Somatic histone H3 alterations in pediatric diffuse intrinsic pontine gliomas and non-brainstem glioblastomas. *Nat. Genet.* **44**, 251–253 (2012).
111. Schwartzentruber, J. *et al.* Driver mutations in histone H3.3 and chromatin remodelling genes in paediatric glioblastoma. *Nature* **482**, 226–231 (2012).
112. Capper, D. *et al.* DNA methylation-based classification of central nervous system tumours. *Nature* **555**, 469–474 (2018).
113. Mitteilungen, K. Ableitung der absoluten Konfiguration yon Alkaloiden der Aspidospermingruppe durch optischen Vergleich mit Alkaloiden der Strychningruppe 5-Azacytidine , a New , Highly Effective Cancerostatic. 202–203 (1964).
114. Silverman, L. R. *et al.* Randomized controlled trial of azacitidine in patients with the myelodysplastic syndrome: A study of the cancer and leukemia group B. *J. Clin. Oncol.* **20**, 2429–2440 (2002).
115. Kantarjlan, H. *et al.* Decitabine improves patient outcomes in myelodysplastic syndromes: Results of a phase III randomized study. *Cancer* **106**, 1794–1803 (2006).
116. Borodovsky, A. *et al.* 5-azacytidine reduces methylation, promotes differentiation and induces tumor regression in a patient-derived IDH1 mutant glioma xenograft. *Oncotarget* **4**, (2013).
117. Turcan, S. *et al.* Efficient induction of differentiation and growth inhibition in IDH1 mutant glioma cells by the DNMT Inhibitor Decitabine. *Oncotarget* **4**, 1729–1736 (2013).
118. Konkankit, V. V. *et al.* Decitabine immunosensitizes human gliomas to NY-ESO-1 specific T lymphocyte targeting through the Fas/Fas Ligand pathway. *J. Transl. Med.* **9**, 13–15 (2011).
119. Riccadonna, C. *et al.* Decitabine treatment of glioma-initiating cells enhances immune recognition and killing. *PLoS One* **11**, 1–20 (2016).
120. Finnin, M. S. *et al.* Structures of a histone deacetylase homologue bound to the TSA and SAHA inhibitors. *Nature* **401**, 188–193 (1999).
121. Eckschlager, T., Plch, J., Stiborova, M. & Hrabeta, J. Histone deacetylase inhibitors as anticancer drugs. *Int. J. Mol. Sci.* **18**, 1–25 (2017).

122. Kim, H. J. & Bae, S. C. Histone deacetylase inhibitors: Molecular mechanisms of action and clinical trials as anti-cancer drugs. *Am. J. Transl. Res.* **3**, 166–179 (2011).
123. Kozikowski, A. P., Tapadar, S., Luchini, D. N., Ki, H. K. & Billadeau, D. D. Use of the Nitrile Oxide Cycloaddition (NOC) reaction for molecular probe generation: A new class of enzyme selective histone deacetylase inhibitors (HDACIs) showing picomolar activity at HDAC6. *J. Med. Chem.* **51**, 4370–4373 (2008).
124. Eom, G. H. & Kook, H. Posttranslational modifications of histone deacetylases: Implications for cardiovascular diseases. *Pharmacol. Ther.* **143**, 168–180 (2014).
125. Mann, B. S., Johnson, J. R., Cohen, M. H., Justice, R. & Pazdur, R. FDA Approval Summary: Vorinostat for Treatment of Advanced Primary Cutaneous T-Cell Lymphoma. *Oncologist* **12**, 1247–1252 (2007).
126. Grant, C. *et al.* Romidepsin: a new therapy for cutaneous T-cell lymphoma and a potential therapy for solid tumors. *Expert Rev. Anticancer Ther.* **10**, 997–1008 (2010).
127. Lee, H. Z. *et al.* FDA approval: Belinostat for the treatment of patients with relapsed or refractory peripheral T-cell lymphoma. *Clin. Cancer Res.* **21**, 2666–2670 (2015).
128. Raedler, L. A. Farydak (Panobinostat): First HDAC Inhibitor Approved for Patients with Relapsed Multiple Myeloma. *Am. Heal. drug benefits* **9**, 84–7 (2016).
129. Galanis, E. *et al.* Phase II trial of Vorinostat in recurrent glioblastoma multiforme: A north central cancer treatment group study. *J. Clin. Oncol.* **27**, 2052–2058 (2009).
130. Friday, B. B. *et al.* Phase II trial of vorinostat in combination with bortezomib in recurrent glioblastoma: A north central cancer treatment group study. *Neuro. Oncol.* **14**, 215–221 (2012).
131. Galanis, E. *et al.* Phase I/II trial of vorinostat combined with temozolomide and radiation therapy for newly diagnosed glioblastoma: Results of Alliance N0874/ABTC 02. *Neuro. Oncol.* **20**, 546–556 (2018).
132. Ghiaseddin, A. *et al.* Phase II Study of Bevacizumab and Vorinostat for Patients with Recurrent World Health Organization Grade 4 Malignant Glioma. *Oncologist* **23**, 157-e21 (2018).
133. Iwamoto, F. M. *et al.* A phase I/II trial of the histone deacetylase inhibitor romidepsin for adults with recurrent malignant glioma: North American brain tumor consortium study 03-03. *Neuro. Oncol.* **13**, 509–516 (2011).
134. Lee, E. Q. *et al.* Phase II study of panobinostat in combination with bevacizumab for recurrent glioblastoma and anaplastic glioma. *Neuro. Oncol.* **17**, 862–867 (2015).
135. Shi, W. *et al.* Phase I trial of panobinostat and fractionated stereotactic re-irradiation therapy for recurrent high grade gliomas. *J. Neurooncol.* **127**, 535–539 (2016).
136. Krauze, A. V. *et al.* A Phase 2 Study of Concurrent Radiation Therapy, Temozolomide, and the Histone Deacetylase Inhibitor Valproic Acid for Patients with Glioblastoma. *Int. J. Radiat. Oncol. Biol. Phys.* **92**, 986–992 (2015).
137. Gurbani, S. S. *et al.* Assessing Treatment Response of Glioblastoma to an HDAC Inhibitor Using Whole-Brain Spectroscopic MRI. **5**, 53–60 (2019).
138. Rotili, D. & Mai, A. Targeting histone demethylases: A new avenue for the fight against cancer. *Genes and Cancer* **2**, 663–679 (2011).

139. McAllister, T. E. *et al.* Recent Progress in Histone Demethylase Inhibitors. *J. Med. Chem.* **59**, 1308–1329 (2016).
140. Sareddy, G. R. *et al.* KDM1 is a novel therapeutic target for the treatment of gliomas. *Oncotarget* **4**, 18–28 (2013).
141. Maes, T. *et al.* ORY-1001, a Potent and Selective Covalent KDM1A Inhibitor, for the Treatment of Acute Leukemia. *Cancer Cell* **33**, 495-511.e12 (2018).
142. Markolovic, S. *et al.* Structure-function relationships of human JmjC oxygenases - demethylases versus hydroxylases. *Curr. Opin. Struct. Biol.* **41**, 62–72 (2016).
143. King, O. N. F. *et al.* Quantitative high-throughput screening identifies 8-hydroxyquinolines as cell-active histone demethylase inhibitors. *PLoS One* **5**, (2010).
144. Wang, L. *et al.* A small molecule modulates Jumonji histone demethylase activity and selectively inhibits cancer growth. *Nat. Commun.* **4**, (2013).
145. Kruidenier, L. *et al.* A selective jumonji H3K27 demethylase inhibitor modulates the proinflammatory macrophage response. *Nature* **488**, 404–408 (2012).
146. Heinemann, B. *et al.* Inhibition of demethylases by GSK-J1/J4. *Nature* **514**, E1–E2 (2014).
147. Horton, J. R. *et al.* Structural basis for KDM5A histone lysine demethylase inhibition by diverse compounds The KDM5/JARID1 family of Fe(II)-and α-ketoglutarate-dependent demethylases removes methyl groups from methylated lysine 4 of histone H3. Accumulating evidence supports . *Cell Chem Biol* **23**, 769–781 (2016).
148. Wu, L. *et al.* KDM5 histone demethylases repress immune response via suppression of STING. *PLoS Biol.* **16**, 1–29 (2018).
149. Tumber, A. *et al.* Potent and Selective KDM5 Inhibitor Stops Cellular Demethylation of H3K4me3 at Transcription Start Sites and Proliferation of MM1S Myeloma Cells. *Cell Chem. Biol.* **24**, 371–380 (2017).
150. Hashizume, R. *et al.* Pharmacologic inhibition of histone demethylation as a therapy for pediatric brainstem glioma. *Nat. Med.* **20**, 1394–1396 (2014).
151. Venteicher, A. S. *et al.* Decoupling genetics, lineages, and microenvironment in IDH-mutant gliomas by single-cell RNA-seq. *Science (80-.).* **355**, (2017).
152. Banelli, B. *et al.* Small molecules targeting histone demethylase genes (KDMs) inhibit growth of temozolomide-resistant glioblastoma cells. *Oncotarget* **8**, 34896–34910 (2017).
153. Romani, M., Daga, A., Forlani, A., Pistillo, M. P. & Banelli, B. Targeting of Histone Demethylases KDM5A and KDM6B Inhibits the Proliferation of. (2019).
154. Dang, L., Yen, K. & Attar, E. C. IDH mutations in cancer and progress toward development of targeted therapeutics. *Ann. Oncol.* **27**, 599–608 (2016).
155. Pusch, S. *et al.* Pan-mutant IDH1 inhibitor BAY 1436032 for effective treatment of IDH1 mutant astrocytoma in vivo. *Acta Neuropathol.* **133**, 629–644 (2017).
156. Stein, E. M. *et al.* Enasidenib in mutant IDH2 relapsed or refractory acute myeloid leukemia. *Blood* **130**, 722–731 (2017).
157. DiNardo, C. D. *et al.* Durable remissions with ivosidenib in IDH1-mutated relapsed or refractory AML. *N. Engl. J. Med.* **378**, 2386–2398 (2018).
158. Turcan, S. *et al.* Mutant-IDH1-dependent chromatin state reprogramming, reversibility, and persistence. *Nat. Genet.* **50**, 62–72 (2018).
159. Viswanath, P. *et al.* Rapid Conversion of Mutant IDH1 from Driver to Passenger in a Model of Human Gliomagenesis. *Mol. Cancer Res.* **14**, 976–983 (2016).
160. Kats, L. M. *et al.* Proto-oncogenic role of mutant IDH2 in leukemia initiation

and maintenance. *Cell Stem Cell* **14**, 329–341 (2014).
161. Fulda, S., Gorman, A. M., Hori, O. & Samali, A. Cellular stress responses: Cell survival and cell death. *Int. J. Cell Biol.* **2010**, (2010).
162. Ashburner, M. & Bonner, J. J. The induction of gene activity in drosophila by heat shock. *Cell* **17**, 241–254 (1979).
163. Craig, E. A. & Schlesinger, M. J. The Heat Shock Respons. *Crit. Rev. Biochem.* **18**, 239–280 (1985).
164. Lindquist, S. THE HEAT-SHOCK RESPONSE. (1986).
165. Heikkila, J. J., Schultz, G. A., Iatrou, K. & Gedamu, L. Expression of a set of fish genes following heat or metal ion exposure. *J. Biol. Chem.* **257**, 12000–12005 (1982).
166. Courgeon, A. M., Maisonhaute, C. & Best-Belpomme, M. Heat shock proteins are induced by cadmium in Drosophila cells. *Exp. Cell Res.* **153**, 515–521 (1984).
167. Michel, G. P. F. & Starka, J. Effect of ethanol and heat stresses on the protein pattern of Zymomonas mobilis. *J. Bacteriol.* **165**, 1040–1042 (1986).
168. Richter, K., Haslbeck, M. & Buchner, J. The Heat Shock Response: Life on the Verge of Death. *Mol. Cell* **40**, 253–266 (2010).
169. Wang, W., Vinocur, B., Shoseyov, O. & Altman, A. Role of plant heat-shock proteins and molecular chaperones in the abiotic stress response. *Trends Plant Sci.* **9**, 244–252 (2004).
170. Gupta, S. C., Sharma, A., Mishra, M., Mishra, R. K. & Chowdhuri, D. K. Heat shock proteins in toxicology: How close and how far? *Life Sci.* **86**, 377–384 (2010).
171. Abravaya, K., Myers, M. P., Murphy, S. P. & Morimoto, R. I. The human heat shock protein hsp70 interacts with HSF, the transcription factor that regulates heat shock gene expression. *Genes Dev.* **6**, 1153–1164 (1992).
172. Zou, J., Guo, Y., Guettouche, T., Smith, D. F. & Voellmy, R. Repression of heat shock transcription factor HSF1 activation by HSP90 (HSP90 complex) that forms a stress-sensitive complex with HSF1. *Cell* **94**, 471–480 (1998).
173. Kourtis, N. & Tavernarakis, N. Cellular stress response pathways and ageing: Intricate molecular relationships. *EMBO J.* **30**, 2520–2531 (2011).
174. Stevens, F. J. & Argon, Y. Protein folding in the ER. *Semin. Cell Dev. Biol.* **10**, 443–454 (1999).
175. Ellgaard, L. & Helenius, A. Quality control in the endoplasmic reticulum. *Nat. Rev. Mol. Cell Biol.* **4**, 181–191 (2003).
176. Munro, S. & Pelham, H. R. B. An hsp70-like protein in the ER: Identity with the 78 kd glucose-regulated protein and immunoglobulin heavy chain binding protein. *Cell* **46**, 291–300 (1986).
177. Wang, M., Wey, S., Zhang, Y., Ye, R. & Lee, A. S. Role of the unfolded protein response regulator GRP78/BiP in development, cancer, and neurological disorders. *Antioxidants Redox Signal.* **11**, 2307–2316 (2009).
178. Lee, A. S. The ER chaperone and signaling regulator GRP78/BiP as a monitor of endoplasmic reticulum stress. *Methods* **35**, 373–381 (2005).
179. Yoshida, H., Matsui, T., Yamamoto, A., Okada, T. & Mori, K. XBP1 mRNA Is Induced by ATF6 and Spliced by IRE1 in Response to ER Stress to Produce a Highly Active Transcription Factor phorylation, the activated Ire1p specifically cleaves HAC1 precursor mRNA to remove an intron of 252 nucle-otides. The cleaved 5 and . *Cell* **107**, 881–891 (2001).
180. Haze, K., Yoshida, H., Yanagi, H., Yura, T. & Mori, K. Mammalian

transcription factor ATF6 is synthesized as a transmembrane protein and activated by proteolysis in response to endoplasmic reticulum stress. *Mol. Biol. Cell* **10**, 3787–3799 (1999).
181. Ye, J. *et al.* ER stress induces cleavage of membrane-bound ATF6 by the same proteases that process SREBPs. *Mol. Cell* **6**, 1355–1364 (2000).
182. Shi, Y. *et al.* Identification and Characterization of Pancreatic Eukaryotic Initiation Factor 2 α-Subunit Kinase, PEK, Involved in Translational Control. *Mol. Cell. Biol.* **18**, 7499–7509 (1998).
183. Vattem, K. M. & Wek, R. C. Reinitiation involving upstream ORFs regulates ATF4 mRNA translation in mammalian cells. *Proc. Natl. Acad. Sci. U. S. A.* **101**, 11269–11274 (2004).
184. Harding, H. P. *et al.* Regulated translation initiation controls stress-induced gene expression in mammalian cells. *Mol. Cell* **6**, 1099–1108 (2000).
185. Pakos-Zebrucka, K. *et al.* The integrated stress response. *EMBO Rep.* **17**, 1374–1395 (2016).
186. Clemens, M. J. & Elia, A. The double-stranded RNA-dependent protein kinase PKR: Structure and function. *J. Interf. Cytokine Res.* **17**, 503–524 (1997).
187. Vazquez de Aldana, C. R., Wek, R. C., Segundo, P. S., Truesdell, A. G. & Hinnebusch, A. G. Multicopy tRNA genes functionally suppress mutations in yeast eIF-2 alpha kinase GCN2: evidence for separate pathways coupling GCN4 expression to unchanged tRNA. *Mol. Cell. Biol.* **14**, 7920–7932 (1994).
188. Castilho, B. A. *et al.* Keeping the eIF2 alpha kinase Gcn2 in check. *Biochim. Biophys. Acta - Mol. Cell Res.* **1843**, 1948–1968 (2014).
189. Han, A. P. *et al.* Heme-regulated eIF2α kinase (HRI) is required for translational regulation and survival of erythroid precursors in iron deficiency. *EMBO J.* **20**, 6909–6918 (2001).
190. Bank, A. Understanding globin regulation in β-thalassemia.pdf. 4–7 (2005). doi:10.1172/JCI25398.1470
191. Ma, K., Vattem, K. M. & Wek, R. C. Dimerization and release of molecular chaperone inhibition facilitate activation of eukaryotic initiation factor-2 kinase in response to endoplasmic reticulum stress. *J. Biol. Chem.* **277**, 18728–18735 (2002).
192. Chan, C. P., Kok, K. H., Tang, H. M. V., Wong, C. M. & Jin, D. Y. Internal ribosome entry site-mediated translational regulation of ATF4 splice variant in mammalian unfolded protein response. *Biochim. Biophys. Acta - Mol. Cell Res.* **1833**, 2165–2175 (2013).
193. Dey, S. *et al.* ATF4-dependent induction of heme oxygenase 1 prevents anoikis and promotes metastasis. *J. Clin. Invest.* **125**, 2592–2608 (2015).
194. Kilberg, M. S., Shan, J. & Su, N. ATF4-dependent transcription mediates signaling of amino acid limitation. *Trends Endocrinol. Metab.* **20**, 436–443 (2009).
195. Rozpedek, W. *et al.* The Role of the PERK/eIF2α/ATF4/CHOP Signaling Pathway in Tumor Progression During Endoplasmic Reticulum Stress. *Curr. Mol. Med.* **16**, 533–544 (2016).
196. Hiramatsu, N., Chiang, W. C., Kurt, T. D., Sigurdson, C. J. & Lin, J. H. Multiple Mechanisms of Unfolded Protein Response-Induced Cell Death. *Am. J. Pathol.* **185**, 1800–1808 (2015).
197. Ma, Y. & Hendershot, L. M. Delineation of a negative feedback regulatory loop that controls protein translation during endoplasmic reticulum stress. *J. Biol. Chem.* **278**, 34864–34873 (2003).

198. Stewart, S. A. *et al.* Lentivirus-delivered stable gene silencing by RNAi in primary cells. *Rna* **9**, 493–501 (2003).
199. Cheng, E. H. Y. *et al.* BCL-2, BCL-XL sequester BH3 domain-only molecules preventing BAX- and BAK-mediated mitochondrial apoptosis. *Mol. Cell* **8**, 705–711 (2001).
200. Sanjana, N. E., Shalem, O. & Zhang, F. Improved vectors and genome-wide libraries for CRISPR screening. *Nat. Methods* **11**, 783–784 (2014).
201. Campeau, E. *et al.* A versatile viral system for expression and depletion of proteins in mammalian cells. *PLoS One* **4**, (2009).
202. Labun, K. *et al.* CHOPCHOP v3: expanding the CRISPR web toolbox beyond genome editing. *Nucleic Acids Res.* **47**, W171–W174 (2019).
203. Chou, T. C. Theoretical basis, experimental design, and computerized simulation of synergism and antagonism in drug combination studies. *Pharmacol. Rev.* **58**, 621–681 (2006).
204. Schmidt, E. K., Clavarino, G., Ceppi, M. & Pierre, P. SUnSET, a nonradioactive method to monitor protein synthesis. *Nat. Methods* **6**, 275–277 (2009).
205. Wingett, S. W. & Andrews, S. FastQ Screen: A tool for multi-genome mapping and quality control. *F1000Research* **7**, 1338 (2018).
206. Kim, D., Paggi, J. M., Park, C., Bennett, C. & Salzberg, S. L. Graph-based genome alignment and genotyping with HISAT2 and HISAT-genotype. *Nat. Biotechnol.* **37**, 907–915 (2019).
207. Sims, D. *et al.* CGAT: Computational genomics analysis toolkit. *Bioinformatics* **30**, 1290–1291 (2014).
208. Cribbs, A. P. *et al.* CGAT-core: a python framework for building scalable, reproducible computational biology workflows. *F1000Research* **8**, 377 (2019).
209. Love, M. I., Huber, W. & Anders, S. Moderated estimation of fold change and dispersion for RNA-seq data with DESeq2. *Genome Biol.* **15**, 1–21 (2014).
210. Subramanian, A. *et al.* Gene set enrichment analysis: A knowledge-based approach for interpreting genome-wide expression profiles. *Proc. Natl. Acad. Sci. U. S. A.* **102**, 15545–15550 (2005).
211. Fang, H., Knezevic, B., Burnham, K. L. & Knight, J. C. XGR software for enhanced interpretation of genomic summary data, illustrated by application to immunological traits. *Genome Med.* **8**, 1–20 (2016).
212. Mootha, V. K. *et al.* PGC-1α-responsive genes involved in oxidative phosphorylation are coordinately downregulated in human diabetes. *Nat. Genet.* (2003). doi:10.1038/ng1180
213. Rozo, A. V. *et al.* ATF5 regulates β-cell survival during stress. *Proc. Natl. Acad. Sci.* **114**, 1341–1346 (2017).
214. Oyadomari, S. & Mori, M. Roles of CHOP/GADD153 in endoplasmic reticulum stress. *Cell Death Differ.* **11**, 381–389 (2004).
215. Li, J., Lee, B. & Lee, A. S. Endoplasmic Reticulum Stress-induced Apoptosis. *J. Biol. Chem.* **281**, 7260–7270 (2006).
216. Lu, Y. *et al.* Chemosensitivity of IDH1-mutated gliomas due to an impairment in PARP1-mediated DNA repair. *Cancer Res.* **77**, 1709–1718 (2017).
217. Greiner, D., Bonaldi, T., Eskeland, R., Roemer, E. & Imhof, A. Identification of a specific inhibitor of the histone methyltransferase su(Var)3-9. *Nat. Chem. Biol.* **1**, 143–145 (2005).
218. Dixit, D., Ghildiyal, R., Anto, N. P. & Sen, E. Chaetocin-induced ROS-mediated apoptosis involves ATM-YAP1 axis and JNK-dependent inhibition of glucose metabolism. *Cell Death Dis.* **5**, e1212-13 (2014).

219. Ozyerli-Goknar, E. *et al.* The fungal metabolite chaetocin is a sensitizer for pro-apoptotic therapies in glioblastoma. *Cell Death Dis.* **10**, (2019).
220. Khan, N. *et al.* Determination of the class and isoform selectivity of small-molecule histone deacetylase inhibitors. *Biochem. J.* **409**, 581–589 (2008).
221. Kusaczuk, M., Krętowski, R., Stypułkowska, A. & Cechowska-Pasko, M. Molecular and cellular effects of a novel hydroxamate-based HDAC inhibitor – belinostat – in glioblastoma cell lines: a preliminary report. *Invest. New Drugs* **34**, 552–564 (2016).
222. Al-Lazikani, B., Banerji, U. & Workman, P. Combinatorial drug therapy for cancer in the post-genomic era. *Nat. Biotechnol.* **30**, 679–692 (2012).
223. Paller, C. J. *et al.* Design of Phase I Combination Trials: Recommendations of the Clinical Trial Design Task Force of the NCI Investigational Drug Steering Committee. *Clin. Cancer Res.* **20**, 4210–4217 (2014).
224. Hanahan, D. Rethinking the war on cancer. *Lancet* **383**, 558–563 (2014).
225. Landry, B. D. *et al.* Tumor-stroma interactions differentially alter drug sensitivity based on the origin of stromal cells. *Mol. Syst. Biol.* **14**, 1–15 (2018).
226. Piaskowski, S. *et al.* Glioma cells showing IDH1 mutation cannot be propagated in standard cell culture conditions. *Br. J. Cancer* **104**, 968–970 (2011).
227. Lee, J. *et al.* Tumor stem cells derived from glioblastomas cultured in bFGF and EGF more closely mirror the phenotype and genotype of primary tumors than do serum-cultured cell lines. *Cancer Cell* **9**, 391–403 (2006).
228. Kelly, J. J. P. *et al.* Proliferation of human glioblastoma stem cells occurs independently of exogenous mitogens. *Stem Cells* **27**, 1722–1733 (2009).
229. Chen, Y. C. *et al.* High-throughput single-cell derived sphere formation for cancer stem-like cell identification and analysis. *Sci. Rep.* **6**, 1–12 (2016).
230. Izumiya, M. *et al.* Chemoresistance is associated with cancer stem cell-like properties and epithelial-to-mesenchymal transition in pancreatic cancer cells. *Anticancer Res.* **32**, 3847–3853 (2012).
231. Corces-Zimmerman, M. R. *et al.* Isocitrate dehydrogenase 1 and 2 mutations induce BCL-2 dependence in acute myeloid leukemia. *Nat. Med.* **21**, 178–184 (2015).
232. Turcan, S. *et al.* Mutant-IDH1-dependent chromatin state reprogramming, reversibility, and persistence. *Nat. Genet.* **50**, 62–72 (2018).
233. Antony, J. M. *et al.* The Human Endogenous Retrovirus Envelope Glycoprotein, Syncytin-1, Regulates Neuroinflammation and Its Receptor Expression in Multiple Sclerosis: A Role for Endoplasmic Reticulum Chaperones in Astrocytes. *J. Immunol.* **179**, 1210–1224 (2007).
234. Antony, J. M., DesLauriers, A. M., Bhat, R. K., Ellestad, K. K. & Power, C. Human endogenous retroviruses and multiple sclerosis: Innocent bystanders or disease determinants? *Biochim. Biophys. Acta - Mol. Basis Dis.* **1812**, 162–176 (2011).
235. Pasquarella, A. *et al.* Retrotransposon derepression leads to activation of the unfolded protein response and apoptosis in pro-B cells. *Development* **143**, 1788–1799 (2016).
236. Sidrauski, C. *et al.* Pharmacological brake-release of mRNA translation enhances cognitive memory. *Elife* **2013**, 1–22 (2013).
237. Mihailidou, C., Papazian, I., Papavassiliou, A. G. & Kiaris, H. CHOP-dependent Regulation of p21/waf1 During ER Stress. *Cell. Physiol. Biochem.* **25**, 761–766 (2010).
238. Cribbs, A. *et al.* Inhibition of histone H3K27 demethylases selectively modulates

inflammatory phenotypes of natural killer cells. *J. Biol. Chem.* **293**, 2422–2437 (2018).
239. Sakaki, H. *et al.* GSKJ4, A Selective Jumonji H3K27 Demethylase Inhibitor, Effectively Targets Ovarian Cancer Stem Cells. *Anticancer Res.* **35**, 6607–6614 (2015).
240. Mandal, C., Kim, S. H., Kang, S. C., Chai, J. C. & Lee, Y. S. Molecules and Cells GSK-J4-Mediated Transcriptomic Alterations in Differentiating Embryoid Bodies. **40**, 737–751 (2017).
241. Floros, K. V. *et al.* Targeted inhibition of histone H3K27 demethylation is effective in high-risk neuroblastoma. *Sci. Transl. Med.* **10**, eaao4680 (2018).
242. Dai, Y. *et al.* Bortezomib interacts synergistically with belinostat in human acute myeloid leukaemia and acute lymphoblastic leukaemia cells in association with perturbations in NF-κB and Bim. *Br. J. Haematol.* **153**, 222–235 (2011).
243. Havas, A. P. *et al.* Belinostat and vincristine demonstrate mutually synergistic cytotoxicity associated with mitotic arrest and inhibition of polyploidy in a preclinical model of aggressive diffuse large B cell lymphoma. *Cancer Biol. Ther.* **17**, 1240–1252 (2016).
244. Kahali, S., Sarcar, B., Prabhu, A., Seto, E. & Chinnaiyan, P. Class I histone deacetylases localize to the endoplasmic reticulum and modulate the unfolded protein response. *FASEB J.* **26**, 2437–2445 (2012).
245. Richon, V. M., Sandhoff, T. W., Rifkind, R. A. & Marks, P. A. Histone deacetylase inhibitor selectively induces p21WAF1 expressjon and gene-associated histone acetylation. *Proc. Natl. Acad. Sci. U. S. A.* **97**, 10014–10019 (2000).
246. Ocker, M. & Schneider-Stock, R. Histone deacetylase inhibitors: Signalling towards p21cip1/waf1. *Int. J. Biochem. Cell Biol.* **39**, 1367–1374 (2007).
247. Ju, R. & Muller, M. T. Histone deacetylase inhibitors activate p21WAF1 expression via ATM. *Cancer Res.* **63**, 2891–2897 (2003).
248. Zhao, S. *et al.* Glioma-Derived Mutations in IDH1 Dominantly Inhibit IDH1 Catalytic Activity and Induce HIF-1. *Science (80-.).* **324**, 261–265 (2009).
249. Kaelin, W. G. & Ratcliffe, P. J. Oxygen Sensing by Metazoans: The Central Role of the HIF Hydroxylase Pathway. *Mol. Cell* **30**, 393–402 (2008).
250. Semenza, G. L. Hypoxia-inducible factors in physiology and medicine. *Cell* **148**, 399–408 (2012).
251. Losman, J.-A. *et al.* (R)-2-Hydroxyglutarate Is Sufficient to Promote Leukemogenesis and Its Effects Are Reversible. *Science (80-.).* **339**, 1621–1625 (2013).
252. Lewis, C. M. *et al.* Suberoylanilide hydroxamic acid, a histone deacetylase inhibitor, ameliorates motor deficits in a mouse model of Huntington's disease. *Proc. Natl. Acad. Sci.* **100**, 2041–2046 (2003).
253. Stapleton, S. L. *et al.* Plasma and cerebrospinal fluid pharmacokinetics of valproic acid after oral administration in non-human primates. *Cancer Chemother. Pharmacol.* **61**, 647–652 (2008).